Spring 2022

Synthesis, characterization and chemistry of two-dimensional transition metal carbides and nitrides (MXenes)

Shuohan Huang
Missouri University of Science and Technology

Department: Chemistry

SYNTHESIS, CHARACTERIZATION AND CHEMISTRY OF TWO-DIMENSIONAL TRANSITION METAL CARBIDES AND NITRIDES (MXENES)

by

SHUOHAN HUANG

A DISSERTATION

Presented to the Graduate Faculty of the

MISSOURI UNIVERSITY OF SCIENCE AND TECHNOLOGY

In Partial Fulfillment of the Requirements for the Degree

DOCTOR OF PHILOSOPHY

in

CHEMISTRY

2021

Approved by:

Vadym N. Mochalin, Advisor
Honglan Shi
Jeffrey G. Winiarz
Amitava Choudhury
Xinhua Liang

PUBLICATION DISSERTATION OPTION

This dissertation consists of the following four articles, formatted in the style used by the Missouri University of Science and Technology:

Paper I, found on pages 26–53, has been published in *Inorganic Chemistry*.

Paper II, found on pages 54–83, has been published in *ACS Nano*.

Paper III, found on pages 84–121, has been published in *Nature Communications*.

Paper IV, found on pages 122–144, has been published in *Materials Today Advances*.

ABSTRACT

MXenes represent a relatively new and quickly growing family of two-dimensional (2D) early transition-metal carbides and nitrides first synthesized in 2011 from bulk layered crystalline MAX phases. Because of their 2D structure and unique combination of high conductivity and hydrophilicity, MXenes have raised a significant interest for various applications. However, it has been found that in some cases colloidal MXene flakes are not stable and can spontaneously degrade on a time scale from hours to days. In this work, we investigate the crucial factors for MXene degradation and demonstrate gas analysis as a powerful method to gain further insights into chemical reactivity of MXenes. The degradation rates of MXenes in water were further investigated depending on their monolayer thickness within the same chemical composition, as well as depending on chemical composition of the materials within the same monolayer thickness.

We further demonstrate the role of chemical properties and reactivity of MXenes in some of their applications, in particular, related to tribology and adhesion. We investigated the tribological properties of Ti_3C_2 MXene and MXene/graphene coatings. We have observed that with a careful control of the environment in order to suppress undesirable chemical decomposition of MXenes, the friction of MXene coated silicon substrates can be reduced to superlubric regime. We also studied adhesion of MXenes to silicon using atomic force microscopy. The obtained adhesion evnergies of two types of MXenes to silicon do not depend on the number of MXene monpayers in a stack and are comparable with that of graphene to silicon, showing a great potential of MXenes for (opto)electronic device assembly.

ACKNOWLEDGEMENTS

First and foremost, I would like to express my profound gratitude to my advisor, Dr. Vadym Mochalin, for his help and support during my Ph.D. study at Missouri S&T. It is impossible for me to stand at this point without his patient help and great encouragement. He led me to be the best I could be in different aspects during my graduate research, trusted me and gave me confidence. He not only guided me to explore wider and dig deeper, but also gave me positive influence on being optimistic towards life. I would like to thank my committee members, Drs. Honglan Shi, Jeffrey G. Winiarz, Amitava Choudhury and Xinhua Liang, for their help on reviewing this work and providing valuable comments.

I am also thankful to my labmates, Dr. Sergii Chertopalov, who helped me at the beginning of my graduate research, and Gabriel Hulliuing, who worked with me for MXene synthesis. I would like to thank our previous group members, Dr. Daisuke Shiro, Dr. Jiangying Qu, Dr. Mei Wang, Dr. Xinmeng Zhang, Ibrahim Abdullahi and Atsushi Kume, for their help and friendship. I am also grateful to my collaborators in Dr. Chenglin Wu's lab (Missouri S&T) and Dr. Anirudha Sumant's lab (Argonne National Labratory). We worked together and made exciting discoveries. Thanks to Dr. Eric Bohannan and Dr. Nathan Leigh for their help with characterizations.

This work was supported by the National Science Foundation under Grant No. MoMS 1930881 and the U.S. Department of Energy, Office of Science, Office of Basic Energy Sciences, under Contract No. DE-AC02-06CH11357.

Last but not least, I would express my special gratitude to my parents for their love, caring and unlimited support.

TABLE OF CONTENTS

Page

LIST OF ILLUSTRATIONS

SECTION Page

PAPER II

PAPER III

PAPER IV

LIST OF TABLES

NOMENCLATURE

Symbol	Description
2D	Two-Dimensional
GC	Gas Chromatography
AFM	Atomic Force Microscopy
MoS_2	Molybdenum Disulfide
h-BN	Hexagonal Boron Nitride
DLC	Diamond-Like Carbon
HREELS	High-Resolution Electron Energy Loss Spectroscopy
MILD	Minimally Intensive Layer Delamination
ILs	Ionic Liquids
$EMIMBF_4$	1-Ethyl-3-Methylimidazolium Tetrafluoroborate
$BMIMPF_6$	1-butyl-3-methylimidazolium hexafluoro-phosphate
CDC	Carbide-Derived Carbon
TMAOH	Tetramethylammounium Hydroxide
NH_4HF_2	Ammonium Dihydrogen Fluoride
XRD	X-Ray Diffraction
SEM	Scanning Electron Microscopy
EDX	Energy Dispersive X-ray Spectroscopy
XPS	X-ray Photoelectron Spectroscopy
NMR	Nuclear Magnetic Resonance
TGA-MS	Thermogravimetric-Mass Spectrometry Analysis

DESs	Deep Eutectic Solvents
ChCl	Choline Chloride
MD	Molecular Dynamics
GO	Graphene Oxide
COF	Coefficient of Friction
CVD	Chemical Vapor Deposition
PMMA	Poly(methyl methacrylate)
TCD	Thermal Conductivity Detector
TEM	Transmission Electron Microscopy
ATR	Attenuated Total Reflection
FTIR	Fourier Transform Infrared Spectroscopy
DLS	Dynamic Light Scattering
RMS	Root Mean Square
RH	Relative Humidity
n	Integer
λ (in Bragg's Law)	Wavelength
d	d-Spacing
θ	Glancing Angle
M	Molarity
A	Absorbance
τ	Time Constant
R	Bond Length
I	Moment of Inertia

B	Rotational Constant
h	Plank Constant
c	Speed of Light
W_{adh}	Adhesion Energy
F_{adh}	Adhesion Force
λ (in the Maugis–Dugdale theory)	Effective Coefficient
R_{tip}	Radius
$R_{tip\text{-}RMS}$	RMS Value
R_{film}	RMS Value
Z_0	Equilibrium Separation
V	Ball Wear Volume
d	Diameter
r	Radius
S	Sliding Distance
W	Load
K_B	Ball Wear Rate

1. INTRODUCTION

Two-dimensional materials have raised significant interest due to their many outstanding properties. MXenes represent a new family of 2D early transition metal (M) carbides and nitrides, which were first synthesized in 2011 [1, 2]. They are produced by selective extraction of group A element atoms (typically Al) from bulk precursor MAX phases using fluorine-containing etchants. MXenes have a general formula $M_{n+1}X_nT_x$, where n=1-4, M represents an early transition metal, X is carbon or nitrogen, and T stands for surface terminations (-OH, -F and -O-), whose fractions in the formula are usually unknown (x) [3]. The combination of hydrophilicity with high electrical conductivity provided by MXenes is unique among 2D materials [2, 4]. Similar to their bulk counterparts (transition metal carbides), MXenes offer high monolayer elastic properties [5-7] and bending rigidity [8], making them potential nanofillers for reinforced composites, *etc.* Because of their 2D structure and many extraordinary physical properties, MXenes have raised a significant interest for various applications, such as optoelectronic devices [9, 10], triboelectric nanogenerators [11], supercapacitors [4, 12, 13], lithium ion batteries [14, 15], lithium-sulfur batteries [16], lasers [17], sensors [10, 18, 19], solid lubricants [20, 21], THz wave transmission and communication technology [9, 22], *etc*.

1.1. MXENE SYNTHESIS

Top-down methodes have been primarily used to synthesize MXenes. This section introduces the precursors and different synthesis methods of MXenes.

1.1.1. Precursors: MAX Phases. MAX phases are a group of layered ternary transition metal carbides and nitrides (space group $P6_3/mmc$), with a general formula of $M_{n+1}AX_n$, where M is an early transition metal (including Sc, Ti, V, Cr, Mn, Zr, Nb, Mo, Lu, Hf, or Ta), A is one of the group A elements (including Al, Si, P, S, Ga, Ge, As, Cd, In, Sn, Tl, or Pb), X represents C and/or N, and n = 1-4 [23]. Figure 1.1 highlights the elements in the Periodic Table that are known to form MAX phases. MAX phases advantageously combine properties of both ceramics and metals, such as good thermal stability, electrical conductivity and resistance to chemical attack [24].

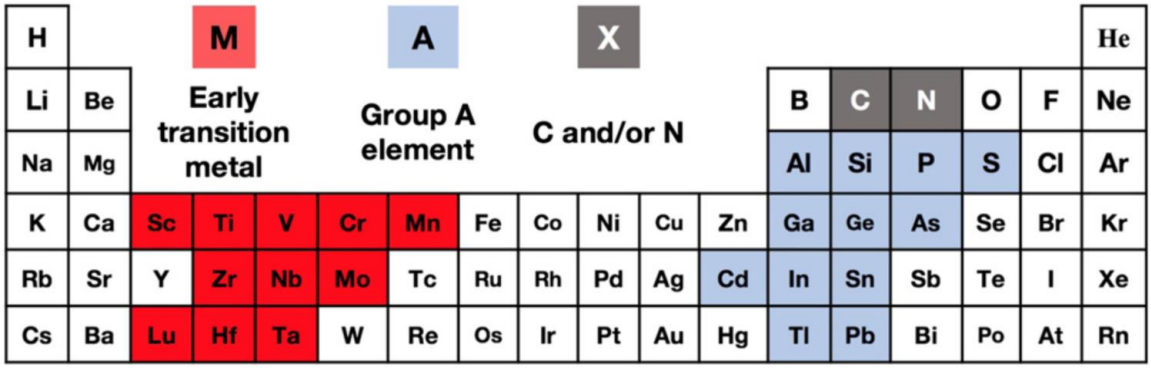

Figure 1.1. Elements in Periodic Table which can form MAX [25].

The chemical bonding within the MAX phase structure is mixed with varied contributions of metallic, ionic, and covalent bonds. M-X bonds are strong and largely covalent in character, similar to the bonds in binary MX compounds. However the M-A bonds are mostly metallic [25]. Unlike other layered bulk materials (e.g. graphite) with weak van der Waals interactions between the layers, MAX phases are held together by strong chemical bonds of different types, which explains why they could not be exfoliated

int MXenes *via* mechanical means so far [26, 27]. At the same time, differences in chemical reactivities of different bond types with the MAX structure have been explored to successfully exfoliate some of them. In particular, a weaker metallic M-A bonding and more reactive A element make it easier to selectively remove the A element layers from the MAX phase structures by etching with acids, yielding the corresponding MXenes [28].

1.1.2. Synthesis Methods. The As of 2021, over 20 different MXenes have been experimentally synthesized [23]. Top-down synthesis, whereupon the A layers are selectively etched from the MAX phase or non-MAX phase precursors (Figure 1.2), has become a general synthesis method for MXenes [29]. Variations of the etching technique allow to produce MXenes with different flake sizes [3], slight variations of surface chemistry (T_x) [30-32], and different interlayer spacing [33, 34].

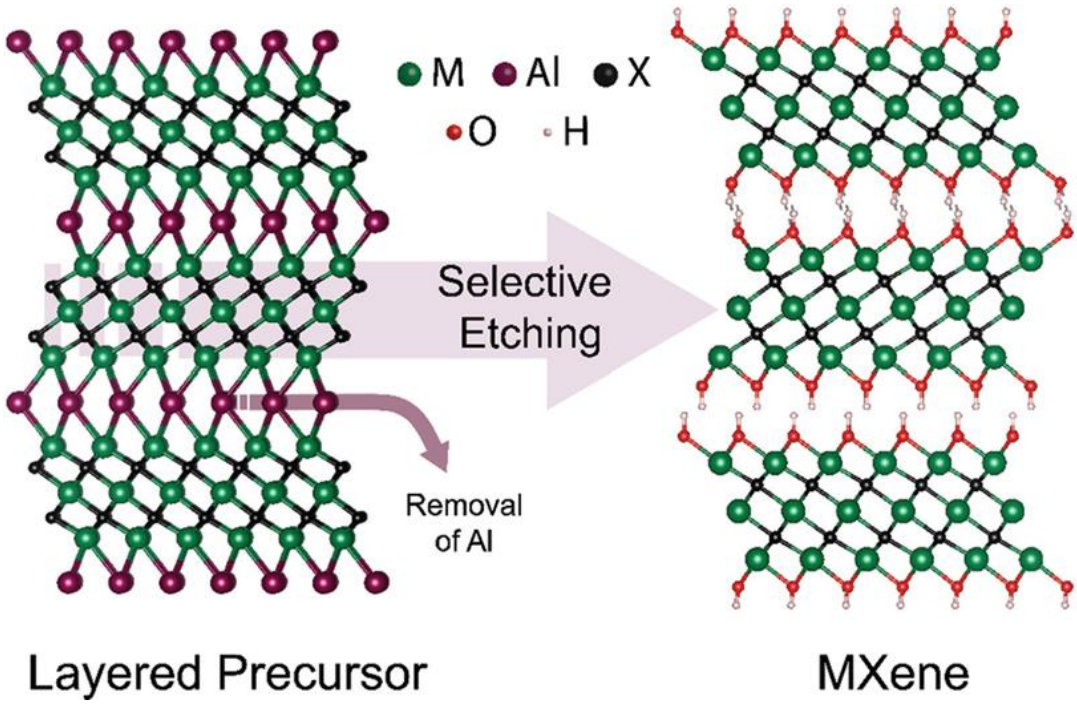

Figure 1.2. Selective etching of Al layer from as M_3AlC_2 MAX phase produces $M_3C_2T_x$ MXene [29].

1.1.2.1. Etching techniques using HF or in-situ formed HF. In 2011, the first discovered MXene Ti_3C_2 was synthesized at Drexel University by selective etching of Al layer out of the MAX phase Ti_3AlC_2 using concentrated HF (50%) [1]. The overall reaction equation can be written as:

$$Ti_3AlC_2 + 3HF = Ti_3C_2 + \frac{3}{2}H_2(gas) + AlF_3 \quad (1)$$

Since then, HF has been widely used as the etchant for synthesis of different MXenes [3, 15, 35-37]. The etching conditions (concentration of HF, etching temperature and etching time) must be adjusted for each MAX phase because of differences in chemical composition, types of bonding, number of atomic layers forming MX block, etc. After aqueous HF etching, the received MXene is always terminated with O, OH and F. Also, this method often leads to over etching, producing defected MXenes with relatively small flake sizes [3].

To avoid hazardous concentrated HF solutions, Ghidiu et al.[4] have discovered in 2014 an *in-situ* HF etching method, using 5 M LiF/6 M HCl as the etchant (Route 1, Figure 1.3), and producing Ti_3C_2 MXene clay. Although varying in the extent of the etching, other fluorides, such as NaF, KF, CsF, Ca_2F etc., also work in this method. In 2016, a minimally intensive layer delamination (MILD) etching method was proposed by adjusting the concentration of LiF and HCl to 7.5 M LiF/9 M HCl (Route 2, Figure 1.3) [38, 39]. In this method, MAX phase etching by *in-situ* formed HF is followed by delamination of multi-layered MXene into individual flakes by hand-shaking (Figure 1.3). The MILD method has become one of the most widely used ways to synthesize and delaminate MXenes.

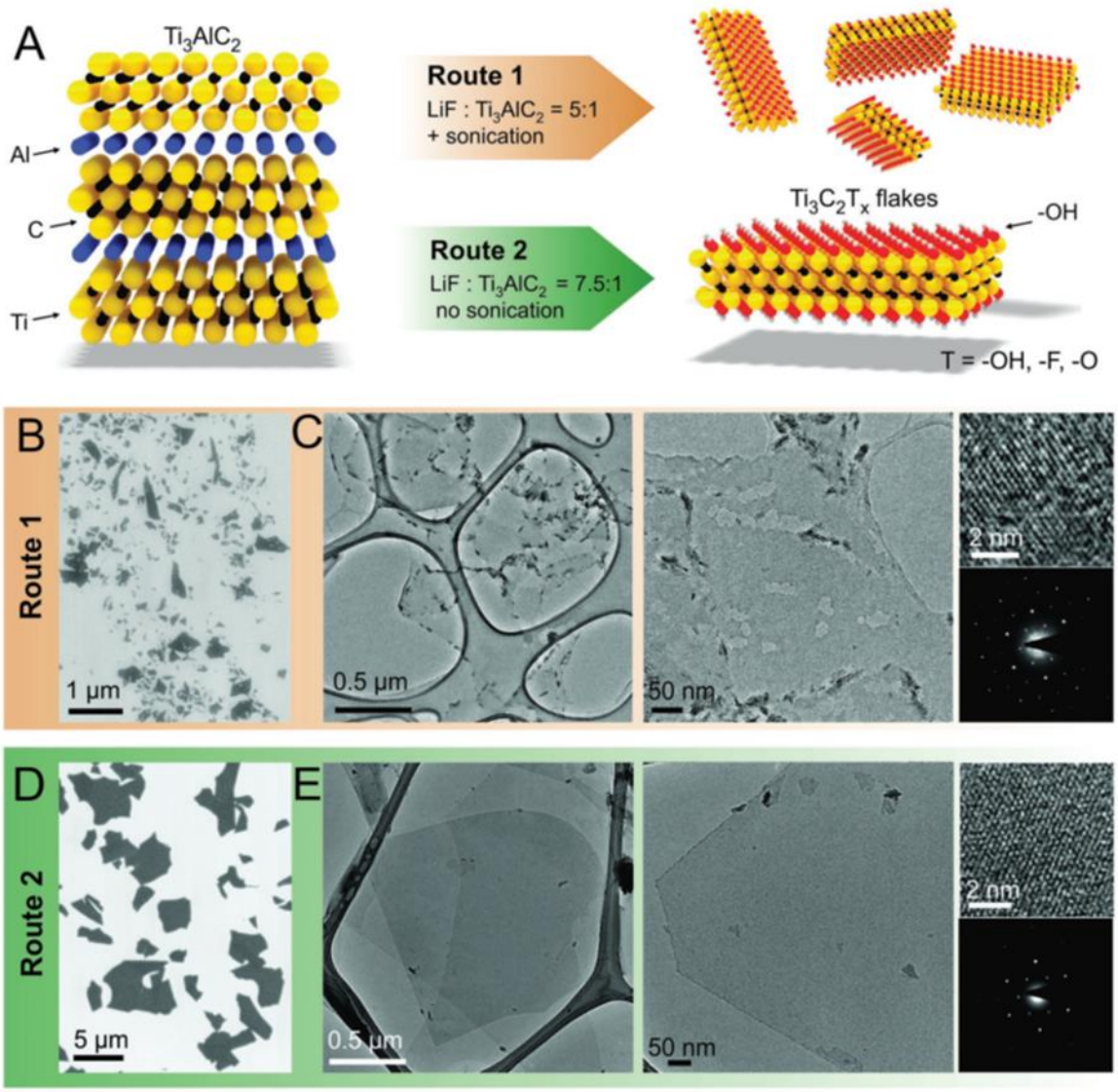

Figure 1.3. Synthesis routes and microscopy images of MXenes produced by the corresponding route [38]. Route 1 used 5 M LiF/6 M HCl and Route 2 used 7.5 M LiF/9 M HCl (MILD method).

1.1.2.2. Etching with fluorine-contained non-acid etchants. Fluorine containing ions must be applied in most of the MXene synthesis techniques because of fluorine's strong binding ability to aluminum [30]; however, it is possible to avoid harmful HF. By

using NH_4HF_2 [40], the Al layer of MAX phase Ti_3AlC_2 can be etched, thus forming $(NH_4)_3AlF_6$. The reaction is expressed as:

$$Ti_3AlC_2 + 3NH_4HF_2 = Ti_3C_2 + \frac{3}{2}H_2\,(gas) + (NH_4)_3AlF_6 \quad (2)$$

Interestingly, the MXene produced by this technique is intercalated with NH_3 and NH_4^+ which expand its interlayer spacing by 25%.

Most recently, in 2021, other studies established that ionic liquids (ILs) such as 1-ethyl-3-methylimidazolium tetrafluoroborate ($EMIMBF_4$) and 1-butyl-3-methylimidazolium hexafluoro-phosphate ($BMIMPF_6$) can act as both etchants and intercalants [41] in MXene synthesis. Hydrolysis of ILs in water formed small amounts of HF, which was responsible for the etching, but the morphology of the MXene produced by this technique is different from HF etched MXene, which has a cave-like structure.

1.1.2.3. Electrochemical etching techniques. Although replacement of hazardous HF by fluorine-contained chemicals is a major step forward, the latter are also harmful to the environment, and therefore, researchers continue to search for other etching techniques. Since the etching processes require electron transfer, electrochemical etching of MAX phases could potentially de-alloy A layer and produce MXenes. However, a previous study shows that electrochemical anodic etching of MAX phases (Ti_2AlC and Ti_3AlC_2) in dilute HCl and NaCl solutions led to formation of carbide-derived carbon (CDC) [42]. Although Sun et al. [43] demonstrated that fluorine-free Ti_2CT_x (T= Cl, O, OH) can be synthesized by electrochemical etching out of the Al layer from Ti_2AlC in dilute HCl, subsequent removal of Ti from MXene forming CDC on MXene surface was unavoidable. In 2018, Yang et al.[44] successfully used an electrochemical etching technique to synthesize Ti_3C_2 (> 90% yield) from Ti_3AlC_2 anode. The electrolyte was composed of 1 M NH_4Cl and 0.2

M tetramethylammounium hydroxide (TMAOH) creating a slightly basic environment (pH > 9). The resulting Ti_3C_2 MXene was fluorine-free and was terminated with O and OH. The reaction of etching out of Al layer was proposed as:

$$Ti_3AlC_2 - 3e^- + 3Cl^- = Ti_3C_2 + AlCl_3 \quad (3)$$

1.1.2.4. Fluorine-free etching techniques. Surface chemistry of as-synthesized MXene largely depends on the etchants and environment during the MAX phases etching processes. Thus, etching with fluorine-contained etchants will yield F-terminated MXene, a type of terminations that are not desirable when using MXene as an electrode material for supercapacitors [44, 45]. Since Al is amphoteric, it is theoretically feasible to etch Al layers using alkali (like NaOH) at ambient environments, but the formation of insoluble aluminum hydroxides or oxide hydroxides hinders the etching process, resulting in an incomplete etching. By treating a MAX phase (Ti_3AlC_2) in concentrated (27.5 M) NaOH in hydrothermal conditions (270 ^oC), Li et al.[30] discovered that $Al(OH)_3$ and AlO(OH), formed in the etching reaction with alkali, can be converted into soluble $Al(OH)_4^-$ exposing the inside Al layers for further reaction. According to the authors, the resulting MXene Ti_3C_2 was free of fluorine and terminated with O and OH. Organic bases, such as tetramethylammonium hydroxide (TMAOH) can also potentially etch Al. Thus, in another work, Xuan et al. [34] applied TAMOH as the etchant, forming $Al(OH)_4^-$ while etching out the Al layer. The MXene sheets produced in this way have $Al(OH)_4^-$ on their surface.

1.1.2.5. Water-free etching techniques. . Most of the MXene synthesis methods reported in literature use water as the main solvent [3]. However, MXenes are unstable in water and will spontaneously transform into corresponding metal oxides over time [46]. Also, MXenes are widely researched as reinforcement particles for polymers, where the

presence of water may interfere with *in situ* polymerization reactions and be otherwise undesirable. Moreover, the traces of intercalated water in MXene layers can have negative impact on Li-ion or Na-ion batteries, which require anhydrous organic electrolytes with no traces of water. Organic solvent etching in a glove box provides a water-free environment while also suppressing MXene degradation [46, 47]. Therefore, Natu et al.[32] reported an etching method using organic polar solvents (e.g. propylene carbonate, acetonitrile, dioxane, N,N-dimethylformamide, dimethyl sulfoxide and N-methyl-2-pyrrolidone) in the presence of ammonium dihydrogen fluoride (NH_4HF_2), to synthesize $Ti_3C_2T_z$ MXene. In this method, HF formed *in-situ* by dissociation of NH_4HF_2 in an organic solvent, is deemed to be the main etchant, playing a role similar to HF in aqueous etchants. $Ti_3C_2T_z$ MXene synthesized in organic solvents is ~70% F terminated, which is the highest content of F terminations reported for MXenes. More recently in 2021, Ti_3C_2 was also produced by halogen etching (with Br_2, I_2, ICl, IBr) of Ti_3AlC_2 MAX phase in cyclohexane, resulting in halogenated Ti_3C_2 [48].

1.1.2.6. Molten salt etching techniques. The wet chemical etching techniques reviewed in the previous sections are widely used for producing carbide or carbonitride MXenes, however, the yield of nitride MXenes in wet etching techniques is low [49]. This may be because nitride MXenes are less stable than their carbide cousins [50], resulting in overetching of MX blocks during removal of A layers. The cohesive energies of nitride MXenes are lower than those of carbide MXenes, while the formation energies are higher [51]. In 2016, the molten salt method was investigated to synthesize $Ti_4N_3T_x$ MXene from Ti_4AlN_3 [50]. The salt etchant (59 wt% of potassium fluoride, 29 wt% of lithium fluoride, and 12 wt% of sodium fluoride) was mixed with Ti_4AlN_3 MAX phase and heated to the

eutectic temperature of 550 ^{o}C for the synthesis under argon flow. The resulting mixture was washed with sulfuric acid and Ti_4C_3 MXene was further delaminated with TBAOH using sonication.

In another study, Li et al.[52] proposed a Lewis acid etching technique to etch various MAX phases (A = Al, Zn, Si and Ga) producing the corresponding MXenes. Using Ti_3SiC_2 as an example, the MAX phase was mixed with $CuCl_2$, NaCl, and KCl in a 1:3:2:2 ratio. The mixture was then heated to 750 ^{o}C under argon flow for 24 h yielding Ti_3C_2/Cu composite. The proposed etching mechanism is:

$$Ti_3SiC_2 + 2CuCl_2 = Ti_3C_2 + SiCl_4\,(gas) + 2Cu \quad (4)$$

Similar to the mechanism of HF etching, Cu^{2+} in molten $CuCl_2$ acts as H^+, while Cl^- acts as F^- in HF. The residual Cu was washed out by ammonium persulfate and the resulting Ti_3C_2 MXene was terminated with O and Cl. Based on that work, researchers have later extended the molten salt technique to $CdCl_2$ and $CdBr_2$, producing Ti_2C and Ti_3C_2 MXenes with Cl and Br terminations, respectively [53].

1.1.2.7. Etching from other A element MAX phases. Various methods were developed for etching Al containing MAX phases producing MXenes but not the MAX phases containing other A elements. This may be because the redox potential of Al in MAX phases is the most negative among all other A elements (A = Si, Ga, Ge, etc.) [54]. In 2015, the first non-Al containing MXene precursor Mo_2Ga_2C (not a MAX phase) was etched by concentrated HF (50%) [55]. Although the corresponding multilayer Mo_2C MXene was produces from this non-MAX precursor, the etching was incomplete. Later, Halim et al.[56] have improved the etching conditions using concentrated HF (14 M) and by increasing the temperature and prolonging the etching time. This was followed by a

TBAOH treatment to produce, for the first time, monolayer Mo_2C. Synthesis of less defective Mo_2C flakes by the MILD method has been reported in the same work.

Compared with Ti_3AlC_2, Ti_3SiC_2 is a more abundant and cheaper precursor for Ti_3C_2 MXene synthesis. However, because of the stronger Ti-Si bonds [25], conventional HF etching method failed to etch this MAX phase. HF is known as an agent that dissolves SiO_2, therefore Alhabeb et al.[54] proposed to oxidize Si first before etching it out of the Si based MAX phase, resulting in an HF/oxidizer etching process (where oxidizer is H_2O_2, $(NH_4)_2S_2O_8$, $KMnO_4$ or $FeCl_3$), which yielded the Ti_3C_2 MXene.

1.2. CHARACTERIZATION OF MXENES

MXene structure and surface physical and chemical properties can be characterized using multiple techniques. This section discusses primarily used characterization techniques used for MXene study.

1.2.1. X-Ray Diffraction (XRD). XRD is one of the simplest and most common ways to confirm successful synthesis of MXene because of clear differences between the XRD patterns of the original MAX phase and the corresponding MXene [1, 35]. When the MAX phase is partially etched, all peaks from the MAX phase remain, along with an extra downshifted peak of (002) reflections (Figure 1.4). When a pure MXene is produced, all the peaks that represent MAX phase disappear, and only the downshifted (002) peak along with higher order (00*l*) peaks that represent MXene can be seen (Figure 1.4). Because of the $P6_3/mmc$ space group of MAX phase, one unit cell of MXene has two MXene layers, resulting in the c-lattice parameter 2 times that of d-spacing as shown in Figure 1.5.

In addition to confirming the presence of MXenes, XRD is used for measuring the interlayer spacing of MXenes. Tailoring the interlayer space by adjusting the functional groups on MXene surface or by intercalation between MXene layers is important for some applications, such as energy storage [33, 57], ion rejection [58], water treatment [59] etc.

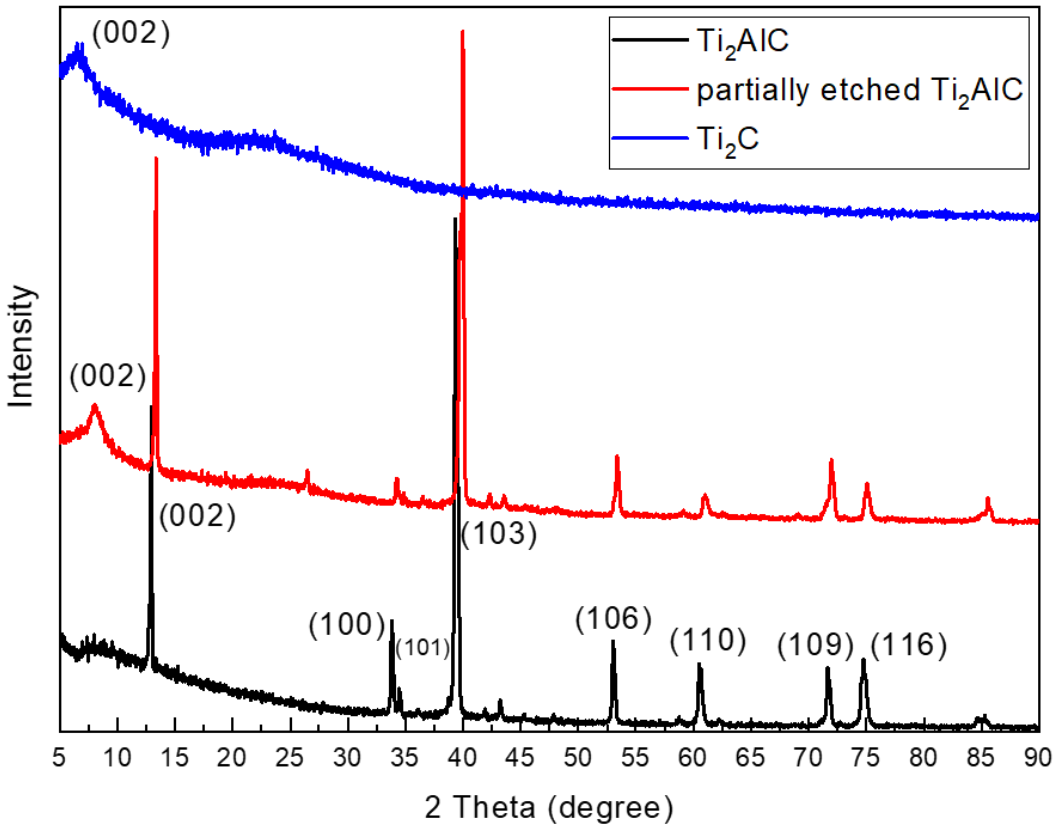

Figure 1.4. XRD patterns of MAX phase Ti_2AlC, partially etched Ti_2AlC, and Ti_2C MXene.

The d-spacing of MXene can be calculated from XRD data using Bragg's law:

$$n\lambda = 2dsin\theta \tag{5}$$

where n is a positive integer, λ is the wavelength of the incident wave, d is the d-spacing shown in Figure 1.5, and θ is the glancing angle, which can be obtained from the peak

position for (002) plane. Heating removes the intercalants like water or other molecules, thus reducing the d-spacing (Figure 1.6), whereas introduction of various intercalants (e.g. ions, molecules) increases the d-spacing [33, 57].

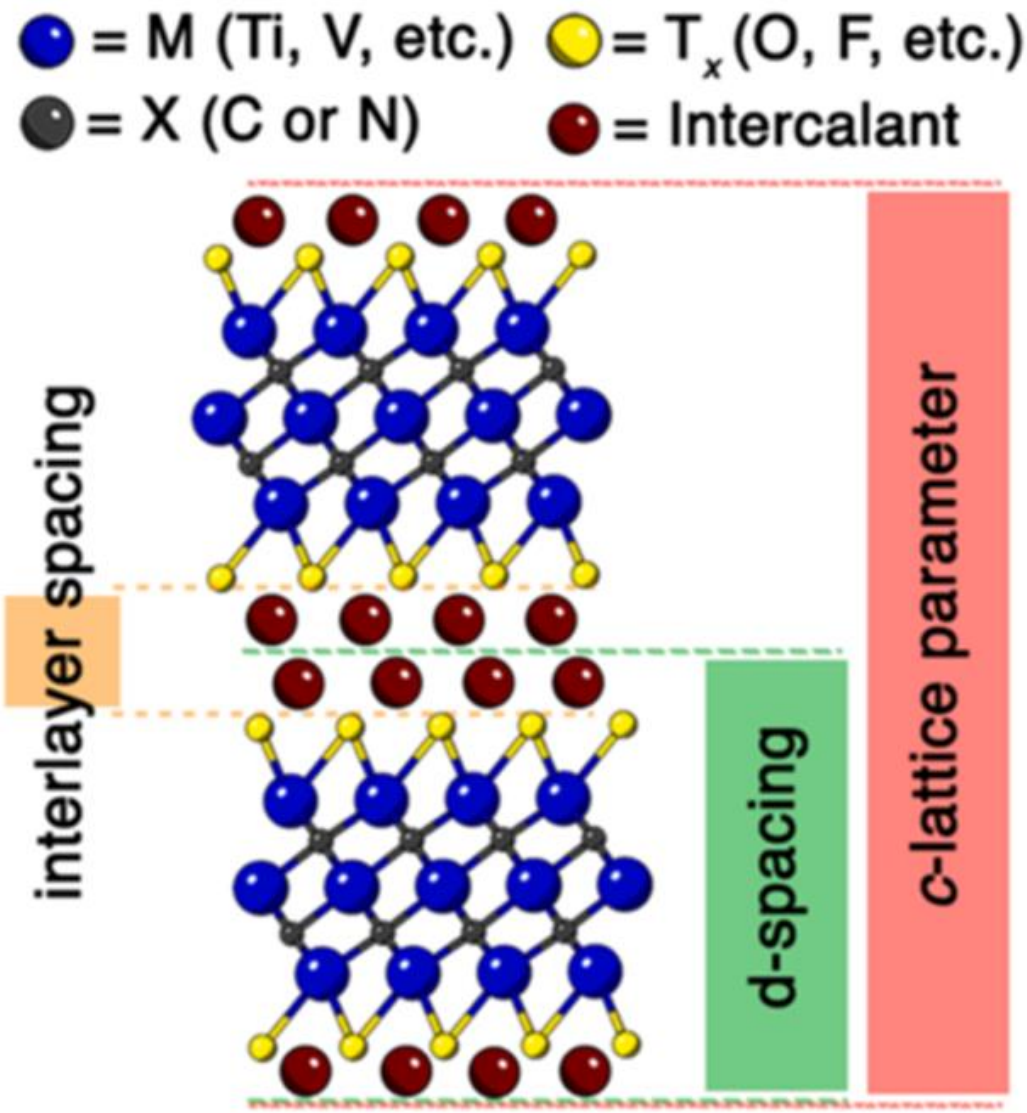

Figure 1.5. The difference among interlayer spacing, d-spacing, and c-lattice parameter for a $M_3X_2T_x$ MXene with intercalants [60].

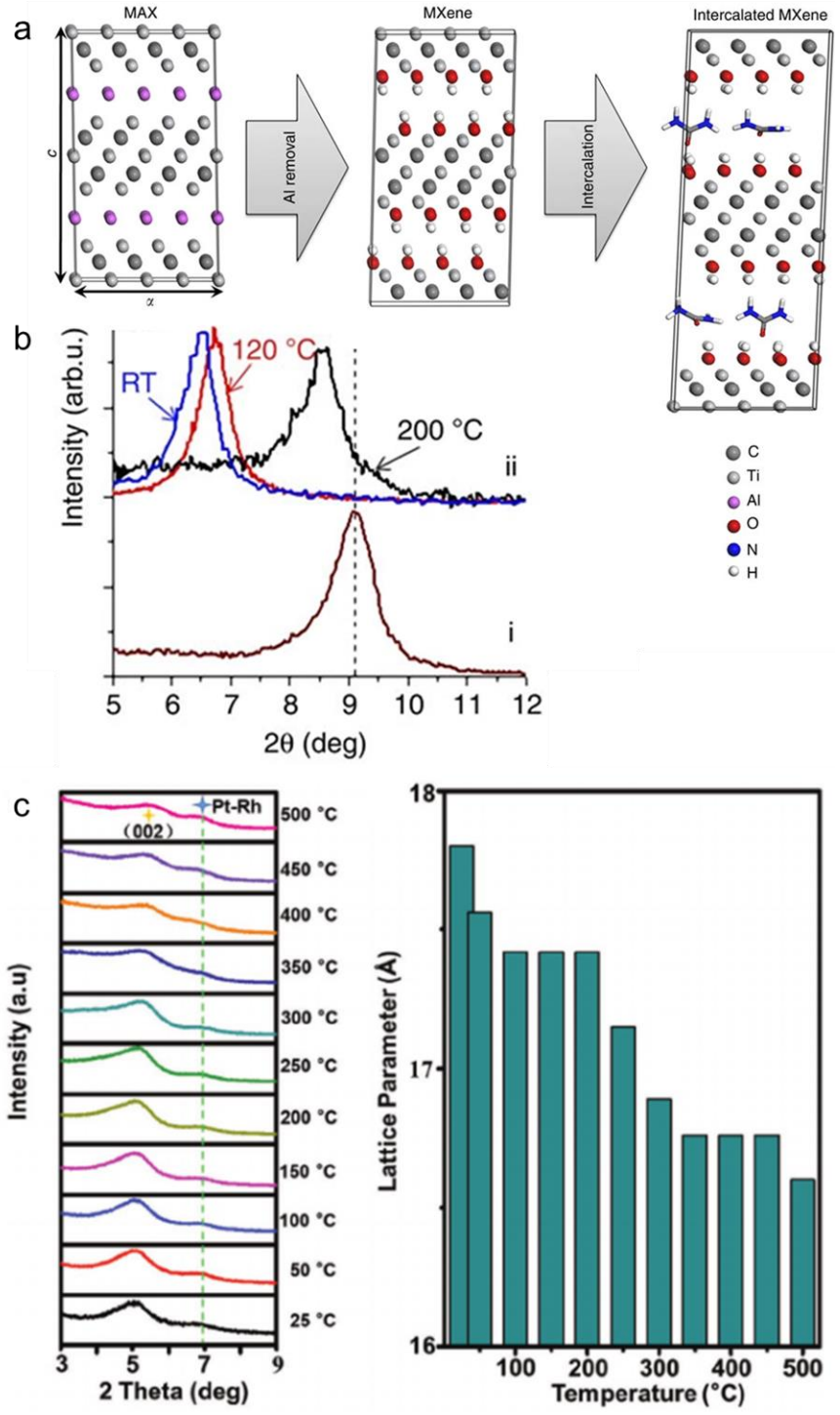

Figure 1.6. (a) Schematics of synthesis and intercalation of MXene. (b) XRD patterns of (i) as received MXene, (ii) after intercalation with hydrazine at room temperature and de-intercalation at elevated temperatures [57] (c) XRD patterns of a $Nb_4C_3T_x$ MXene film at different temperatures in vacuum and c-lattice parameters calculated from XRD data at different temperatures [33].

1.2.2. Raman Spectroscopy. XRD is a powerful structure analysis technique for multilayer MXenes, it is less informative when it comes to characterization of monolayer MXenes. Raman spectroscopy probes interaction between light and chemical bonds within the material, and it is, therefore, applicable to monolayer or few layer flakes, powders, films, as well as liquids and gases. Requiring minimal sample preparation, Raman spectroscopy can be used to investigate chemical structure of MXenes and their degradation products in solid, liquid or gas phases [61-64]. In 2020, Sarycheva et al. [64] reported detailed characterization of chemical structure, surface chemistry, and stacking of $Ti_3C_2T_x$ using Raman, as shown in Figure 1.7a. The deconvoluted MXene spectrum has 3 regions, including the flake region, surface group region, and the carbon region. This study showed that excitation with different wavelengths produces different Raman spectra. For example, Ti_3C_2 has a plasmon resonance at ~800 nm [63], so there were several peaks selectively enhanced when the Raman spectrum was acquired under 785 nm laser (Figure 1.7b). The type of etchant used for MXene synthesis can also be inferred from the Raman spectra of MXene because different etchants produce different relative densities of functional groups on the MXene surface (Figure 1.7c) [63].

1.2.3. Microscopy. Scanning electron microscopy (SEM) provides an opportunity to investigate the morphology of MXenes. Compared with bulk MAX phase, multilayered MXene particles have a characteristic “accordion-like” appearance after HF etching (Figure 1.8a, b). However, this multilayer structure with large gaps should not be used as a decisive proof of MXene presence in the sample. The well-separated gaps are formed when a vigorous reaction with concentrated HF results in a rapid formation of H_2 gas that expands the structure. The etching reactions with less concentrated HF are less vigorous

and the structure of the resulting multilayer MXene is tighter. Energy dispersive X-ray spectroscopy (EDX) is usually conducted as complementary technique along with SEM to confirm successful MXene synthesis.

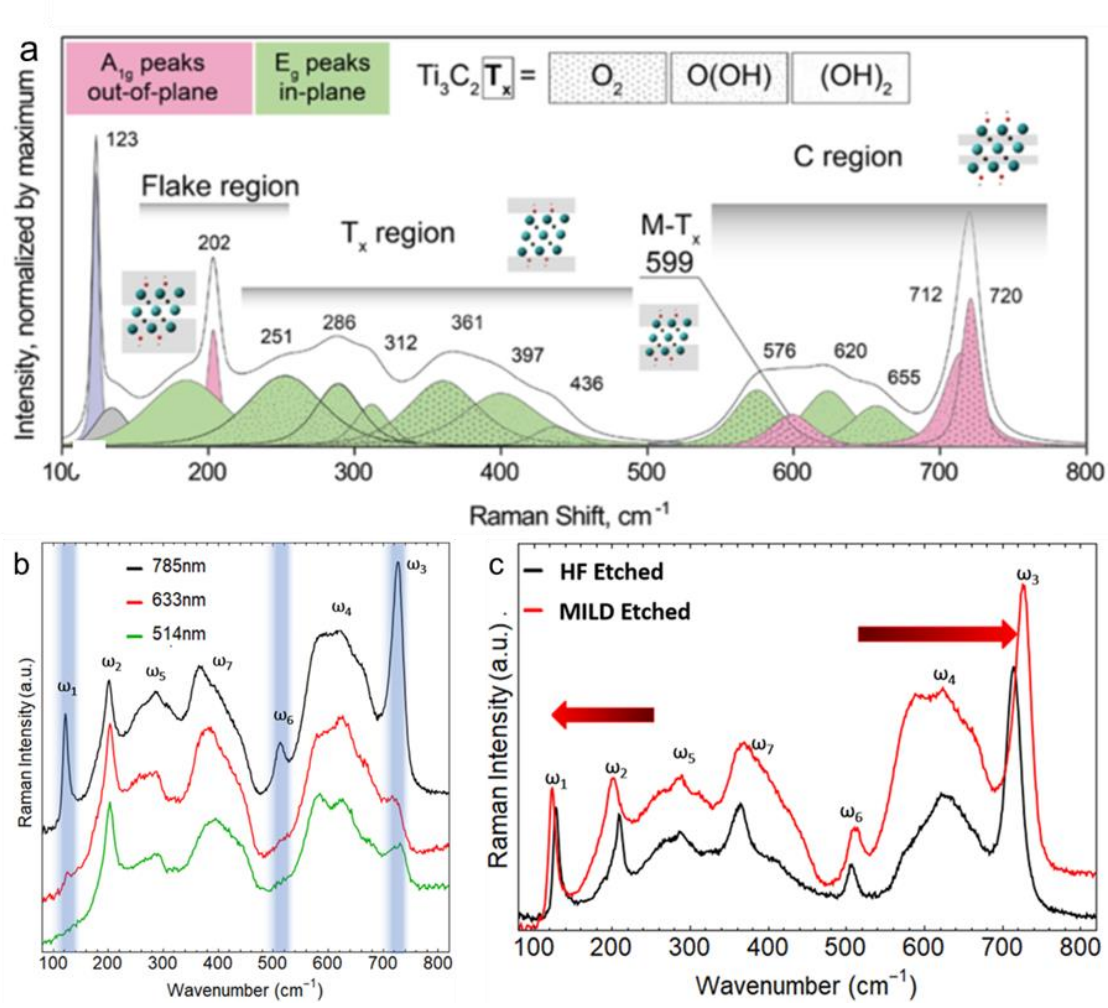

Figure 1.7. (a) Deconvoluted Raman spectrum of $Ti_3C_2T_x$ synthesized using HF-HCl as the etchant excited with 785 nm laser [64]. Raman spectra of the MXene flakes (b) measured by different excitation wavelengths, (c) synthesized from different etchants [63].

After delamination of multilayered MXene, the images of monolayer or few-layered flakes can be acquired using SEM and transmission electron microscopy (TEM).

Moreover, MXene crystalline structure can also be confirmed from selected area electron diffraction (SAED) patterns in TEM. MXene has hexagonal structure and therefore, indexing of SAED pattern can be done with:

$$\frac{1}{\mathrm{d}^2} = \frac{4}{3}\frac{h^2+hk+k^2}{a^2} + \frac{l^2}{c^2} \quad (6)$$

where d is the d-spacing, which can be measured from the image, h, k, and l are the Miller indices of the lattice planes, a and c are lattice parameters.

Atomic force microscopy (AFM) is used to measure flake size and thickness of MXenes [38, 65, 66]. According to Lipatov et al. [5], the height measured from the MXene layer directly attached to the substrate may not be accurate because the trapped water molecules may contribute to the thickness. Thus, this technique has limitations in determining the monolayer thickness of MXenes in some cases. However, this is still a powerful method to investigate mechanical properties of MXenes on the microscale [5, 65-68].

1.2.4. UV-Vis-NIR Spectroscopy. Vivid colors of colloidal solutions is another feature of MXenes. The color of the MXene colloidal solution or film is characteristic for each MXene, also depending on its state (solid film or colloidal solution). For example, Ti_3C_2 solution shows a greenish color, while the Ti_3C_2 film yields a purpleish color. Different MXenes absorb light of different energies, which corresponds to their plasmon resonance (Figure 1.9) [60, 69]. UV-Vis-NIR spectroscopy is a simple technique to confirm the presence of a particular MXene in solution or in thin film state. The plasmonic peaks of MXenes vary because of their different chemical composition (M and X elements) or different number of atomic layers in a monolayer.

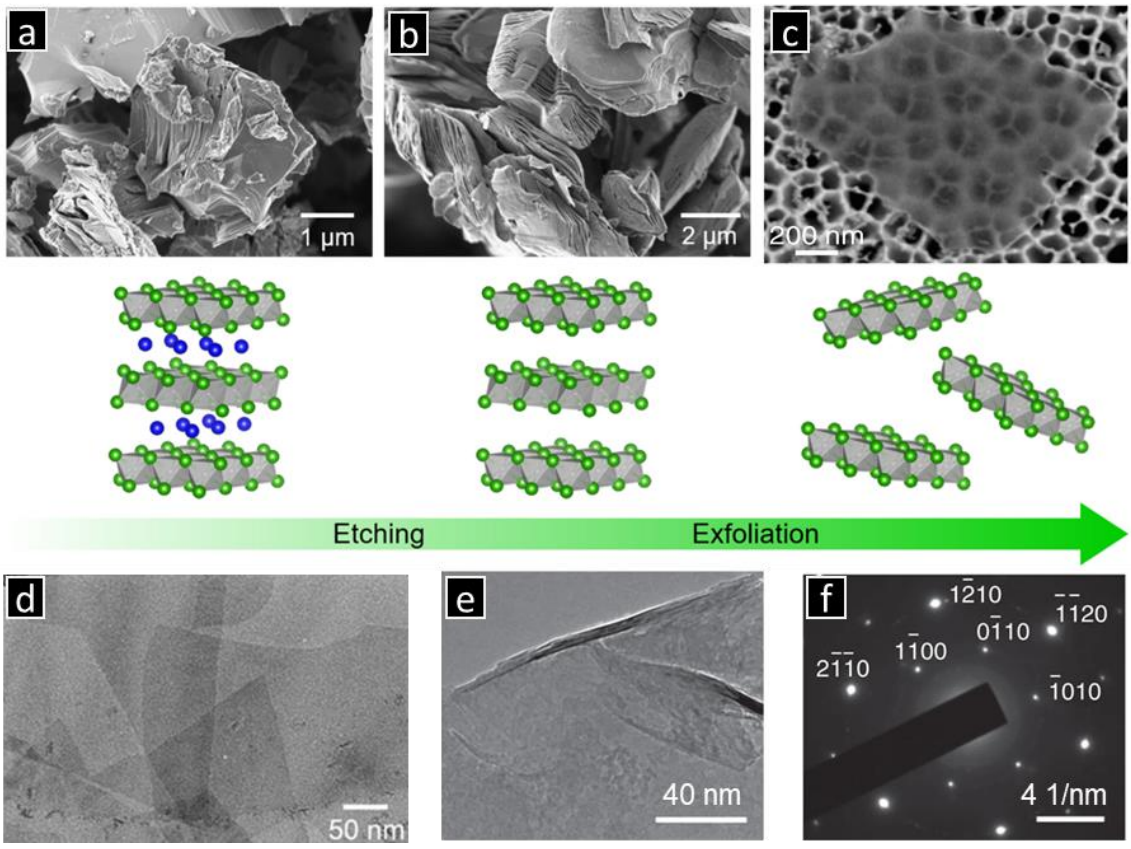

Figure 1.8. SEM characterizations of MXene synthesis at each step: (a) MAX phase Ti_3AlC_2, (b) Ti_3C_2 after etching of the Al layer and (c) delaminated Ti_3C_2 MXene single layers. (d, e) TEM images of Ti_3C_2 MXene flakes and (f) SAED pattern of Ti_3C_2 [57, 70, 71].

1.2.1. Other Characterization Techniques. Many other complementary techniques are used for MXene characterization, such as X-ray photoelectron spectroscopy (XPS), nuclear magnetic resonance (NMR), thermogravimetric-mass spectrometry analysis (TGA-MS) etc. XPS is mostly used to characterize chemical composition, extent of degradation, and surface chemistry of MXene [72-74]. NMR can analyze the functional groups on MXene surfaces produced using different etchants or the surface chemistry of different MXenes [31, 75-78]. TGA-MS allows to investigate the thermostability and the

surface chemistry (e.g. functional groups like O and F) and intercalants, such as water, HF, TBA^+ of MXenes based on analysis of gaseous products produced by heating [79, 80].

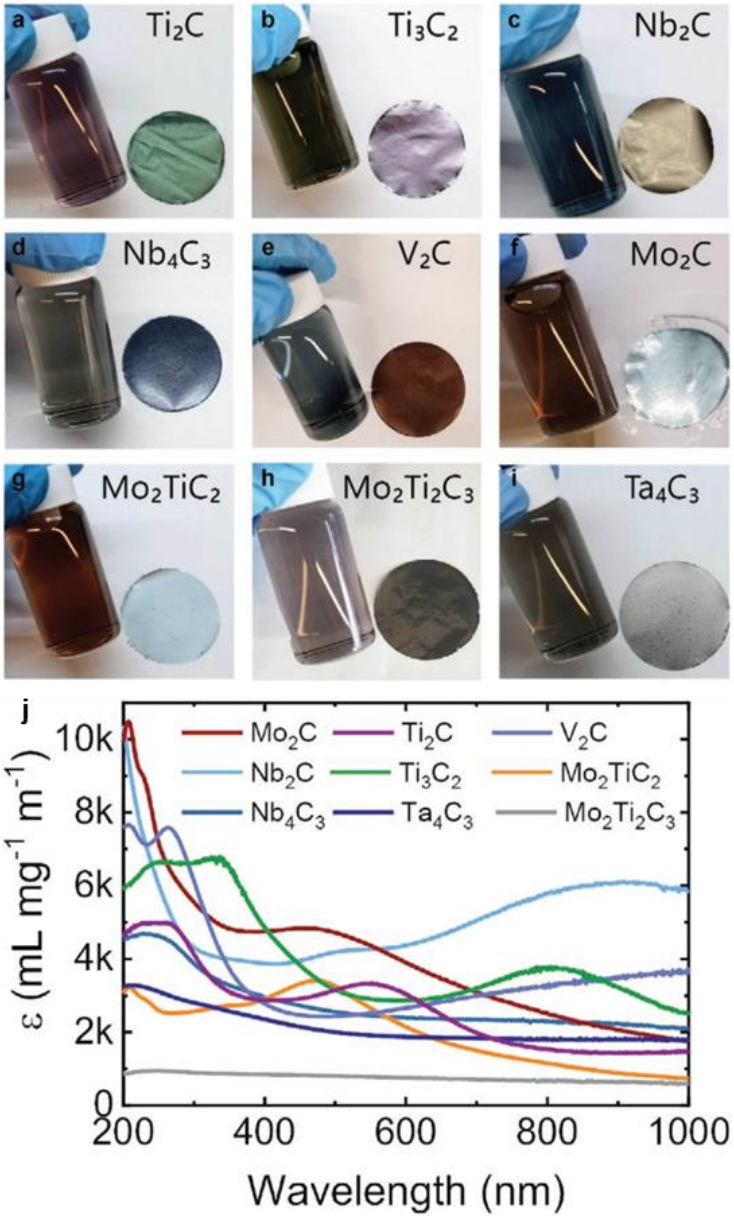

Figure 1.9. Visual color of MXene colloidal solutions and films for (a-i) Ti_2C, Ti_3C_2, Nb_2C, Nb_4C_3, V_2C, Mo_2C, Mo_2TiC_2, $Mo_2Ti_2C_3$, and Ta_4C_3, respectively. Including (j) UV-Vis-NIR extinction spectra of different MXenes [69].

1.3. CHEMISTRY OF MXENES

Because of the great potential and many applications of MXenes, understanding the chemistry of MXenes is of importance. This section discusses the chemistry, especially chemical stabilities of MXenes.

1.3.1. Surface Chemistry and Chemical Modification of MXenes. To a large extent, the surface chemistry of MXenes is controlled by the etchants or etching environments [3, 32, 41, 44, 81], regardless of the type of M, X elements or the number of atomic layers in MXene structure [82]. Many efforts have been made to investigate the surface chemistry of MXenes. Among them, XPS is the most widely used technique [72]. Combining the XPS and EDS is and efficient way to demonstrate the type of functional groups and their proportions. However, when it comes to quantitative resolving of -O- and -OH contributions, this tequnique is often non-conclusive. Solid state NMR was used as a powerful tool to solve this problem [31]. For different etchants, more -F terminations (relative to -O- and -OH) are formed when using HF as the etchant, while more -O-terminations can be found when using LiF/HCl etchant (Figure 1.10). Kobayashi et al. [77] have further devised the -OH terminations into external Ti-OH and interlayer Ti-OH, and confined water presence in MXenes using solid state NMR. Seredych et al. [79] have demonstrated that TGA-MS could be used to investigate the surface terminations as well as the intercalants of MXenes synthesized by different etchants. Literature results show that HF concentration affects the ratio of F to O on MXene surface. Also, a higher concentration of HF results in more intercalated water trapped between MXene layers.

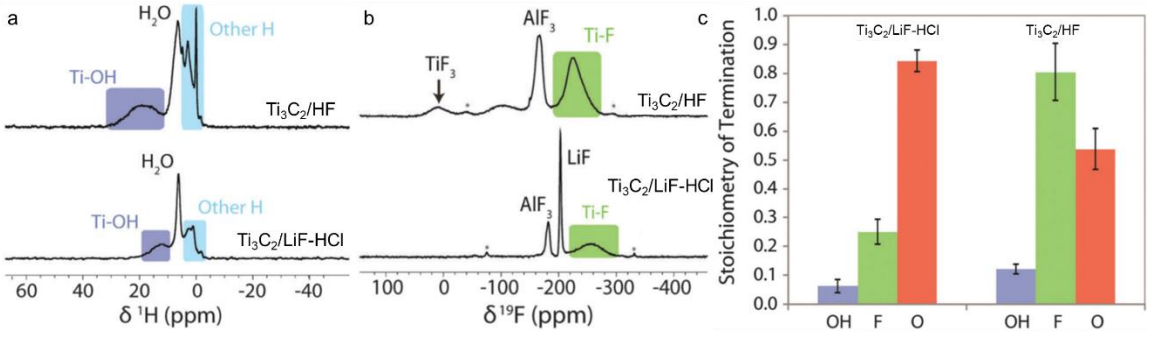

Figure 1.10. (a) ^{1}H NMR spectra, (b) ^{19}F NMR spectra, and (c) surface functional group compositions of Ti_3C_2 MXenes synthesized by using HF and LiF/HCl etchants [31].

Surface chemistry of MXenes has many effects on their performance. One of the efficient methods of improving the electronic conductivity of MXene is to remove the surface terminations. Vacuum annealing was demonstrated to partially remove the functional groups on MXene surface, resulting in an increased conductivity [80]. Besides, Kamysbayev et al. [53] synthesized different MXenes (Ti, Mo, Nb, and V) with none, O, S, Cl, Br, Se, Te or NH surface terminations using Lewis acidic molten salt method (Figure 1.11), which can be beneficial for various applications. Surface functionalizations also affect the interlayer distance, allowing tailoring of MXenes for energy storage performance. For example, Chen et al.[83] functionalized $Ti_3C_2T_x$ MXene with glycine which increased the d-spacing by 1.19 Å, resulting in a better rate and cycling performance. A comparative performance of $Ti_3C_2T_x$ MXenes prepared with different etchants (HF, HF/HCl, and HF/H_2SO_4) in Na-ion storage has also been studied, and results show that the MXene synthesized with HF/H_2SO_4 has a better electrochemical performance because of the cleaner surface and less structural water [81]. Very recently, Pazniak et al. [84] demonstrated low-energy ion implantation as a new route to modify Ti_3C_2 MXene surface by introducing Mn^{+} ions. This modification not only introduced manganese ions on the

MXene surface, but also produced defective structure, resulting in an increasing amount of O on MXene, in order to modify its electronic properties.

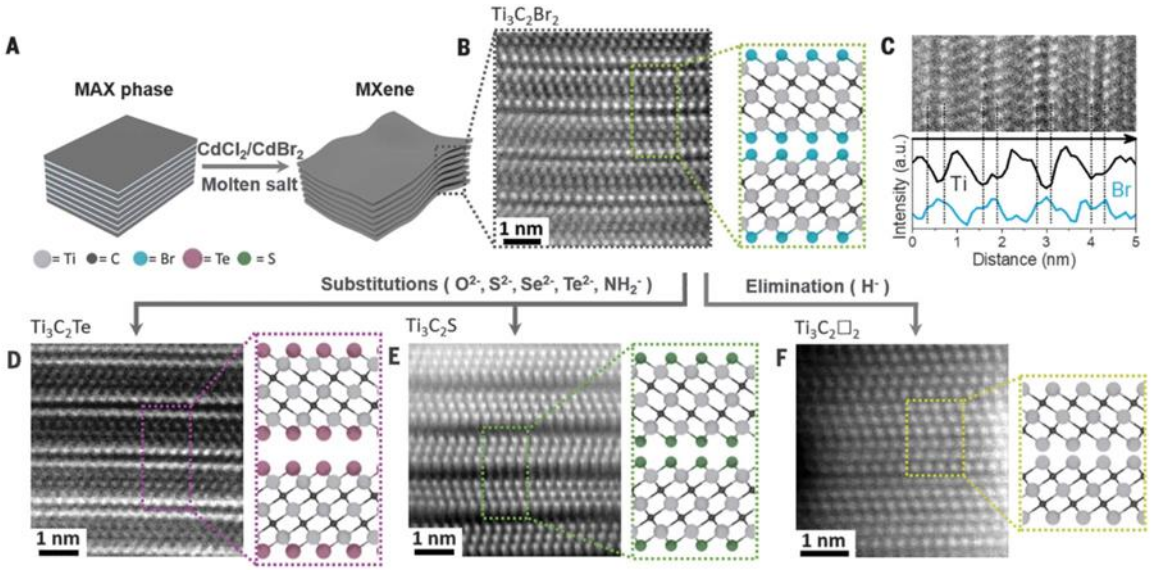

Figure 1.11. Schematics for MXene synthesis using molten salts and atomic resolution high-angle annular dark-field (HAADF) images of $Ti_3C_2Br_2$, Ti_3C_2Te, Ti_3C_2S, and $Ti_3C_2\square_2$ MXenes.

1.3.2. Stability and Reactivity of MXenes. MXenes raised significant interest for various applications but were found to spontaneously transform into the corresponding transition metal oxides [47, 62, 85]. Until recently, the commonly accepted opinion was that the transformation of the titanium containing MXenes into titania observed in their aqueous colloidal solutions is mainly due to MXene oxidation (reaction with oxygen). Lipatov et al. reported that when a colloidal solution of delaminated $Ti_3C_2T_x$ in water was exposed to air at room temperature, MXene flakes were completely oxidized within several days [38]. Although previous studies from Gogotsi's group mentioned that MXene sheets in aqueous solutions may slowly react and transform into titanium hydroxide [47, 85], the

main oxidizer in this process was thought to be dissolved oxygen, while the role of water was reduced to merely a solvent. Not surprisingly, attempts to protect MXenes against oxidation were reported, particularly in aqueous solutions [86-88]. Zhang et al. proposed that refrigeration and de-aerated environment substantially improve shelf life of $Ti_3C_2T_x$ and Ti_2CT_x MXenes in aqueous colloidal solutions (Figure 1.12a) [62]. Zhao et al. also demonstrated that sodium L-ascorbate, used as antioxidant, can effectively protect MXenes from oxidation (Figure 1.12c) [87]. It is well known that the degradation of MXenes starts from the edges and defects of MXene flakes [89]. Thus, Natu et al. discovered that supposedly positively charged edges of MXene flakes could be capped using polyanions: polyphosphates, polysilicates and polyborates, thus suppressing the degradation of MXenes (Figure 1.12b) [86]. Tailoring surface chemistry of MXenes is another approach to prevent oxidation. Etching out Al layers from Ti_3AlC_2 with TMAOH resulted in $Al(OH)_4^-$ terminated Ti_3C_2 MXene [88]. Because of the shielding and passivating effects on MXene surface, the $Al(OH)_4^-$ terminated MXenes survived longer time in water with strong oxidizer (H_2O_2) added than the MXenes with -OH and -F terminated synthesized using HF.

In 2019 we have demonstrated hydrolysis as one of the main factors in MXene degradation in aqueous colloids [46, 61]. Due to hydrolysis, merely preventing oxidation of MXenes is not enough to avoid their degradation. Low temperature slows down many reactions, *e.g.*, hydrolysis and oxidation reactions. Simply freezing of MXene solutions at low temperatures (below -20 ^oC) was an efficient way to reduce the degradation [90, 91]. However, this method cannot completely solve the problem. Very recently, in 2021, Kim et al. discovered deep eutectic solvents (DESs) as efficient agents to suppress MXene

degradation (Figure 1.13) [92]. The DES, consisting of choline chloride (ChCl) and urea, can be hydrated in water forming DES-water clusters. The DES used in this study attached to MXene surface *via* hydrogen bonding thus passivating it and hindering access of oxygen and water to MXene, resulting in suppression of its degradation.

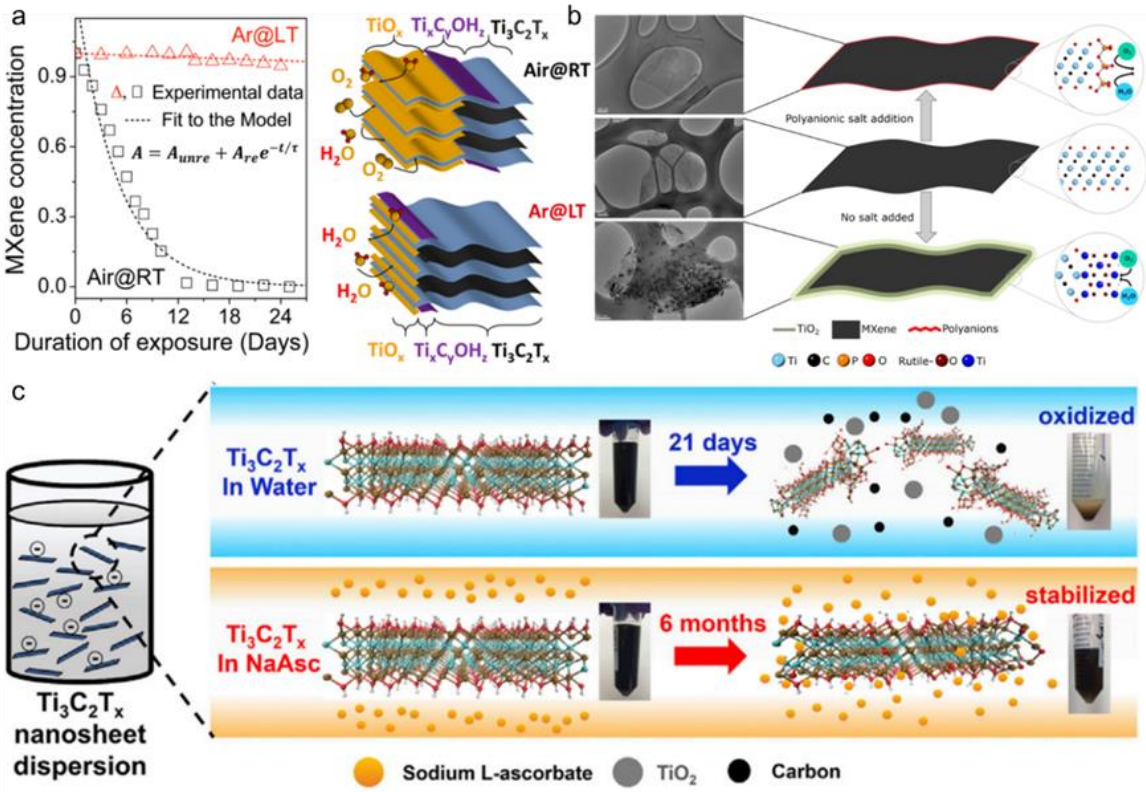

Figure 1.12. (a) Degradation kinetics and schematics of Ti_3C_2 MXene in Ar atmosphere at low temperature (5 ^oC, LT) and Air atmosphere at room temperature [62]. (b) Schematic of Ti_3C_2 MXene flakes with and without protection by polyanions [86]. (c) TEM and schematics of degradation of Ti_3C_2 MXene in water and sodium L-ascorbate solution [87].

While all the methods reviewed above are applied after receiving MXenes, another way to suppress their reactivity and stabilize MXenes in colloids originates from the idea that less defective MXenes must be also less reactive. Along these lines, Mathis et al.

demonstrated that the modified synthesis method (changing the composition of TiC:Ti:Al = 2:1:1 from molar ratio to mass ratio) produced a less defective MAX phase because of excess of Al, resulting in less defective MXene sheets (Figure 1.14) [93]. According to this report, the produced MXene can be stored for years in ambient environment, which certainly is a breakthrough.

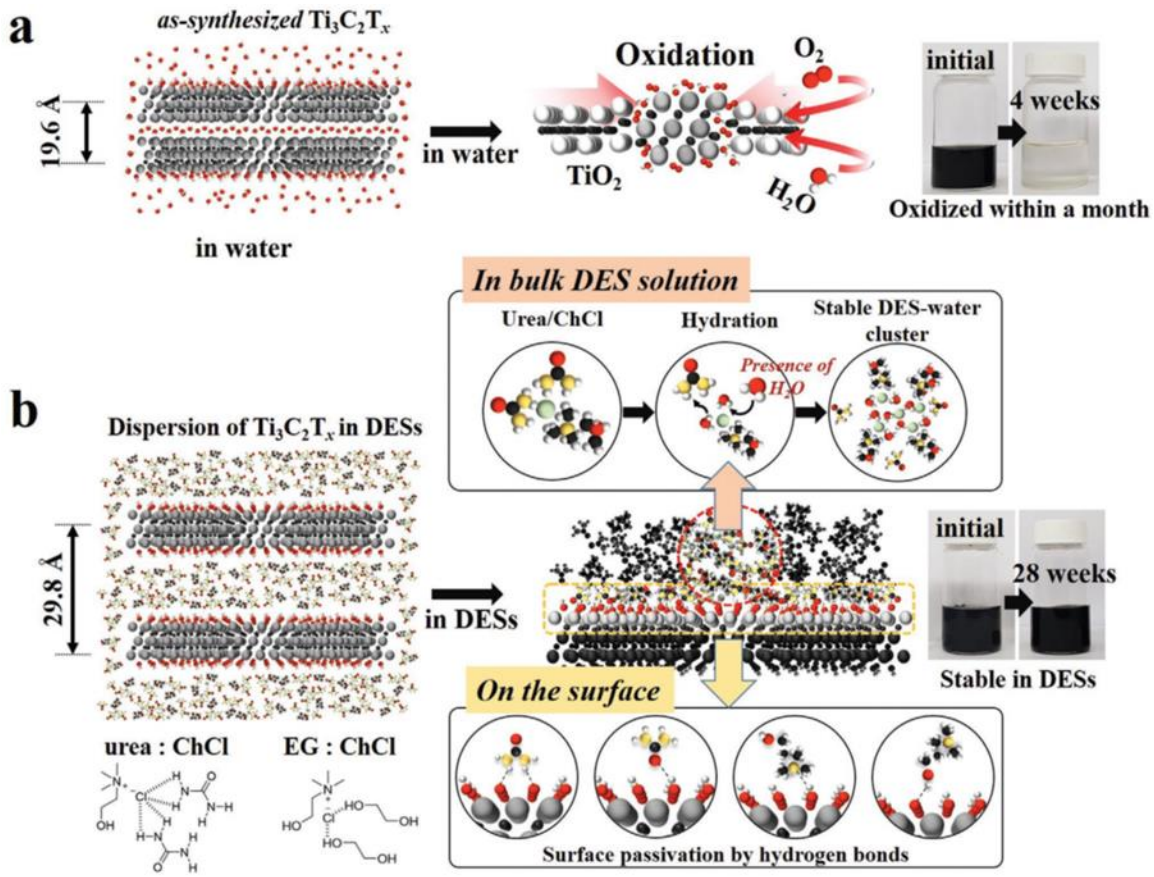

Figure 1.13. Schematics of (a) bare Ti_3C_2 MXene and (b) Ti_3C_2 in DES solution [92].

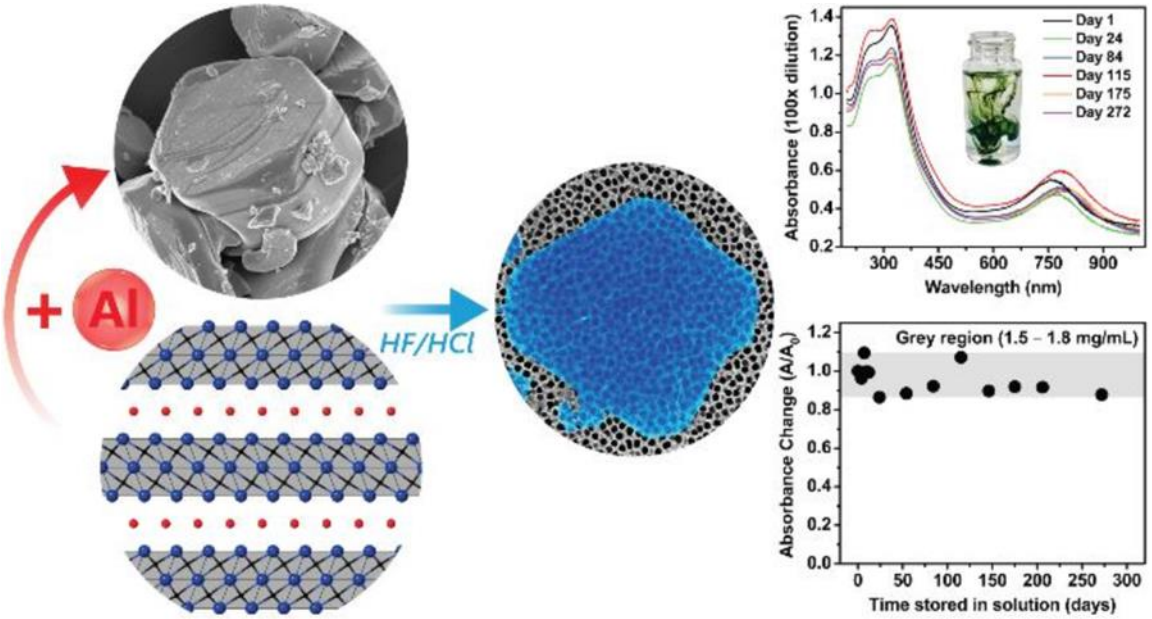

Figure 1.14. Schematic illustration of MAX phase produced with excess of Al in the initial mix and of subsequent MXene synthesis, leading to a more stable Ti_3C_2 MXene colloid [93].

PAPER

I. HYDROLYSIS OF 2D TRANSITION METAL CARBIDES (MXENES) IN COLLOIDAL SOLUTIONS

Shuohan Huang[†] and Vadym N. Mochalin[*,†,‡]
[†]Department of Chemistry, Missouri University of Science & Technology, Rolla, Missouri 65409, United States
[‡]Department of Materials Science & Engineering, Missouri University of Science & Technology, Rolla, Missouri 65409, United States
*Correspondence to: mochalinv@mst.edu

ABSTRACT

Although oxidation was deemed as the main factor responsible for the instability of MXenes in aqueous colloids, here we put forward and test a hypothesis about the central role of water as the primary factor. We show that water and related processes of MXene hydrolysis play the main role in the phenomena leading to complete transformations of 2D titanium carbide MXenes into titania in aqueous environments. To demonstrate the role of water, the stability of two MXenes, $Ti_3C_2T_x$ and Ti_2CT_x, has been systematically studied in aqueous and nonaqueous colloids exposed to oxygen and inert gas atmospheres. The calculated time constant for degradation of $Ti_3C_2T_x$ dispersed in anhydrous iso-propanol saturated with pure oxygen exceeds 5 years, in striking contrast to the same MXene dispersed in water, where more than a half of it would transform into titania even in an oxygen-less atmosphere over ~41 days. A thinner Ti_2CT_x MXene showed similar behavior, albeit with shorter time constants in both solvents, correspondingly. UV−vis and Raman spectroscopy were used to analyze the oxidation kinetics and composition of fresh and aged

MXenes. An intense anatase peak was observed in MXenes stored in aqueous solutions under Ar atmosphere, while no signs of oxidation could be found in iso-propanol solutions of the MXenes stored under O_2 atmosphere over a similar period of time.

1. INTRODUCTION

MXenes represent a relatively new and quickly growing family of two-dimensional (2D) early transition-metal (M) carbides and nitrides, which were first synthesized in 2011 from bulk layered crystalline $M_{n+1}AX_n$ (n = 1, 2, 3) phases, where A represents group IIIA or IVA elements and X could be C, N, or both [1]. By etching off the A element, 2D transition-metal carbides/nitrides (MXenes) with a general formula $M_{n+1}X_nT_x$ (n = 1, 2, 3) are obtained, where T stands for the surface terminations −OH, −F, and −O− that render MXenes hydrophilic (x is their fractions) [2, 3] The combination of hydrophilicity with high electrical conductivity provided by MXenes is unique among 2D materials, having earned them a nickname “conductive clays” [2, 4]. Similar to their bulk counterparts (transition-metal carbides), MXenes offer high monolayer elastic properties [5−7] and bending rigidity [8], making them potential nanofillers for reinforced composites and more. Because of their 2D structure and many extraordinary physical properties, MXenes have raised a significant interest for various applications, such as optoelectronic devices [9, 10], triboelectric nanogenerators [11], supercapacitors [4, 12, 13], lithium ion batteries [14, 15], lithium−sulfur batteries [16], sensors [17−19], etc. However, it has been found that in some cases MXene flakes are not stable and can be spontaneously oxidized on a time scale from hours to days [20−22], a process which may limit their usage or, if understood and

harnessed, lead to novel materials and applications, for example in photosensors [19]. Since most of the applications of MXenes rely upon single- or few-layer flakes obtained from colloidal solutions rather than dry powders, it is important to explore the reactivity, in particular oxidation and hydrolysis, of MXenes in colloidal solutions and understand the underlying processes.

So far, some attempts have been made to investigate the oxidation stability of titanium-based MXenes [23−25]. The current commonly accepted opinion is that the transformation of the MXenes into titania observed in their aqueous colloidal solutions is mainly due to oxidation (reaction with oxygen). Lipatov et al. reported that when a colloidal solution of delaminated $Ti_3C_2T_x$ in water was exposed to air, MXene flakes were completely oxidized within several days [26]. Zhang et al. concluded that refrigeration and deaerated environment substantially improve the shelf life of $Ti_3C_2T_x$ and Ti_2CT_x MXenes in aqueous colloidal solutions [21]. Although previous studies from Gogotsi's group have mentioned that MXene sheets in aqueous solutions may slowly react and transform into titanium hydroxide [20,22], the main oxidizer in this process was thought to be dissolved oxygen, while the role of water has been reduced to merely a solvent.

Reactivity of carbides toward water ranges in wide limits. Some carbides such as methides (Be2C, Al4C3) and acetylides (CaC2, MgC2) are known to vigorously react with water to produce large volumes of CH4 or C2H2, respectively. In contrast, bulk interstitial (e.g., TiC) and covalent (e.g., SiC) carbides are known as "not hydrolyzed" [27] and resistant to attack by water [28]. On the other hand, many years ago Avgustinik et al. studied slow and seemingly insignificant reactions of bulk TiC with water yielding small quantities of hydrocarbons and titania [29]. They mentioned that the hydrolysis of TiC is

limited by the very surface, propagating no more than 10−15 nm into the carbide crystal structure. However, this length covers the entire thickness of both $Ti_3C_2T_x$ and Ti_2CT_x MXene monolayers, which are 0.82 and 0.57 nm, respectively, as estimated from their DFT optimized models (Figure 1). More recently, using high-resolution electron energy loss spectroscopy (HREELS) [30, 31], Merrill et al. and Didziulis et al. have found that bulk titanium carbide is capable of dissociating water molecules. Reactions of MXenes with water were never studied in detail; however, it is obvious now that chemical reactivity of MXenes toward water should not be underestimated and deserves more detailed investigations.

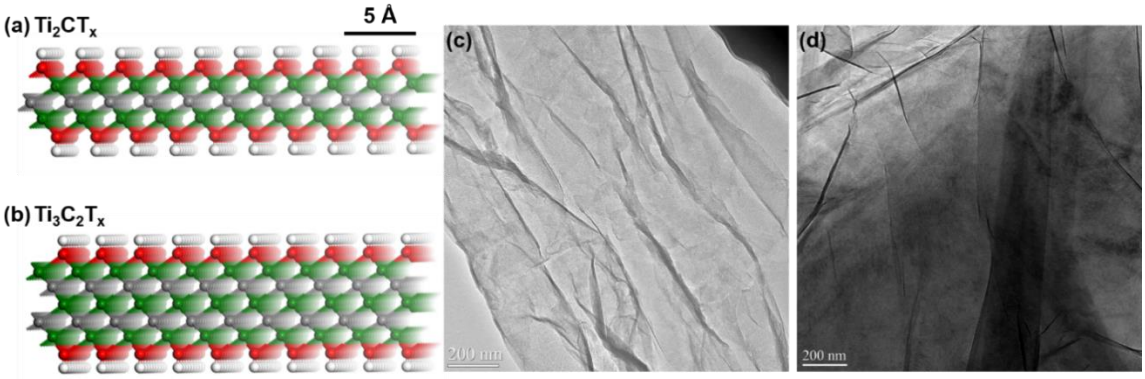

Figure 1. Atomic structures of (a) Ti_2CT_x, (b) $Ti_3C_2T_x$ MXenes and TEM images of (c) Ti_2CT_x, (d) $Ti_3C_2T_x$ MXenes.

Here, we analyze the role of water as the primary reagent, not only as a solvent, in the processes of conversion of 2D titanium carbide MXenes into titania. As we show below, this analysis leads to important conclusions about the oxidation stability of MXenes and the choice of solvent for long-term storage of MXene sheets in the colloidal state. Based on our analysis, the presence of water, even under inert atmosphere, is detrimental

for long-term MXene stability. These conclusions will also have important implications for fundamental chemistry of 2D carbides and the development of many applications of MXenes.$Ti_3C_2T_x$ and Ti_2CT_x 2D transitionmetal carbides were chosen as representative MXenes for this study. They were produced using similar techniques, have the same elemental composition and bonding, and differ only in the thickness of the monolayer (Figure 1). The opportunity to study chemical properties as a function of monolayer thickness within the same elemental composition and bonding provided by MXenes is another unique advantage rendering them particularly well suited among 2D materials for fundamental studies of the thickness effect on different properties, including reactivity.

2. EXPERIMENTAL SECTION

2.1. SYNTHESIS OF MAX PHASES

Ti_3AlC_2 was synthesized by known techniques [19,32]. Briefly, a mix of titanium (−325 mesh, 99%, Alfa Aesar), aluminum (−325 mesh, 99.5%, Alfa Aesar), and graphite (−325 mesh, 99%, Alfa Aesar) powders in a 3:1.1:1.88 molar ratio (7.0000, 1.4462, and 1.1001 g, respectively) were ball-milled for 8 h at 100 rpm using zirconia milling cylinders in a polyethylene jar. The mixture then was transferred into an alumina boat, placed in an alumina tube furnace (GSL-1800X-KS60-UL, MTI Corporation), and purged with Ar at RT for 1 h, followed by heating at 10 °C/min to 1550 °C and holding at this temperature for 2 h under argon flow. After that, the system was cooled to room temperature at 10 °C/min in Ar flow. Ti_2AlC was synthesized by ball-milling of titanium carbide (typically 2-μm size powder, 99.5%, Alfa Aesar), titanium (−325 mesh, 99%, Alfa Aesar), and

aluminum (−325 mesh, 99.5%, Alfa Aesar) powders in a 0.85:1.15:1.05 molar ratio (5.0896, 5.5047, and 2.8330 g, respectively) for 8 h (100 rpm) using zirconia milling cylinders in a polyethylene jar.33 The mixture was then transferred into an alumina boat, placed in an alumina tube furnace (GSL-1800XKS60-UL, MTI Corporation), purged with Ar at RT for 1 h, and then heated at 10 °C/min to 1400 °C and held at this temperature for 4 h in Ar flow. After that, the sample was cooled to room temperature at 10 °C/min in Ar flow. The resulting samples of MAX phase ceramics, shown in Figure S1 in the Supporting Information, were manually crushed by mortar and pestle.

2.2. PREPARATION OF MXENE COLLOIDAL SOLUTIONS

$Ti_3C_2T_x$ was synthesized using the MILD method [26,34]. The fresh etchant was prepared by dissolving 0.3 g of LiF in 6 mL of 6 M HCl in a 50 mL plastic centrifuge tube. Then, 0.3 g of Ti_3AlC_2 (−325 mesh, particle size ≤ 45 μm) was added to the etchant gradually.34 The etching lasted for 24 h at room temperature (∼23 °C). After that, the etched powder was washed with fresh deaerated water prepared by purging boiling deionized water with Ar for 30 min and then cooling it to room temperature while continuing Ar purging. The MXene washing steps were performed several times until the pH of the supernatant reached ∼6. After that, the $Ti_3C_2T_x$ aqueous colloidal solution was obtained via 5 min of hand-shaking followed by 1 h of centrifugation at 3500 rpm to precipitate and separate the excess of MXene. $Ti_3C_2T_x$ colloidal solution in anhydrous iso-propanol was obtained by centrifugation and washing of $Ti_3C_2T_x$ aqueous solution 4 times with an excess of fresh anhydrous iso-propanol (99.5+%, anhydrous, Alfa Aesar) to remove water from the system. Then, 1 h bath sonication was applied to disperse $Ti_3C_2T_x$ flakes in

iso-propanol. Finally, $Ti_3C_2T_x$ iso-propanol solution was centrifuged at 4500 rpm for 1 h to separate the excess of MXene. Colloidal solutions of Ti_2CT_x in deaerated water and anhydrous iso-propanol were obtained using the same methods except that the MAX phase in this case was Ti_2AlC (−325 mesh, particle size ≤ 45 μm). The resulting MXene monolayers were imaged by transmission electron microscopy (TEM) as shown in Figure 1. All MXene solutions were stored in closed drawers between measurements to reduce a possible effect of light on MXene decomposition.

3. CHARACTERIZATION

UV−vis spectra of MXene colloidal solutions were recorded in a glass cuvette (1 cm optical path length) in the wavelength range of 400−900 nm using a fiber optics QE Pro UV−vis spectrometer (Ocean Optics).

Raman spectra were obtained using a Horiba Jobin Yvon LabRAM Aramis m-Raman spectrometer with a 633 nm He− Ne laser. All Raman spectra were collected with a 10× objective and 1200 lines/mm grating. At least three different spots on each sample were examined by Raman analysis to ensure representability of the spectra.

TEM images of MXene thin films were acquired on an FEI Tecnai F20 transmission electron microscope with an accelerating voltage of 200 kV. The samples for TEM were prepared by depositing MXene thin films on 2000 mesh copper TEM grids.

The crystal structures of Ti_3AlC_2 and Ti_2AlC MAX phases were characterized using X-ray diffraction (XRD, PANalytical, Phillips MPD) with Cu Kα radiation (λ = 1.5406 Å) at U = 45 kV and I = 40 mA (Figure S2).

4. RESULTS AND DISCUSSION

4.1. Ti_2CT_x MXENE

The as-prepared Ti_2CT_x MXene colloidal solutions in deaerated water (referred to as "water" hereafter) and iso-propanol were of approximately same concentrations (~0.55 mg/mL), as confirmed by UV−vis transmittance spectra (Figure 2). The transmittance at 505 nm was used as the analytical signal proportional to the concentrarion of Ti_2CT_x MXene colloidal solutions. Freshly prepared Ti_2CT_x MXene colloidal solutions were purged with O_2 or Ar and sealed in 20 mL glass vials labeled as Ti_2CT_x−water/O_2, Ti_2CT_x−water/Ar, Ti_2CT_x−iso-propanol/O_2, and Ti_2CT_x− iso-propanol/Ar (Table 1). Figure 3 shows changes in the visual appearance of the samples over time at room temperature.

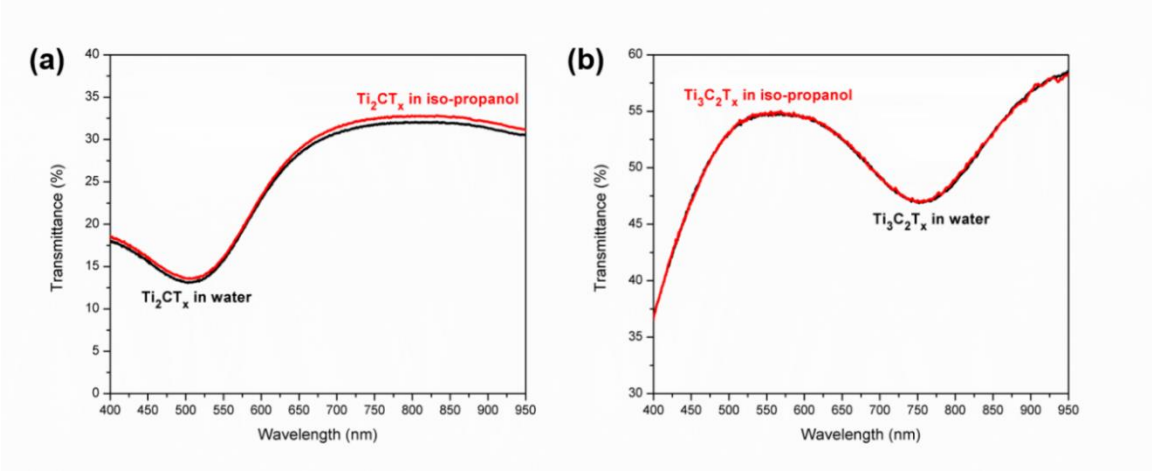

Figure 2. UV-Vis transmittance spectra of freshly made: (a) Ti_2CT_x water colloidal solution and Ti_2CT_x iso-propanol colloidal solution at same MXene concentrations (~0.55 mg/mL), (b) $Ti_3C_2T_x$ water colloidal solution and $Ti_3C_2T_x$ iso-propanol colloidal solution at same MXene concentrations (~0.04 mg/mL).

According to the photographs, Ti_2CT_x completely degrades in a water/O_2 environment within 12 to 24 h. Although the change of gas atmosphere from O_2 to Ar slows the degradation, Ti_2CT_x in water/Ar does not survive beyond 1 day. However, the color of the Ti_2CT_x−iso-propanol colloidal solution was visually unchanged even after 3 days in either O_2 or Ar atmosphere.

Table 1. Description of Ti_2CT_x and $Ti_3C_2T_x$ Colloidal Solution Samples Used in This Study.

Sample Name	**Description**
Ti_2CT_x-water/O_2	Ti_2CT_x in dearated DI water saturated with O_2 and sealed under O_2 atmosphere
Ti_2CT_x-water/Ar	Ti_2CT_x in dearated DI water saturated with Ar and sealed under Ar atmosphere
Ti_2CT_x-iso-propanol/O_2	Ti_2CT_x in anhydrous iso-propanol saturated with O_2 and sealed under O_2 atmosphere
Ti_2CT_x-iso-propanol/Ar	Ti_2CT_x in anhydrous iso-propanol saturated with Ar and sealed under Ar atmosphere
$Ti_3C_2T_x$-water/O_2	$Ti_3C_2T_x$ in dearated DI water saturated with O_2 and sealed under O_2 atmosphere
$Ti_3C_2T_x$-water/Ar	$Ti_3C_2T_x$ in dearated DI water saturated with Ar and sealed under Ar atmosphere
$Ti_3C_2T_x$-iso-propanol/O_2	$Ti_3C_2T_x$ in anhydrous iso-propanol saturated with O_2 and sealed under O_2 atmosphere
$Ti_3C_2T_x$-iso-propanol/Ar	$Ti_3C_2T_x$ in anhydrous iso-propanol saturated with Ar and sealed under Ar atmosphere

In order to quantify MXene transformation processes, UV−vis transmittance spectra of Ti_2CT_x in different environments were recorded over time (Figure 4). A broad plasmon resonance band of Ti_2CT_x MXene nanosheets with a measured maximum at 505 nm disappears after 3 days for both Ti_2CT_x−water/O_2 and Ti_2CTx−water/Ar, while in an iso-propanol/O_2 environment, it can be detected even after 15 days, suggesting that it is water, not oxygen, that plays the most important role in the degradation of Ti_2CT_x MXene nanosheets. The kinetics of Ti_2CT_x MXene degradation in different environments is shown in Figure 5. The exponential decay fit

$$A = A_{Initial}\, e^{-t/\tau} \quad (1)$$

was applied, similar to published studies [21, 35, 36], where Ainitial is proportional to the amount of the initial MXene nanosheets in solution and τ is the time constant.

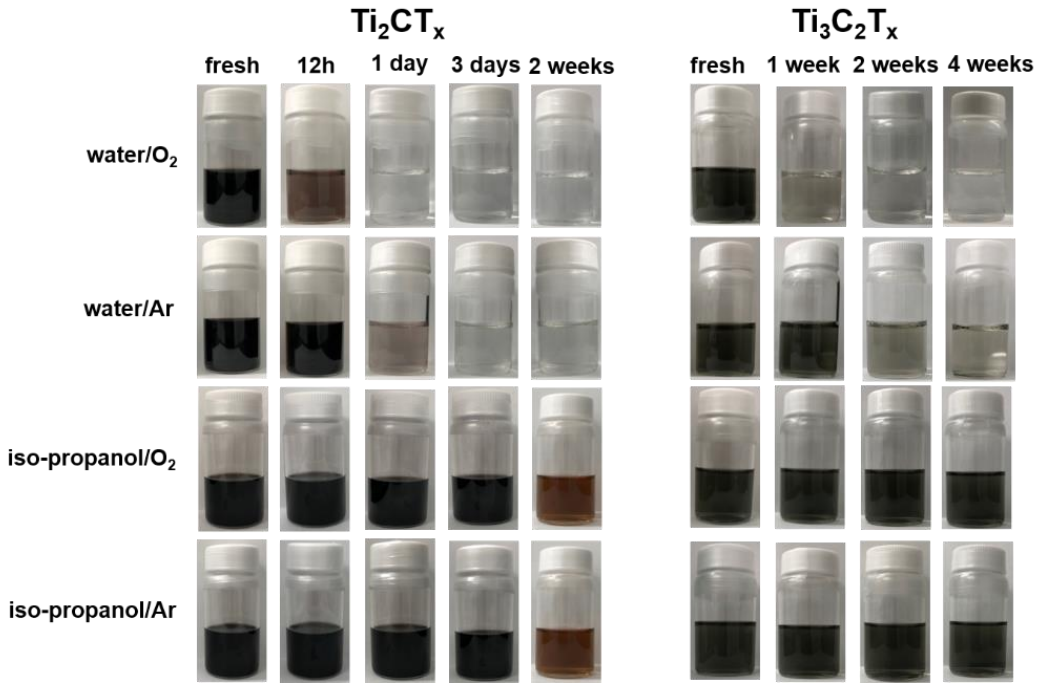

Figure 3. Visual appearance of Ti_2CT_x and $Ti_3C_2T_x$ colloidal solutions in different environments over time.

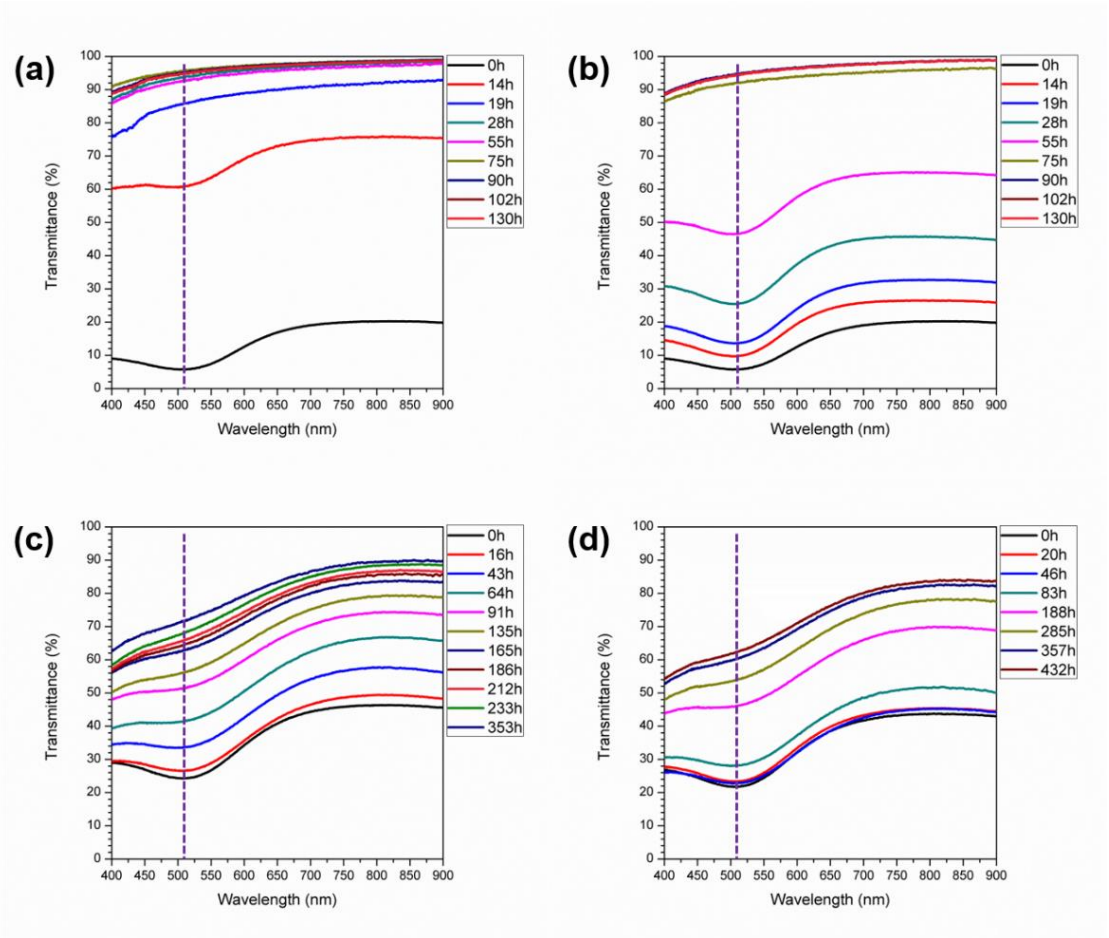

Figure 4. Changes in UV-Vis transmittance spectra of Ti_2CT_x colloids in different environments over time (from bottom to top for each graph). (a) Ti_2CT_x-water/O_2; (b) Ti_2CT_x-water/Ar; (c) Ti_2CT_x-iso-propanol/O_2; (d) Ti_2CT_x-iso-propanol/Ar. Dashed lines indicate the plasmon resonance peak of the MXene.

The results in Table 2 show that the time constant for Ti_2CT_x nanosheets in water/ O_2 is small (0.31 days or 7 h), meaning that only $\sim 1/e \approx 0.37$ of initial MXene is left after 7 h in this environment. In contrast, iso-propanol is a less harsh environment for Ti_2CT_x compared to water, even in those cases when isopronanol has been saturated with O_2, whereas water has been boiled, purged, and saturated with Ar. This is indicated by the ~4 times larger time constant of Ti_2CT_x nanosheets in the iso-propanol/O_2 system (τ = 6.85 days) compared to that of the water/Ar system (τ = 1.50 days). In other words, Ti_2CT_x

MXene in the water-less environment, even saturated with oxygen, remains stable for at least 4 times longer compared to when water is present without oxygen. This further demonstrates the crucial role of water as the central factor in the MXene degradation process. According to this, Ti_2CT_x nanosheets in iso-propanol/Ar show the slowest decay, since there is no water nor oxygen present in the environment. However, even in this case the changes in the spectra and visual appearance become noticeable after ~13 days (Figures 3 and 4), probably signifying a reaction between Ti_2CT_x and isopropanol itself, which is another example of hitherto unknown MXene chemistry. It should be noted that the color of isopropanol MXene colloids eventually changes to brown-red in contrast to aqueous colloids where the color changes to white; thus, the reactions of the MXene with iso-propanol are different compared to its reactions with water.

4.2. $Ti_3C_2T_x$ MXENE

To further test our hypothesis about the crucial role of water in MXene degradation and to illustrate the effect of 2D material monolayer thickness on its chemical properties, we studied another common MXene, $Ti_3C_2T_x$, using the same methods and techniques. $Ti_3C_2T_x$ is composed of the same elements as Ti_2CT_x, but its monolayer is ~1.2 times thicker than that of Ti_2CT_x (Figure 1). Since the measured plasmon resonance band of $Ti_3C_2T_x$ is located at ~780 nm, transmittance at this wavelength has been monitored. After adjusting $Ti_3C_2T_x$ concentrations in deaerated water and anhydrous iso-propanol to the same initial values at ~0.04 mg/mL (Figure 2), the fresh $Ti_3C_2T_x$ MXene colloidal solutions were purged with O_2 or Ar and sealed in 20 mL glass vials labeled as

$Ti_3C_2T_x$–water/O_2, $Ti_3C_2T_x$–water/Ar, $Ti_3C_2T_x$–iso-propanol/O_2, and $Ti_3C_2T_x$–iso-propanol/Ar, respectively (Table 1 and Figure 3).

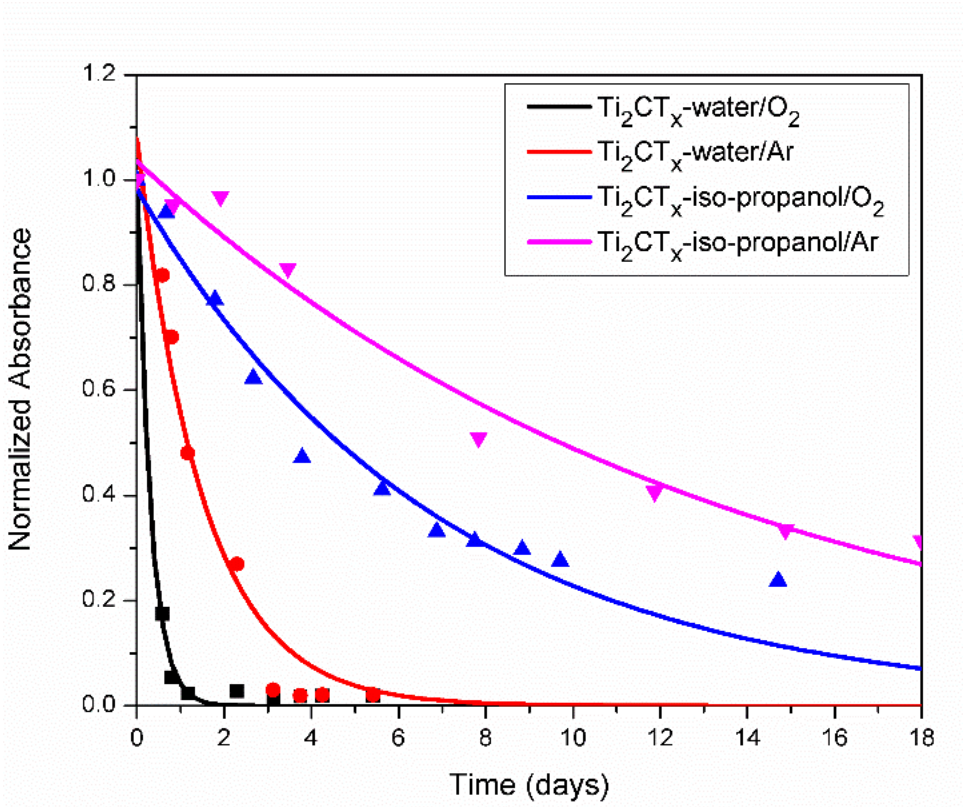

Figure 5. Stability of Ti_2CT_x colloidal solutions in different environments over time. Solid lines represent fits to equation (1).

After 1 week, the $Ti_3C_2T_x$–water/O_2 sample was almost completely colorless while the other three samples still retained their initial dark appearance (Figure 3). It is worth noting that both $Ti_3C_2T_x$–iso-propanol samples with and without O_2 ($Ti_3C_2T_x$–iso-propanol/O_2 and $Ti_3C_2T_x$–iso-propanol/Ar) remained intesely dark-colored even after one month, while both $Ti_3C_2T_x$–water samples became almost transparent, indicating that in anhydrous iso-propanol $Ti_3C_2T_x$ stays intact for a much longer time, even when the system

is saturated with oxygen. In other words, the presence of water leads to quick degradation of $Ti_3C_2T_x$ nanosheets even in an oxygen-less environment.

Table 2. Fitting Parameters of Experimental Degradation Kinetic Data to Equation 1 for Ti_2CT_x and $Ti_3C_2T_x$ Colloidal Solutions in Different Environments.

Sample	**Time Constant (τ, days)** [a]	**$A_{Initial}$**	**R-square**
Ti_2CT_x-water/O_2	0.31	1.001	0.996
Ti_2CT_x-water/Ar	1.50	1.077	0.969
Ti_2CT_x-iso-propanol/O_2	6.85	0.982	0.958
Ti_2CT_x-iso-propanol/Ar	13.35	1.035	0.977
$Ti_3C_2T_x$-water/O_2	4.64	1.021	0.991
$Ti_3C_2T_x$-water/Ar	41.31	0.989	0.984
$Ti_3C_2T_x$-iso-propanol/O_2	2025.52	0.998	0.140
$Ti_3C_2T_x$-iso-propanol/Ar	4752.85	0.985	0.007
[a] one day is equal to 24 h			

Figure 6 shows the changes in UV−vis spectra of $Ti_3C_2T_x$ in different environments over time. The transmittance of $Ti_3C_2T_x$ in water gradually increased with time, while no significant changes have been detected in anhydrous isopropanol (note the stretched transmittance axis in Figure 6 (c, d) to magnify any differences). Thus, we conclude again that for $Ti_3C_2T_x$, same as for Ti_2CT_x, it is water, and not oxygen, which is the main reagent in reactions leading to MXene degradation.

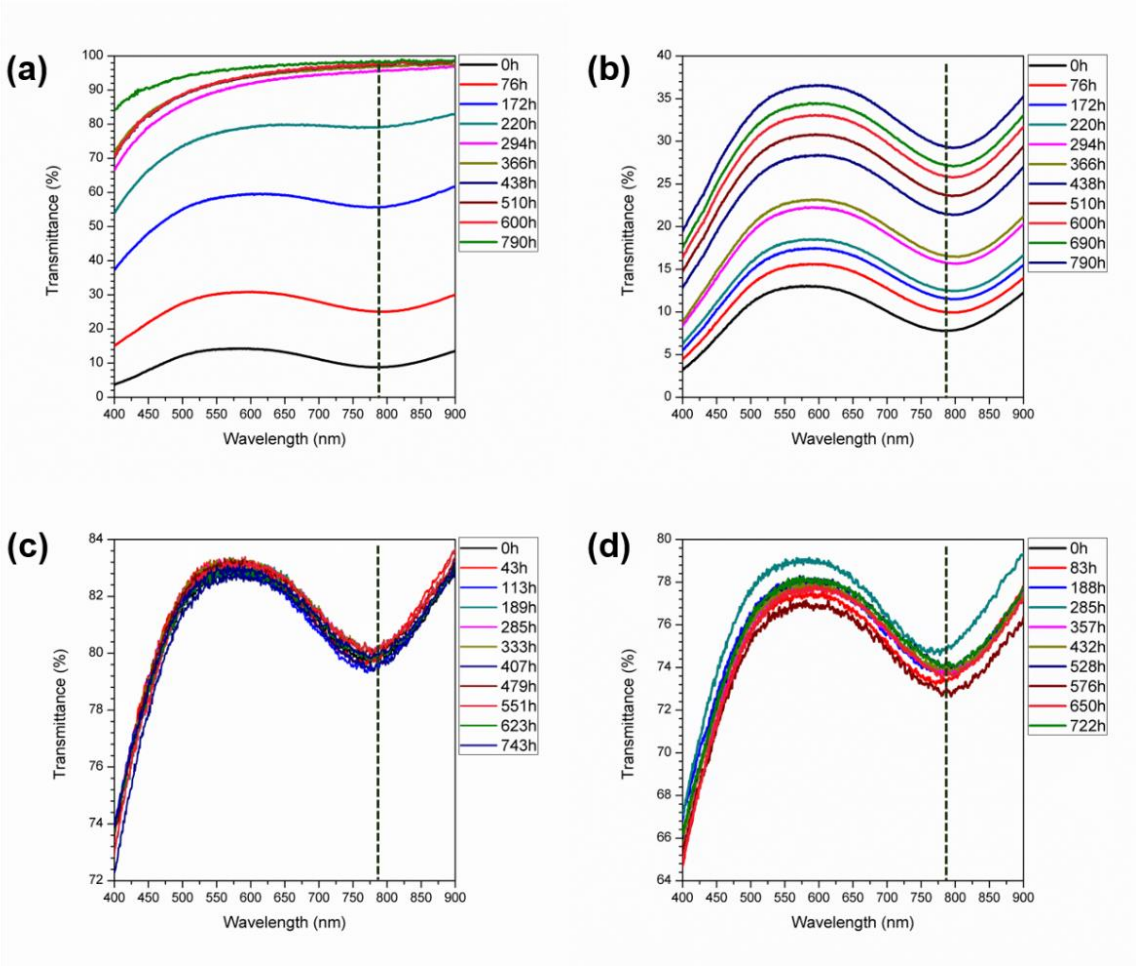

Figure 6. Changes in UV−vis transmittance spectra of $Ti_3C_2T_x$ colloids in different environments over time (from bottom to top for each graph). (a) Ti_3C_2Tx−water/O_2, (b) $Ti_3C_2T_x$−water/Ar, (c) $Ti_3C_2T_x$−iso-propanol/O_2, and (d) $Ti_3C_2T_x$−iso-propanol/Ar. Dashed lines indicate the plasmon resonance peak of the MXene.

Similar to the above analysis, we plot degradadtion kinetics data and fit the curves to eq 1 (Figure 7). There is a continuous decrease in the concentration of $Ti_3C_2T_x$ in water over time, and as Table 2 shows, the time constants (τ) for $Ti_3C_2T_x$ in water are ~5 days in O_2 atmosphere and ~41 days in Ar atmosphere, respectively. However, there are no apparent changes in concentrations of $Ti_3C_2T_x$ in anhydrous isopropanol, where the calculated time constants are fairly large, i.e., ~2026 days in O_2 atmosphere and ~4753

days in Ar atmosphere. It seems that the absorbance of $Ti_3C_2T_x$ in anhydrous iso-propanol colloids simply does not depend on time, as also signified by the nearly zero R-square values in Table 2. Thus, we conclude that both MXenes, especially the thicker $Ti_3C_2T_x$ nanosheets, could survive for quite a long time in their colloidal states in the absence of water. Raman spectra (Figure 8) of the MXenes recorded after liquid evaporation from their freshly prepared colloidal solutions showed the expected vibrational modes for $Ti_3C_2T_x$ and Ti_2CT_x [21, 37, 38].

After storing Ti_2CT_x in water for 3 days (Figure 8 b) the solids collected from the Ti_2CT_x−water/O_2 and Ti_2CT_x−water/Ar samples showed only the anatase Raman peak [39, 40] at 149−155 cm^{-1} and no Raman bands of MXene, while the solids collected from Ti_2CT_x−iso-propanol/O_2 and Ti_2CT_x−iso-propanol/Ar showed MXene peaks and no changes compared to the freshly prepared solutions (Figure 8 a). Similar conclusions could be drawn for $Ti_3C_2T_x$ solutions; after one month the anatase TiO_2 peak dominates the Raman spectra of solids collected by evaporation of $Ti_3C_2T_x$−water/Ar and $Ti_3C_2T_x$−water/O_2 samples. However, in a striking contrast to the water-based colloids, $Ti_3C_2T_x$ in iso-propanol remains intact (as long as Raman spectroscopy is concerned) after 30 days storage (Figure 8 d), which again emphasizes the importance of water rather than oxygen in MXene degradation processes.

Another argument pointing to the central role of water in degradation of colloidal MXenes comes from the analysis of oxygen solubility in water and iso-propanol. According to Battino et al. [41], the mole fraction solubility of O_2 at 298.15 K and 101.3 kPa in water is 2.29×10^{-5}, whereas in iso-propanol it is ∼34 times higher (7.82×10^{-4}). Based on these data, if the main reason for MXene degradation were dissolved O_2, then the

process should be much faster in anhydrous iso-propanol where O_2 solubility is higher than in water. However, the experimental results for the samples saturated with oxygen and kept under oxygen atmosphere tell the opposite; degradation kinetics do not correlate with the solution concentration of oxygen, and instead it is clearly sensitive to the presence of water, regardless of oxygen (see Figures S3 and S4, where the environment was a mix of 20 vol % iso-propanol and 80 vol % water).

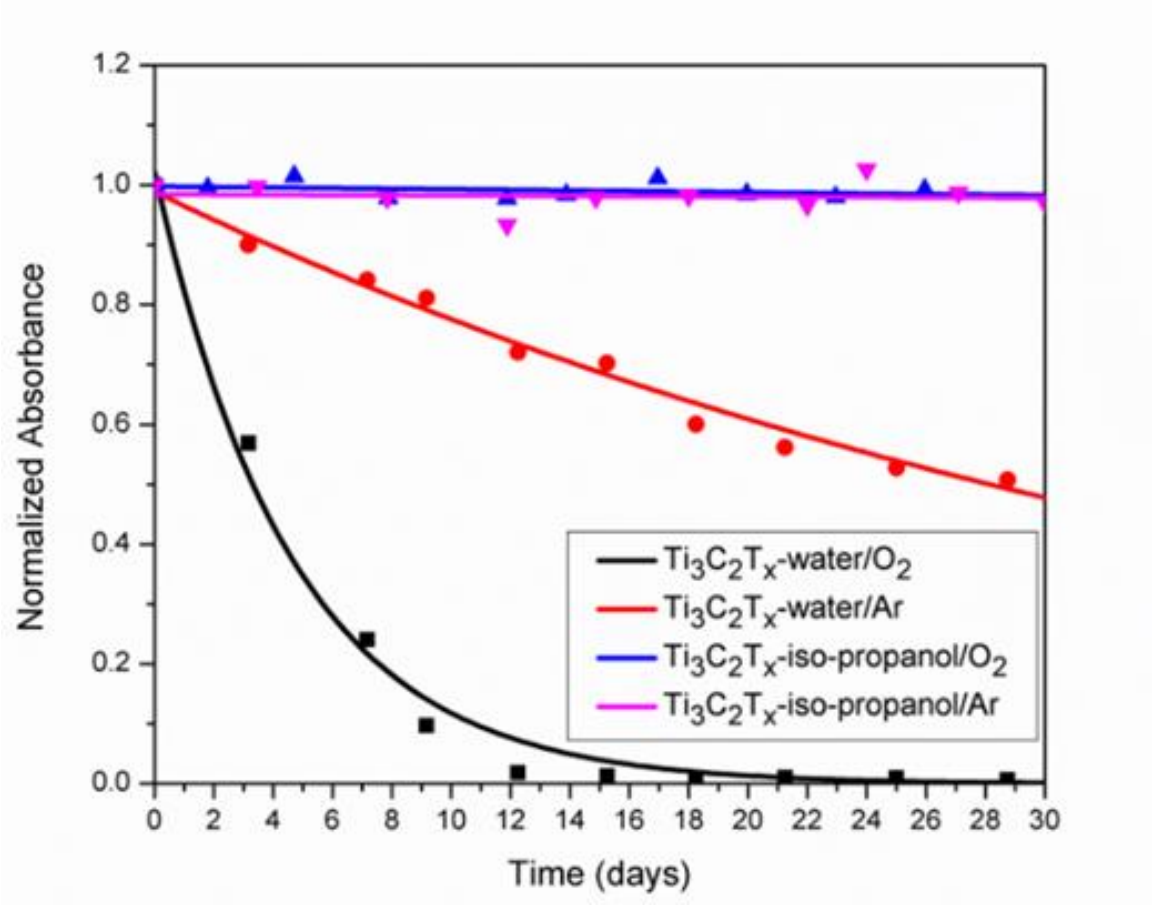

Figure 7. Stability of $Ti_3C_2T_x$ colloidal solutions in different environments over time. Solid lines represent fits to eq 1.

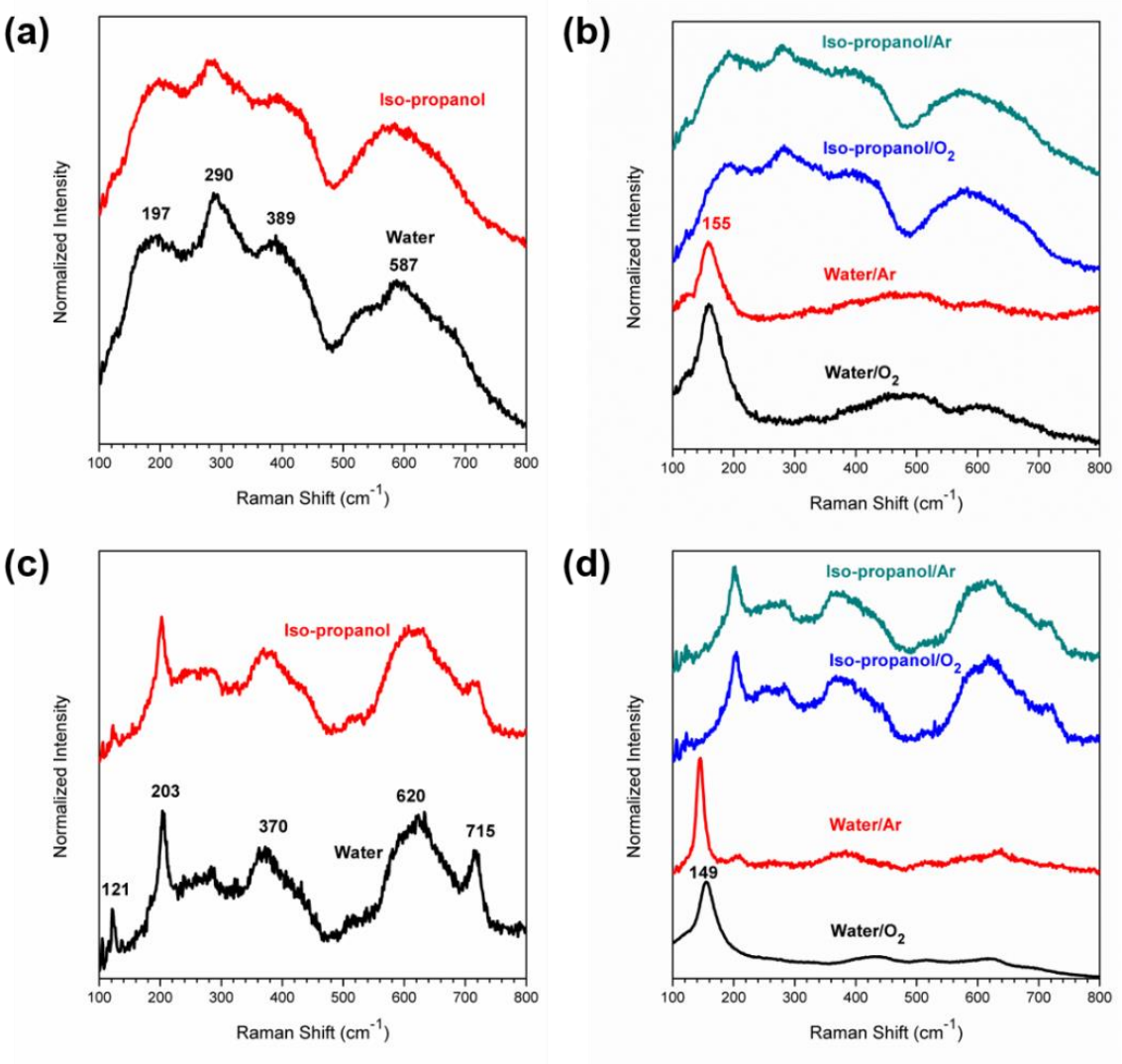

Figure 8. Raman spectra of (a) freshly made Ti_2CT_x in water and iso-propanol; (b) Ti_2CT_x–water/O_2, Ti_2CT_x–water/Ar, Ti_2CT_x–iso-propanol/O_2, and Ti_2CT_x–iso-propanol/Ar after 3 days; (c) freshly made $Ti_3C_2T_x$ in water and iso-propanol; (d) $Ti_3C_2T_x$–water/O_2, $Ti_3C_2T_x$–water/Ar, $Ti_3C_2T_x$–iso-propanol/O_2, and $Ti_3C_2T_x$–iso-propanol/Ar after 1 month.

Therefore, the main reaction in MXene degradation processes, at least for $Ti_3C_2T_x$ and Ti_2CT_x, is hydrolysis and not direct oxidation by oxygen. Accordingly, to prevent fast and complete degradation, Ti-based carbide MXenes should be isolated from water in the first place, and not from oxygen, as deemed before; using deaerated water is less helpful in

this respect than using aerated anhydrous organic solvent, such as iso-propyl alcohol or others [22]. The final formation of TiO_2 in the process of MXene degradation in the presence of water is most likely a result of several processes, including formation of amphoteric amorphous titanium hydroxide due to hydrolysis of the MXenes with water first (similar to what has been proposed by Avgustinik et al. for hydrolysis of bulk TiC [29]), followed by its polymerization and conversion through several equilibrium steps and intermediates into TiO_2 particles. The fate of the MXene carbon atoms during these transformations still remains unclear. Most likely, carbon atoms of MXenes also undergo chemical reactions as evidenced by the color of colloids after hydrolysis of MXenes (Figure 3). We have not observed any noticeable release of gas or pressure build-up in the sealed vials over time. We believe that the carbon is either converted into CO_2 and stays dissolved in the liquid phase, partially in the form of carbonic acid H_2CO_3 or carbonates, or may form some more complex organic molecules, such as hydrocarbons, etc. The net hypothetical chemical reactions can be represented by the following equations:

$$2Ti_3C_2O_2 + 11H_2O = 6TiO_2 + CO + CO_2 + 2CH_4 + 7H_2 \quad (2)$$

or

$$2Ti_3C_2(OH)_2 + 11H_2O = 6TiO_2 + CO + CO_2 + 2CH_4 + 9H_2 \quad (3)$$

for $Ti_3C_2T_x$ with two possible types of T. An experimental evidence supporting formation of CO_2 and H_2CO_3 is provided by acidification of the MXene aqueous colloids in O_2 or Ar atmosphere that progressed in parallel to MXene degradation (Figure S5). In the reactions of MXenes with water and isopropanol we cannot exclude formation of more complex organic molecules, such as aldehydes, alcohols, esters, etc. These reactions can be quite

complex, taking into account that MXenes may potentially also act as catalysts. Their detailed analysis is beyond the scope of this study.

5. CONCLUSIONS

In summary, we have studied the stability of $Ti_3C_2T_x$ and Ti_2CT_x MXenes in water and water-less colloidal solutions saturated with O_2 or Ar, using UV−vis and Raman spectroscopy. When water and O_2 were present together, both MXenes oxidized at an extremely fast rate with time constants at ∼5 days for $Ti_3C_2T_x$ and ∼7 h for Ti_2CT_x. When water or O_2 were present separately, the degradation rates decreased, as evidenced by larger time constants of ∼41 days for $Ti_3C_2T_x$−water/Ar, ∼2026 days for $Ti_3C_2T_x$−iso-propanol/O_2, ∼2 days for Ti_2CT_x−water/Ar, and ∼7 days for Ti_2CT_x−iso-propanol/O_2. Presented data and analysis clearly show that water, and not O_2, plays a key role in the reactions leading to MXene degradation, and it is water rather than oxygen that MXenes need to be protected from. These results will have important implications for MXene manufacturing and storage methods. Moreover, this study indicates the complexity of MXene chemistry, which still largely remains terra incognita but will certainly play a central role in developing MXenes for catalysis and adsorption, as well as biomedical, optical, mechanical, sensing, and electrochemical applications.

SUPPORTING INFORMATION

Figure S1. Photographs of synthesized Ti_3AlC_2 and Ti_2AlC MAX phases.

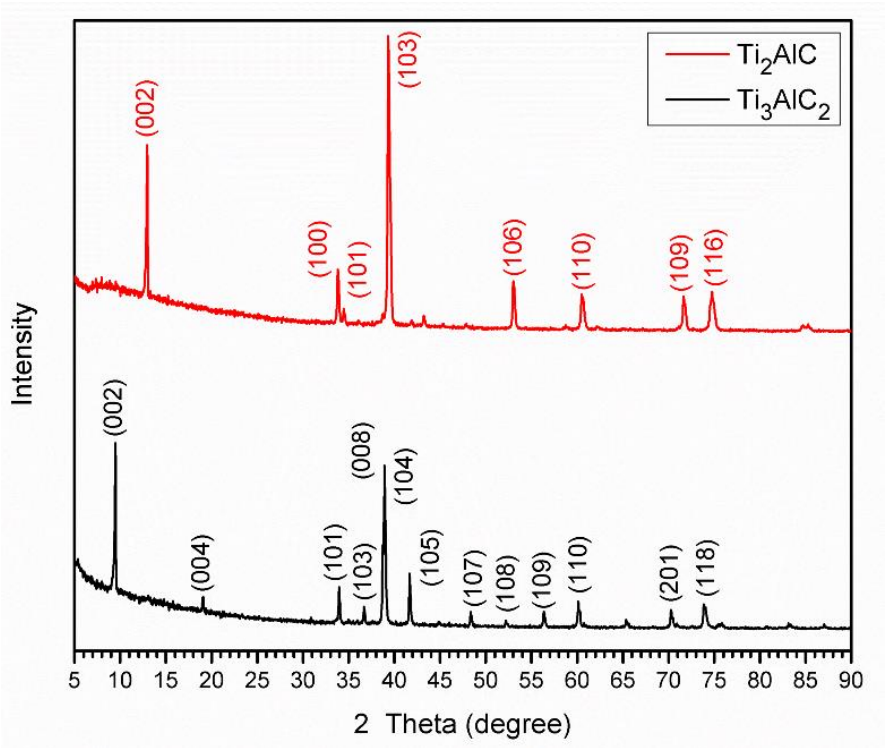

Figure S2. XRD patterns of synthesized Ti_3AlC_2 and Ti_2AlC MAX phases.

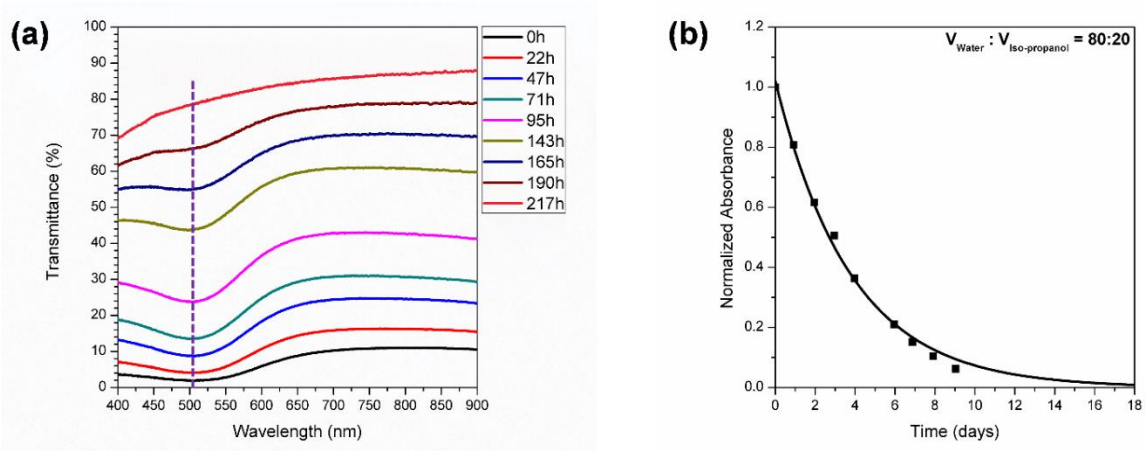

Figure S3. (a) UV-vis transmittance spectra of Ti_2CT_x colloid in water - iso-propanol system (V_{water}:$V_{iso\text{-}propanol}$ = 80:20) in Ar atmosphere over time, where dashed line indicates the position of plasmon resonance peak of the MXene; (b) Stability of the MXene in the same colloidal solution (the absorbance at 505 nm was used as analytical signal proportional to MXene concentration). Solid line is fit to the equation (1) in the main text with time constant τ = 3.8 days.

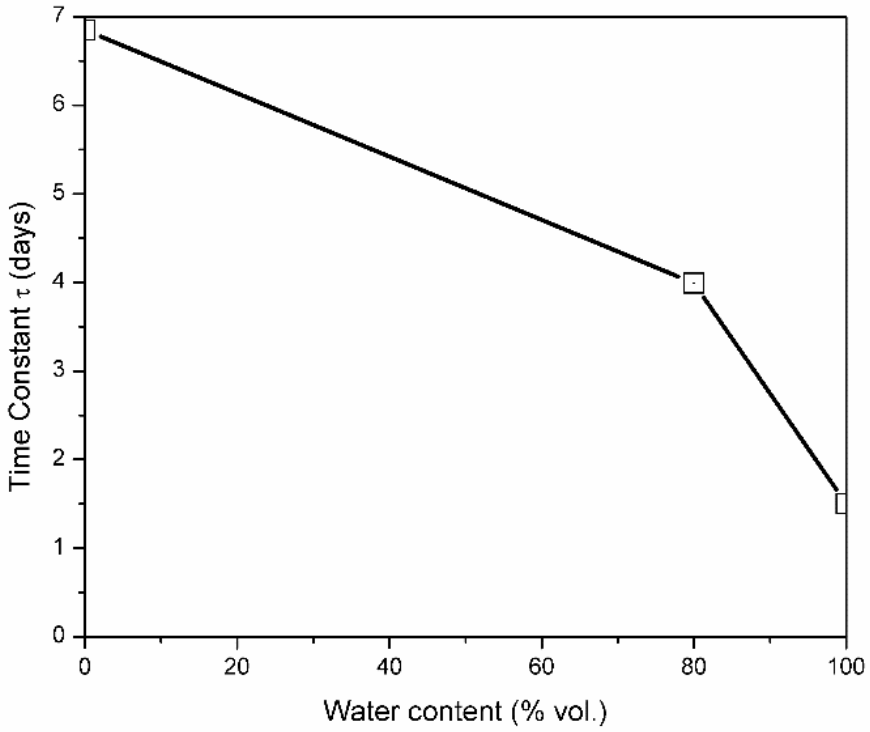

Figure S4. Degradation time constant for Ti_2CT_x colloidal solutions as a function of solvent composition from pure water to pure iso-propanol.

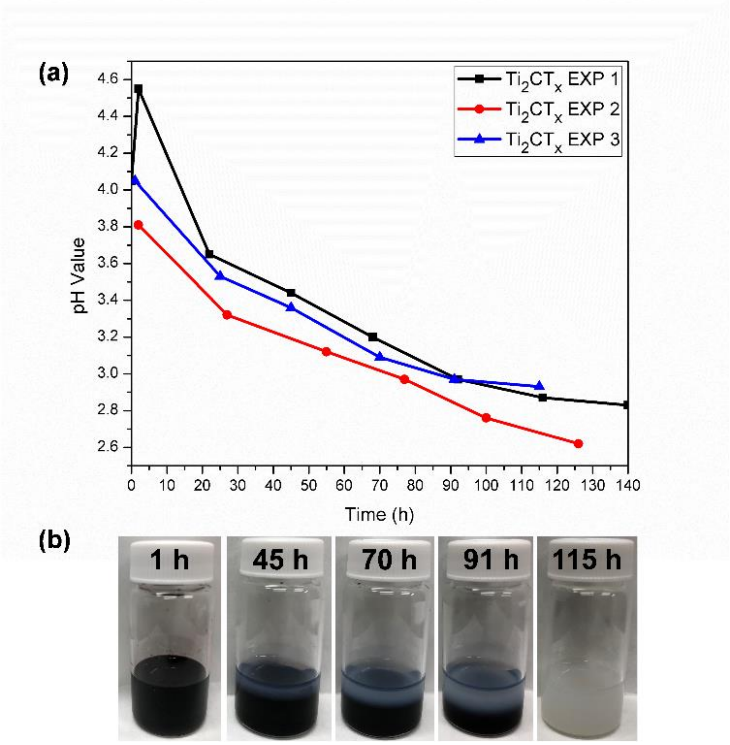

Figure S5. (a) Changes in pH of Ti_2CT_x-water/Ar over time. (b) Visual appearance of Ti_2CT_x colloidal solutions over time in one of the experiments (EXP 3 in panel a).

ASSOCIATED CONTENT

SUPPORTING INFORMATION

The Supporting Information is available free of charge on the ACS Publications website at DOI: 10.1021/acs.inorgchem.8b02890.

Photographs of synthesized Ti_3AlC_2 and Ti_2AlC MAX phases; XRD patterns of synthesized Ti_3AlC_2 and Ti_2AlC MAX phases; UV−vis transmittance spectra and degradation kinetics of Ti_2CT_x colloidally dispersed in a water−iso-propanol system (Vwater/Viso-propanol = 80:20) in an Ar atmosphere over time; degradation time constants for Ti_2CT_x colloidal solutions at three Figure 8. Raman spectra of (a) freshly

made Ti_2CT_x in water and iso-propanol; (b) Ti_2CT_x−water/O_2, Ti_2CT_x−water/Ar, Ti_2CT_x−iso-propanol/ O_2, and Ti_2CT_x−iso-propanol/Ar after 3 days; (c) freshly made $Ti_3C_2T_x$ in water and iso-propanol; (d) Ti3C2Tx−water/O_2, $Ti_3C_2T_x$−water/Ar, $Ti_3C_2T_x$−iso-propanol/O_2, and $Ti_3C_2T_x$−iso-propanol/Ar after 1 month. Inorganic Chemistry Article DOI: 10.1021/acs.inorgchem.8b02890 Inorg. Chem. 2019, 58, 1958−1966 1964 different dispersant compositions; and changes in pH of Ti_2CT_x−water/Ar over time (PDF)

CORRESPONDING AUTHOR

*E-mail: mochalinv@mst.edu

NOTES

The authors declare no competing financial interest.

ACKNOWLEDGEMENTS

The authors thank Dr. R. Brow (Missouri S&T) for providing access to the Raman spectrometer used in this study and Dr. J. Duan (Missouri S&T) for his help with the TEM images of the MXenes.

REFERENCES

[1] M. Naguib, M. Kurtoglu, V. Presser, J. Lu, J.J. Niu, M. Heon, L. Hultman, Y. Gogotsi, M.W. Barsoum, Two-dimensional nanocrystals produced by exfoliation of Ti_3AlC_2, *Advanced Materials*, 23 (**2011**) 4248-4253.

[2] M. Naguib, V.N. Mochalin, M.W. Barsoum, Y. Gogotsi, 25th anniversary article: MXenes: A new family of two-dimensional materials, *Advanced Materials*, 26 (**2014**) 992-1005.

[3] J. Zhu, E. Ha, G. Zhao, Y. Zhou, D. Huang, G. Yue, L. Hu, N. Sun, Y. Wang, L.Y.S. Lee, Recent advance in MXenes: A promising 2D material for catalysis, sensor and chemical adsorption, *Coordination Chemistry Reviews*, 352 (**2017**) 306-327.

[4] M. Ghidiu, M.R. Lukatskaya, M.Q. Zhao, Y. Gogotsi, M.W. Barsoum, Conductive two-dimensional titanium carbide 'clay' with high volumetric capacitance, *Nature*, 516 (**2014**) 78-81.

[5] A. Lipatov, H. Lu, M. Alhabeb, B. Anasori, A. Gruverman, Y. Gogotsi, A. Sinitskii, Elastic properties of 2D $Ti_3C_2T_x$ MXene monolayers and bilayers, *Science Advances*, 4 (**2018**) eaat0491.

[6] V.N. Borysiuk, V.N. Mochalin, Y. Gogotsi, Molecular dynamic study of the mechanical properties of two-dimensional titanium carbides $Ti_{n+1}C_n$ (MXenes), *Nanotechnology*, 26 (**2015**) 265705.

[7] N. Zhang, Y. Hong, S. Yazdanparast, M.A. Zaeem, Superior structural, elastic and electronic properties of 2D titanium nitride MXenes over carbide MXenes: a comprehensive first principles study, *2D Materials*, 5 (**2018**) 045004.

[8] V.N. Borysiuk, V.N. Mochalin, Y. Gogotsi, Bending rigidity of two-dimensional titanium carbide (MXene) nanoribbons: A molecular dynamics study, *Computational Materials Science*, 143 (**2018**) 418-424.

[9] K. Chaudhuri, M. Alhabeb, Z. Wang, V.M. Shalaev, Y. Gogotsi, A. Boltasseva, Highly broadband absorber using plasmonic titanium carbide (MXene), *ACS Photonics*, 5 (**2018**) 1115-1122.

[10] Y. Dong, S. Chertopalov, K. Maleski, B. Anasori, L. Hu, S. Bhattacharya, A.M. Rao, Y. Gogotsi, V.N. Mochalin, R. Podila, Saturable absorption in 2D Ti_3C_2 MXene thin films for passive photonic diodes, *Advanced Materials*, 30 (**2018**) 1705714.

[11] Y. Dong, S.S.K. Mallineni, K. Maleski, H. Behlow, V.N. Mochalin, A.M. Rao, Y. Gogotsi, R. Podila, Metallic MXenes: A new family of materials for flexible triboelectric nanogenerators, *Nano Energy*, 44 (**2018**) 103-110.

[12] M.R. Lukatskaya, O. Mashtalir, C.E. Ren, Y. Dall'Agnese, P. Rozier, P.L. Taberna, M. Naguib, P. Simon, M.W. Barsoum, Y. Gogotsi, Cation intercalation and high volumetric capacitance of two-dimensional titanium carbide, *Science*, 341 (**2013**) 1502-1505.

[13] C. Zhang, M.P. Kremer, A. Seral-Ascaso, S.H. Park, N. McEvoy, B. Anasori, Y. Gogotsi, V. Nicolosi, Stamping of flexible, coplanar micro-supercapacitors using MXene inks, *Advanced Functional Materials*, 28 (**2018**) 1705506.

[14] Y. Xie, M. Naguib, V.N. Mochalin, M.W. Barsoum, Y. Gogotsi, X. Yu, K.W. Nam, X.Q. Yang, A.I. Kolesnikov, P.R. Kent, Role of surface structure on Li-ion energy storage capacity of two-dimensional transition-metal carbides, *Journal of the American Chemical Society*, 136 (**2014**) 6385-6394.

[15] M. Naguib, J. Halim, J. Lu, K.M. Cook, L. Hultman, Y. Gogotsi, M.W. Barsoum, New two-dimensional niobium and vanadium carbides as promising materials for Li-ion batteries, *Journal of the American Chemical Society*, 135 (**2013**) 15966-15969.

[16] H. Tang, W. Li, L. Pan, C.P. Cullen, Y. Liu, A. Pakdel, D. Long, J. Yang, N. McEvoy, G.S. Duesberg, In situ formed protective barrier enabled by sulfur@ titanium carbide (MXene) ink for achieving high-capacity, long lifetime Li-S batteries, *Advanced Science*, 5 (**2018**) 1800502.

[17] S.J. Kim, H.J. Koh, C.E. Ren, O. Kwon, K. Maleski, S.Y. Cho, B. Anasori, C.K. Kim, Y.K. Choi, J. Kim, Y. Gogotsi, H.T. Jung, Metallic $Ti_3C_2T_x$ MXene Gas Sensors with Ultrahigh Signal-To-Noise Ratio, *ACS Nano*, 12 (**2018**) 986-993.

[18] E.S. Muckley, M. Naguib, H.-W. Wang, L. Vlcek, N.C. Osti, R.L. Sacci, X. Sang, R.R. Unocic, Y. Xie, M. Tyagi, Multimodality of structural, electrical, and gravimetric responses of intercalated MXenes to water, *ACS Nano*, 11 (**2017**) 11118-11126.

[19] S. Chertopalov, V.N. Mochalin, Environment Sensitive Photoresponse of Spontaneously Partially Oxidized $Ti_3C_2T_x$ MXene Thin Films, *ACS Nano*, 12 (**2018**) 6109-6116.

[20] O. Mashtalir, K.M. Cook, V.N. Mochalin, M. Crowe, M.W. Barsoum, Y. Gogotsi, Dye adsorption and decomposition on two-dimensional titanium carbide in aqueous media, *J Mater Chem A*, 2 (**2014**) 14334-14338.

[21] C. Zhang, S. Pinilla, N. McEvoy, C.P. Cullen, B. Anasori, E. Long, S.H. Park, A. Seral-Ascaso, A. Shmeliov, D. Krishnan, Oxidation Stability of Colloidal 2D Titanium Carbides (MXenes), *Chemistry of Materials*, 29 (**2017**) 4848-4856.

[22] K. Maleski, V.N. Mochalin, Y. Gogotsi, Dispersions of two-dimensional titanium carbide MXene in organic solvents, *Chemistry of Materials*, 29 (**2017**) 1632-1640.

[23] A.N. Enyashin, A.L. Ivanovskii, Structural and electronic properties and stability of MXenes Ti_2C and Ti_3C_2 functionalized by methoxy groups, *J Phys Chem C*, 117 (**2013**) 13637-13643.

[24] L.-Y. Gan, D. Huang, U. Schwingenschlögl, Oxygen adsorption and dissociation during the oxidation of monolayer Ti_2C, *J Mater Chem A*, 1 (**2013**) 13672.

[25] G. Deysher, S. Sin, Y. Gogotsi, B. Anasori, Oxidized 2D titanium carbide MXene: Flash oxidized powders, *Materials Today*, 21 (**2018**) 1064-1065.

[26] A. Lipatov, M. Alhabeb, M.R. Lukatskaya, A. Boson, Y. Gogotsi, A. Sinitskii, Effect of synthesis on quality, electronic properties and environmental stability of individual monolayer Ti_3C_2 MXene flakes, *Advanced Electronic Materials*, 2 (**2016**) 1600255.

[27] M.C. Sneed, Comprehensive Inorganic Chemistry, Van Nostrand, New York, **1953**.

[28] J.C. Bailar, A. Trotman-Dickenson, Comprehensive inorganic chemistry, Pergamon press Oxford, **1973**.

[29] A.I. Avgustinik, G.V. Drozdetskaya, S.S. Ordan'yan, Reaction of titanium carbide with water, *Soviet Powder Metallurgy and Metal Ceramics*, 6 (**1967**) 470-473.

[30] P.B. Merrill, S.S. Perry, P. Frantz, S.V. Didziulis, Adsorption of water on TiC (100): Evidence for complex reaction and desorption pathways, *Journal of Physical Chemistry B*, 102 (**1998**) 7606-7612.

[31] S.V. Didziulis, P. Frantz, S.S. Perry, O. El-bjeirami, S. Imaduddin, P.B. Merrill, Substrate-dependent reactivity of water on metal carbide surfaces, *Journal of Physical Chemistry B*, 103 (**1999**) 11129-11140.

[32] M.W. Barsoum, The $M_{N+1}AX_N$ phases: A new class of solids: Thermodynamically stable nanolaminates, *Progress in Solid State Chemistry*, 28 (**2000**) 201-281.

[33] Z.W. Seh, K.D. Fredrickson, B. Anasori, J. Kibsgaard, A.L. Strickler, M.R. Lukatskaya, Y. Gogotsi, T.F. Jaramillo, A. Vojvodic, Two-dimensional molybdenum carbide (MXene) as an efficient electrocatalyst for hydrogen evolution, *ACS Energy Letters*, 1 (**2016**) 589-594.

[34] M. Alhabeb, K. Maleski, B. Anasori, P. Lelyukh, L. Clark, S. Sin, Y. Gogotsi, Guidelines for synthesis and processing of two-dimensional titanium carbide ($Ti_3C_2T_x$ MXene), *Chemistry of Materials*, 29 (**2017**) 7633-7644.

[35] A. Favron, E. Gaufrès, F. Fossard, A.-L. Phaneuf-L’ Heureux, N.Y. Tang, P.L. Lévesque, A. Loiseau, R. Leonelli, S. Francoeur, R. Martel, Photooxidation and quantum confinement effects in exfoliated black phosphorus, *Nature Materials*, 14 (**2015**) 826.

[36] D. Hanlon, C. Backes, E. Doherty, C.S. Cucinotta, N.C. Berner, C. Boland, K. Lee, A. Harvey, P. Lynch, Z. Gholamvand, Liquid exfoliation of solvent-stabilized few-layer black phosphorus for applications beyond electronics, *Nature Communications*, 6 (**2015**) 8563.

[37] M. Naguib, O. Mashtalir, M.R. Lukatskaya, B. Dyatkin, C. Zhang, V. Presser, Y. Gogotsi, M.W. Barsoum, One-step synthesis of nanocrystalline transition metal oxides on thin sheets of disordered graphitic carbon by oxidation of MXenes, *Chem Communications*, 50 (**2014**) 7420-7423.

[38] F. Liu, A. Zhou, J. Chen, H. Zhang, J. Cao, L. Wang, Q. Hu, Preparation and methane adsorption of two-dimensional carbide Ti_2C, *Adsorption*, 22 (**2016**) 915-922.

[39] V. Swamy, A. Kuznetsov, L.S. Dubrovinsky, R.A. Caruso, D.G. Shchukin, B.C. Muddle, Finite-size and pressure effects on the Raman spectrum of nanocrystalline anatase TiO_2, *Physical Review B*, 71 (**2005**) 184302.

[40] J. Zhu, Y. Tang, C. Yang, F. Wang, M. Cao, Composites of TiO_2 nanoparticles deposited on Ti_3C_2 MXene nanosheets with enhanced electrochemical performance, *Journal of The Electrochemical Society*, 163 (**2016**) A785-A791.

[41] R. Battino, T.R. Rettich, T. Tominaga, The solubility of oxygen and ozone in liquids, *Journal of Physical and Chemical Reference Data*, 12 (**1983**) 163-178.

II. UNDERSTANDING CHEMISTRY OF TWO-DIMENSIONAL TRANSITION METAL CARBIDES AND CARBONITRIDES (MXENE) WITH GAS ANALYSIS

Shuohan Huang[†] and Vadym N. Mochalin[*,†,‡]
[†]Department of Chemistry, Missouri University of Science & Technology, Rolla, Missouri 65409, United States
[‡]Department of Materials Science & Engineering, Missouri University of Science & Technology, Rolla, Missouri 65409, United States
*Correspondence to: mochalinv@mst.edu

ABSTRACT

MXenes, a large family of two-dimensional materials that are intensely investigated for a broad range of applications, are unstable in water, spontaneously forming TiO_2. Several hypotheses have been proposed recently to explain the transformations of MXenes in aqueous environments based on characterization of solid products and measurements of solution pH. However, no studies of the gaseous products of these reactions have been reported. In this work, we demonstrate the use of Raman spectroscopy and gas chromatography techniques to study the gaseous reaction products of Ti_2C, Ti_3C_2, Ti_3CN, and Nb_2C MXenes in aqueous environment. Based on the analysis of gases, the reactivities of MXenes with different monolayer thickness and chemical composition have been analyzed. We demonstrate the analysis of gases produced during MXene transformations as a powerful technique that can be used for better understanding of their non-trivial chemistry.

Keywords: MXene chemistry, gas analysis, reactivity of 2D materials, gas chromatography, Raman spectroscopy

1. INTRODUCTION

Two-dimensional (2D) materials have raised significant interest due to their many outstanding properties. MXenes are a large family of two-dimensional early transition metal carbides/nitrides discovered in 2011 [1, 2]. MXenes are produced by selective extraction of group A element atoms (typically Al) from bulk precursor MAX phases using fluorine-containing etchants. MXenes have a general formula $M_{n+1}X_nT_x$, where n=1-4, M represents an early transition metal, X is carbon or nitrogen, and T stands for surface terminations (-OH, -F and -O-) whose fraction in the formula is usually unknown (x) [3]. Because of their 2D structure and outstanding combination of properties [2, 4], MXenes have demonstrated promise in various applications, such as optoelectronic devices [5], lasers [6], sensors [7-9], THz wave transmission and communication technology [10, 11], *etc.* Although the interest in using MXenes for a broad range of applications is quickly growing, their basic chemical properties remain largely unexplored. This is particularly worrying since MXenes, especially in their most commonly used aqueous colloidal state, are known to be unstable, spontaneously transforming into the corresponding M element oxides over time, resulting in structure degradation and loss of properties [12-14]. Not surprisingly, attempts have been reported to protect MXenes against oxidation, particularly in aqueous solutions [15-17]. However, in most of these reports, only an indirect evidence (such as electrical conductivity or electrochemical performance) was used to demonstrate

the suppression of MXene degradation. Although important from practical standpoint, these indirect evidences of prolonged MXene stability may not reflect the real degree of chemical transformations in the system. Therefore, the question as to the extent of MXene degradation, even in the situations when it was reportedly suppressed, still remains open. Besides practical importance, direct studies of MXene transformations may shed more light onto currently poorly understood chemistry of 2D transition metal carbides and nitrides. Whereas the fate of transition metal atoms (most typically titanium) in the processes of MXene degradation is more or less clear (they end up in the corresponding transition metal oxides, *e.g.,* titanium oxide), much less is known about the fate of carbon and nitrogen atoms of MXenes. Some reports mention that the oxidative degradation of Ti_3C_2 MXene in aqueous solutions yields titanium dioxide and CO_2 [18], while other authors believe that the final products of MXene degradation are TiO_2 and carbon [12, 13, 17, 19, 20]. And, to our best knowledge, no reports on the degradation products of nitrogen containing MXenes have been published so far.

As an example of complex chemistry of MXenes, we have recently shown that in addition to oxidation, MXenes directly react with water in ambient conditions [21]. This experimental observation of MXene reactivity towards water in ambient conditions differs from chemistry of their bulk counterparts – transition metal carbides. The interactions of bulk carbides with water and aqueous acid or base solutions have received mixed representation in textbooks and papers. While reports and common inorganic chemistry textbooks mention that titanium carbide is resistant to decomposition in water as well as aqueous acid and base solutions [22-24], Avgustinik *et al.* [25] have reported long ago the reaction between group IV metal carbides and water yielding hydrocarbons and hydroxides.

Their results also showed that the extent of the attack by water is limited by 5-30 surface atomic layers of the carbide, which for a bulk material was properly deemed to be insignificant. However, such an attack will have dramatic consequences in case of 2D forms of these carbides where the entire thickness of the monolayer is just several atomic layers. Thus, traditional knowledge of chemistry of bulk carbides can be misleading if transferred directly to carbide based MXenes.

Clearly, studying MXene reactivity is important for synthesis, storage, device fabrication, as well as almost any of their applications. Water colloids are most commonly used to synthesize, process, and store MXenes, as well as in device fabrication. Hence, chemical reactivity of MXenes towards water is of great importance and should be studied further. It is logical to speculate that carbon and nitrogen in the course of these transformations will finally form gaseous species, probably CH_4, CO, CO_2, N_2, *etc.* [21]. However, no experimental confirmation of these products has been obtained whatsoever.

In this work we demonstrate gas analysis as a powerful technique to gain further insights into chemical reactivity of MXenes. Gases produced during chemical transformations of Ti_2C, Ti_3C_2, Ti_3CN, and Nb_2C MXenes in aqueous colloidal solutions (UV-vis spectra and photographs of these solutions are shown in Figure S1) have been collected and analyzed *via* gas chromatography (GC) and Raman spectroscopy. The degradation rates of the MXenes in water were further investigated depending on their monolayer thickness within the same chemical composition, as well as depending on chemical composition of the materials within the same monolayer thickness.

2. RESULTS AND DISCUSSION

Experiments of three types, referred hereafter as Experiment 1, 2, and 3 (Table 1, further details are provided in Experimental section and Figure S2 in Supporting Information), were conducted to collect and characterize the transformation products of different MXenes in water. Figure 1a shows chromatograms of the corresponding gas phases collected from Experiment 1 with different MXenes, as well as pure H_2, CO, CO_2, and CH_4 gases used as references. Comparison of the retention times allows unambiguous identification of CH_4 as the main gaseous product of the transformations of all four studied MXenes in water (retention time of CH_4 reference in the conditions of our GC experiment is ~5 min, see Supporting Information for gas analysis and materials characterization details). This result indicates that carbon in all studied carbide and carbonitride MXene structures ends up forming CH_4 during their transformations in water. Because our GC instrument equipped with thermal conductivity detector is not particularly sensitive to CO_2 (Figure 1a), we further investigated evolved gas composition using other techniques.

Raman spectra of the gas phase bubbles produced and collected in sealed glass vials from Experiment 1 are shown in Figure 1b. The peak at 2331 cm^{-1} represents the symmetric stretching mode of N_2, which probably originates from the small amount of air dissolved in DI water,[26] while the peaks at 2918 and 3020 cm^{-1} correspond to symmetric and asymmetric C-H stretching modes in methane, respectively.[27] Surrounding series of regularly spaced smaller peaks within 2850-3200 cm^{-1} range represent rotational Raman spectrum of CH_4, as confirmed by the bond length calculation provided in Supporting Information (Figure S3). Thus, Raman spectroscopy provides further strong support to GC

observations of methane evolution during the transformations of carbide and carbonitride MXenes in water. In contrast to previously published hypotheses,[18, 21] no traces of CO and CO_2 were observed in our experiments either in GC or in Raman, although these gaseous products would be expected in an oxidative degradation of our MXenes.

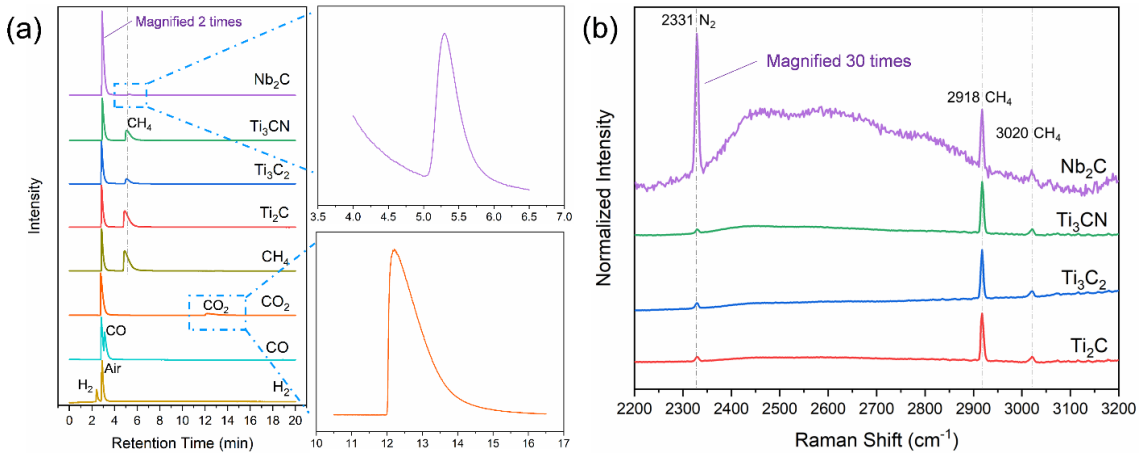

Figure 1. (a) GC analysis of gaseous products of Ti_2C, Ti_3C_2, Ti_3CN, and Nb_2C MXene transformations in water and standard H_2, CO, CO_2, and CH_4 gases. The insets on the right show enlarged areas of CH_4 peak produced in Nb_2C degradation and CO_2 peak of reference CO_2 gas. (b) Raman spectra of gas bubbles collected and analyzed in sealed vials in the course of Ti_2C, Ti_3C_2, Ti_3CN, and Nb_2C MXene transformations in water.

An alternative hypothesis regarding the fate of carbide carbon during MXene degradation expressed in literature is that it remains in the form of "carbon" [12, 13, 17, 19, 20]. To test this hypothesis and answer the question whether there is any solid carbon left, we have analyzed solid products of complete MXene degradation from Experiment 2 using Raman spectroscopy. Obviously, the M elements in the final solid products are anticipated to form the corresponding metal oxides in all our experiments. Accordingly, Raman spectra of solid transformation products of Ti_2C, Ti_3C_2, and Ti_3CN (Figure 2) show a strong peak at 150 cm^{-1} along with three other peaks at 395, 510, and 628 cm^{-1},

respectively, all of which can be assigned to the anatase form of TiO_2 [19, 21]. The Raman spectrum of solid transformation product of Nb_2C shows peaks at 120, 231, 681, and 957 cm^{-1}, representative of Nb_2O_5 [19, 28]. No peaks have been detected in the range of Raman shift typical for carbon (1200-1700 cm^{-1}), thus ruling out the hypothesis of solid carbon present in the transformation products of the MXenes. Furthermore, energy-dispersive X-ray spectroscopy (EDS) also shows no traces of carbon or nitrogen in the solid degradation products of different MXenes (Figure S4). Thus, we conclude that titanium carbide MXenes in aqueous environment ultimately transform into TiO_2 and CH_4, while Nb_2C MXene transforms into Nb_2O_5 and CH_4, respectively. These final products are most likely formed in multistage reactions and detailed mechanisms of their formation still remain unknown.

Another interesting MXene with respect to its chemistry is carbonitride Ti_3CN, especially since chemical transformations of carbonitride MXenes have never been studied before. Similar to carbon, nitrogen in the MXene structure is expected to form gaseous products. Based on the high strength of the triple bond in N_2, *a priori* there is a high chance that nitrogen atoms from the MXene structure will form N_2 gas. However, apart from CH_4, no accumulation of N_2 (besides N_2 from air) nor other gases were detected in the reactions of Ti_3CN with water, neither by GC nor Raman (Figure 1). Another possibility is the formation of ammonia NH_3, which further chemically interacts with water forming NH_4OH. Formation of ammonium hydroxide in the solution must result in the corresponding increase of pH.

Table 1. Description of experiments conducted in this study.

Name	Brief Description	Purpose
Experiment 1	10 ml glass headspace vial fully filled with MXene solution and sealed, kept at 70 ^{o}C upside down with a plastic needle inserted through septum as outlet with the other end of the needle submerged in water	Collect enough volume of gas for GC measurements
Experiment 2	20 ml closed glass vial filled with 10 ml solution kept at 70 ^{o}C in sand bath	1. pH measurements over time 2. Separate supernatant from solid after complete degradation of Ti_3CN for ATR FTIR measurements 3. Separate solid phases from MXene solutions after their complete degradation for Raman measurements
Experiment 3	10 ml headspace vial filled with 6 ml solution and sealed, then kept upside down in an oven at 70, 80, and 90 ^{o}C, correspondingly	Raman measurements of gas phase over the time of reaction

Thus, Experiment of type 2 was conducted and pH values of the Ti_3CN aqueous solution were recorded over time during its transformation. The solution was kept in a 70 ^{o}C sand bath to accelerate the reactions. For comparison, pH values of Ti_2C, Ti_3C_2, and Nb_2C MXene aqueous colloids were also monitored in same conditions. These pH

monitoring experiments were repeated 3 times for each MXene and all collected data are summarized in Figure S5 (Supporting Information). The average pH values shown in Figure 3a initially drop with time over the first ~20 h in Ti_2C, Ti_3C_2, and Ti_3CN solutions, perhaps due to release of the intercalated acidic species (HF or HCl) when MXene structure degrades.[29] The rate of the drop in pH correlates with the MXene degradation rate (compare curves for Ti_2C and Ti_3C_2 in Figure 3a). There is no significant change of pH during the degradation of Nb_2C, perhaps indicating its lower reactivity (also manifested by a lower rate of methane production, see Figure 4a below) or low concentration of Nb_2C colloidal solution. However, as the reaction progressed beyond 20 h, the pH trend of Ti_3CN solution turned from drop to growth (Figure 3a) in striking difference to other, carbide MXene solutions. Therefore, the pH trends support the hypothesis of ammonia formation during Ti_3CN degradation in water. In the presence of anions ammonium will form the corresponding ammonium salts, which can be discovered using spectroscopic techniques. Indeed, bending (1450 cm^{-1}) and stretching (3051 cm^{-1}) modes[30] of N-H in NH_4^+ were observed in addition to H-O-H bending (1645 cm^{-1}) and O-H stretching (3494 cm^{-1}) vibrations of water[31] in the attenuated total reflection (ATR) FTIR spectrum of liquid supernatant collected from Ti_3CN solution after complete MXene degradation (Figure 3b). These results confirm formation of NH_3 (or NH_4^+) during the transformation of Ti_3CN in water. Moreover, Raman spectrum shows only TiO_2 in the water rinsed solid degradation products of Ti_3CN (Figure 2), no solid carbon remains. Thus, the combination of results from gas, liquid, and solid products analysis, leads us to conclude that the transformation of the titanium carbonitride MXene in water produces TiO_2, CH_4, and NH_3.

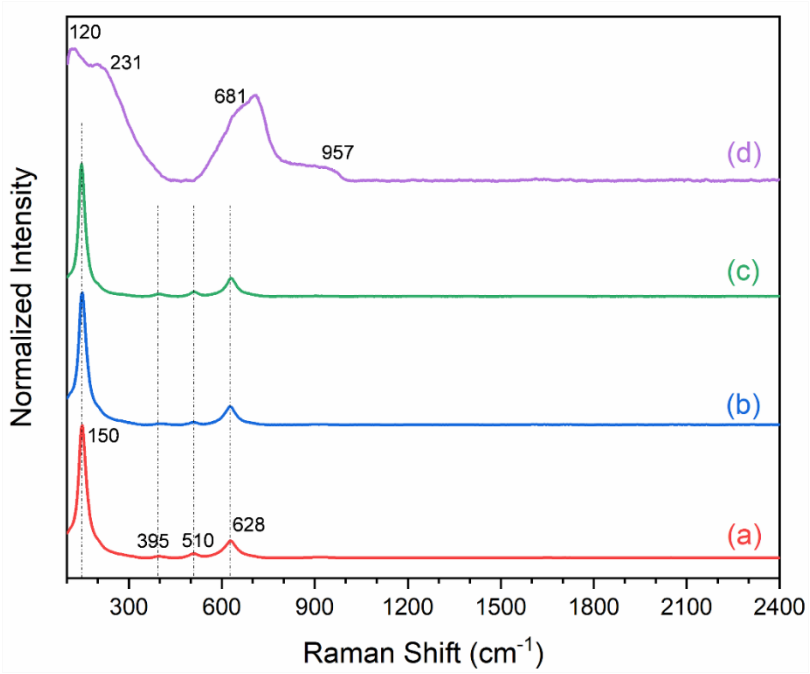

Figure 2. Raman spectra of final solid transformation products of (a) Ti_2C, (b) Ti_3C_2, (c) Ti_3CN, and (d) Nb_2C MXenes in aqueous solutions. Dashed vertical lines mark peak positions of TiO_2 anatase.

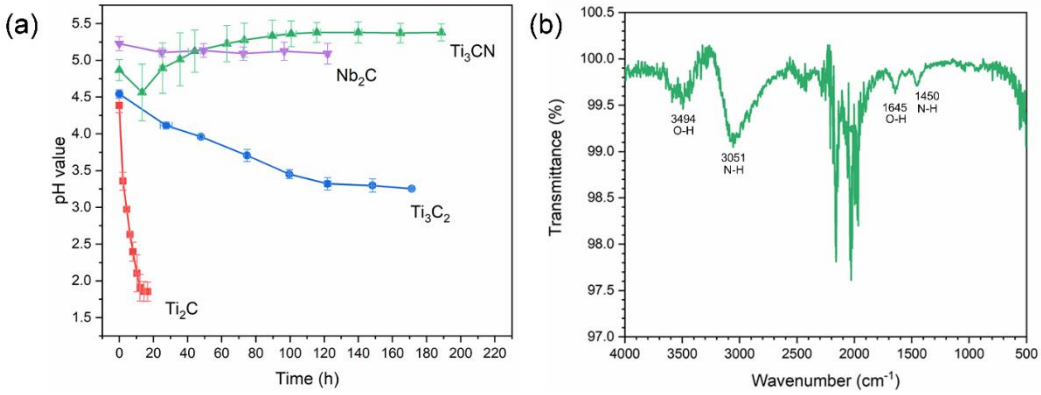

Figure 3. (a) Averaged pH values of Ti_2C, Ti_3C_2, Ti_3CN, and Nb_2C MXene aqueous colloidal solutions kept at 70 ^oC over time. Error bars indicate standard deviations in time and pH values. (b) ATR FTIR spectrum of liquid supernatant from a fully degraded Ti_3CN solution.

One of the unique advantages provided by MXenes is that they allow to disentangle the effects of material composition from the monolayer thickness effects on various

properties (chemical and others) of 2D materials, thus offering a rare opportunity for systematic fundamental studies of these effects in their most pure form.[21, 32] To illustrate the effects of the monolayer thickness and chemical composition of a MXene monolayer on reactivity of the material, we studied kinetics of transformations of different MXenes in water using Raman spectroscopy of gaseous decomposition products, comparing the rates of evolution of their common degradation product, CH_4, collected in conditions of Experiment 3 (Figure 4a, Table 1). Since the amount of air in the closed vials was fixed and was same for all samples, and assuming that N_2 will not react with MXenes, the amount of CH_4 divided by the amount of N_2 (from air in the vials) gives the relative amount of CH_4 formed in the reaction. Among two titanium carbide MXenes (Ti_2C and Ti_3C_2) CH_4 was produced much faster from Ti_2C than from Ti_3C_2, indicating that the transformation rate of the 3 atomic layer thick Ti_2C MXene is higher than the 5 atomic layer thick Ti_3C_2 MXene. Similar relative reactivities of these MXenes have been reported before.[21] This comparison gives a direct estimate of the effect of monolayer thickness within the same chemical composition and bonding on the reactivity of the 2D material. In contrast, both Ti_3C_2 and Ti_3CN have 5 atomic layer thick monolayer, but compared with Ti_3C_2, Ti_3CN reacts faster as evidenced by a higher CH_4 evolution rate (Figure 4a). In the structure of this titanium carbonitride MXene N atoms randomly substitute C atoms in X element sublattice,[33] thus either one acts as defects in the structure of another, and defected 2D material, as expected, has higher reactivity, perhaps explaining why Ti_3CN reacts faster than Ti_3C_2 MXene. This comparison gives a direct estimate of the effects of composition and defects on chemical properties of 2D materials with the same monolayer thickness. At this point we should also mention that other factors, such as MXene flake

size and the extent of exfoliation, presence of M and X vacancies, distribution of surface functional groups, *etc.* may also contribute to the differences in chemical reactivity. While detailed analysis of all these factors is needed in future studies, here we focused on just first of these factors, the relative differences in flake size and exfoliation extent of MXenes, measured using Dynamic Light Scattering (DLS) for MXene solutions and Atomic Force Microscopy (AFM) for dried MXene flakes on silicon (Supporting Information Figure S6 and S7, respectively). The results show that the thickness of our four MXenes is at a similar level (4-5 nm or ~3 monolayers), while the lateral flake size of Nb_2C is smaller compared with other MXenes. DLS size measurements give consistently smaller diameter values compared to lateral flake size measured by AFM. This is due to a known limitation of the standard DLS (which represents particles of any shape by spheres) when it is used for plate-like colloidal particles of 2D materials; however, the trends in size between our MXenes extracted from DLS are consistent with the AFM data. With the flake size results in mind, it is ever more interesting that Nb_2C, which is three atomic layer thick monolayer but in contrast to Ti_2C is composed of Nb and C, demonstrates strikingly different degradation kinetics compared to Ti_2C (Figure 4a). In fact, although Nb_2C flakes are the smallest, this material shows the lowest degradation rate among the four studied MXenes, thus indicating that the chemistry of 2D material not only depends on the monolayer thickness, but also on its chemical composition and the type of bonding within the monolayer. In this regard, again, MXenes provide an interesting opportunity for systematic studies of these effects in their most disentangled form, which was not possible before with any other family of 2D materials.

To investigate the role of temperature in MXene transformations, we studied kinetics of these processes at 70, 80, and 90 °C. The kinetic curves for each MXene at different temperatures are shown in Supporting Information (Figure S8), while the curves at the same temperature for different MXenes are shown in Figure S9. The rate constants calculated from the slopes of the lines fitting the initial parts of the kinetic curves were further used to produce the corresponding Arrhenius plots (Figure 4b). The activation energies calculated from the slopes of the Arrhenius plots are 1.62, 5.72, 0.31, and 2.43 kJ/mol for Ti_2C, Ti_3C_2, Ti_3CN, and Nb_2C MXenes, respectively.

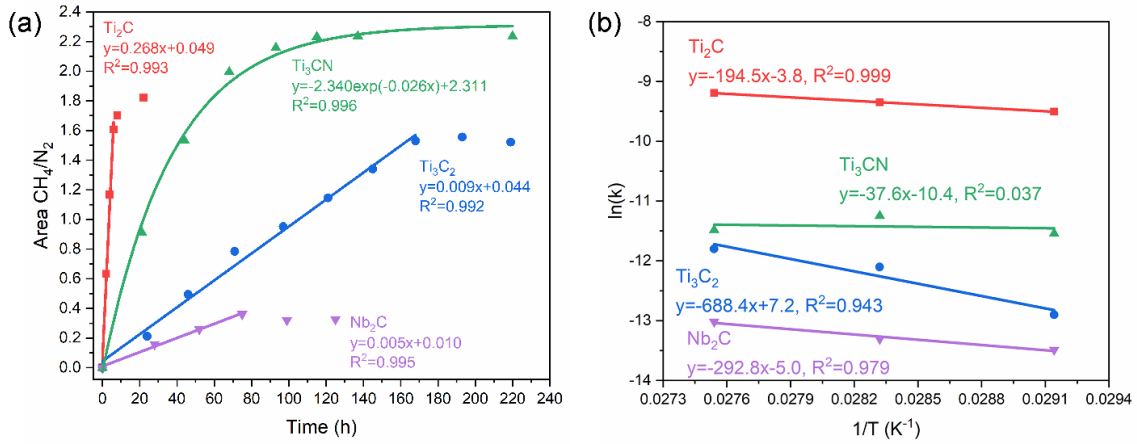

Figure 4. (a) Transformation kinetics of Ti_2C, Ti_3C_2, Ti_3CN, and Nb_2C MXenes in aqueous solutions at 70 °C. Solid lines represent fits to the corresponding color-coded equations indicated in the graph. (b) Arrhenius plots for transformations of Ti_2C, Ti_3C_2, Ti_3CN, and Nb_2C MXenes in water.

3. CONCLUSIONS

In summary, analysis of gaseous products resulting from chemical transformations of MXenes in aqueous environment was demonstrated as a powerful technique to study

chemistry of these materials. In particular, a combination of GC and Raman spectroscopy along with solution pH measurements was used as an efficient way to analyze the products of transformations of four different MXenes, including carbides and a carbonitride. According to experimental data, CH_4 is formed during reactions of carbide MXenes in water, whereas both CH_4 and NH_3 are formed during transformations of the Ti_3CN carbonitride MXene in water.

We further illustrate how to use the fundamental advantages provided by MXenes to disentangle and analyze the effects of monolayer thickness and composition on chemical properties of 2D materials. Transformation rates of MXenes with common transition metal in aqueous environment depend on the monolayer thickness and, additionally, are higher for Ti_3CN carbonitride compared to pure carbide MXenes. However, two MXenes with the same monolayer thickness but different transition metals in their structure (for example, Ti_2C and Nb_2C) may have vastly different chemical reactivities, thus demonstrating that chemical properties of 2D materials also depend on their chemical composition and type of bonding within the monolayer when the monolayer thickness and structure are otherwise same. In this context the effects of flake size are less important compared to the effects of monolayer thickness and composition. These results will be important for fundamental studies into chemistry of MXenes and other 2D materials and will also provide guidelines for development of many practical applications of MXenes where their stability is of paramount concern.

4. METHODS

4.1. SYNTHESIS OF MAX POWDERS

Ti_2AlC was synthesized by mixing TiC (typically 2 μm size powder, 99.5%, Alfa Aesar), Ti (-325 mesh, 99.5%, Alfa Aesar), and Al (-325 mesh, 99.5%, Alfa Aesar) powders in a 0.85:1.15:1.05 molar ratio for 12 h , followed by heating at 10 ^oC/min to 1400 ^oC and holding at this temperature for 4 h under Ar flow. Ti_3AlC_2 was synthesized by mixing Ti, Al, and graphite (-325 mesh, 99%, Alfa Aesar) powders in a 3:1.1:1.88 molar ratio for 12 h, followed by heating at 10 ^oC/min to 1550 ^oC and holding at this temperature for 2 h under Ar flow. Ti_3AlCN was synthesized by mixing Ti, AlN (10 μm size powder, 98%, Sigma-Aldrich), and graphite powders in a 3:1:1 molar ratio for 12 h, followed by heating at 10 ^oC/min to 1500 ^oC and holding at this temperature for 2 h under Ar flow. Nb_2AlC was synthesized by mixing Nb (-325 mesh, 99.8%, Alfa Aesar), Al, and graphite powders in a 2:1.1:1 molar ratio for 12 h, followed by heating at 5 ^oC/min to 1600 ^oC and holding at this temperature for 4 h under Ar flow. The resulting samples of MAX phase ceramics were manually crushed by mortar and pestle.

4.2. SYNTHESIS OF MXENE AND SAMPLE PREPARATION

Synthesis of Ti_2C and Ti_3C_2 MXenes was described before.[21] The as-synthesized powder of a MAX phase (Ti_2AlC or Ti_3AlC_2, 0.5g, 325 mesh, particle size < 38 μm) was slowly added to the etchant prepared by dissolving 0.5 g LiF (97%, Alfa Aesar) in 5 ml of 9 M HCl (36 wt%, Alfa Aesar) in a plastic centrifuge tube. The mixture was stirred for 36 h at 35 ^oC.

Ti_3CN MXene was synthesized from Ti_3AlCN MAX phase.[34] 0.5 g of Ti_3AlCN powder (325 mesh, particle size < 38 µm) was slowly added to the etchant, prepared by dissolving 0.8 g LiF in 10 ml of 9 M HCl in a plastic centrifuge tube. The mixture was stirred for 18 h at 40 ^oC.

Nb_2C MXene was synthesized from Nb_2AlC MAX phase. 0.5 g of Nb_2AlC powder (325 mesh, particle size < 38 µm) was slowly added to the etchant, prepared by dissolving 1.0 g LiF in 10 ml of 12 M HCl in a plastic centrifuge tube. The mixture was stirred for 96 h at 60 ^oC.

After etching, the mixtures were washed with deionized water several times until the pH of the supernatant reached ~6. MXene aqueous colloidal solutions were obtained *via* 30 min room temperature bath ultra-sonication (Bransonic M2800H) followed by 1 h centrifugation (Thermo Fisher Scientific Sorvall ST8 Centrifuge) at 3500 rpm. DI water used in this study was not deaerated. The concentrations of the freshly prepared MXene colloidal solutions were measured by weight after drying 5 aliquots (500 uL each) of the solution on small pieces of weighing paper and averaging the results. The UV-vis spectra and photographs of as prepared MXene colloids are shown in Figure S1. Each fresh as-received MXene colloidal solution was used to carry out Experiments 1-3 as described below.

For Experiment 1 (Figure S2a), three 10 ml headspace vials (Wheaton, 18mm diameter) were fully filled with MXene colloidal solutions to the rim to ensure that no air bubbles remained in the vial and sealed by a threaded cap with septum. A Metcal 22 gauge polypropylene needle (to avoid potential hydrogen evolution due to reaction of metal needle with the acidic aqueous liquid) was inserted into each vial through the septum and

the vials were placed upside down into a large beaker partially filled with DI water so that the open ends of the plastic needles were submerged into water for the entire duration of the experiment to prevent air coming into the system while providing outlet for liquid pushed out of the vials by the evolving gas. The whole setup was placed in a 70 ^{o}C oven to accelerate the reaction. The initial concentrations of different MXenes used in this experiment were 3.83, 2.80, 3.74, and 1.10 mg/ml for Ti_2C, Ti_3C_2, Ti_3CN, and Nb_2C, respectively.

For Experiment 2 (Figure S2b), 10 ml of each MXene colloidal solution was transferred into a 20 ml glass vial (Wheaton, borosilicate glass vial with polypropylene foamed polyethylene lined screw cap) and kept in a 70 ^{o}C sand bath until complete degradation. The pH of the solution was measured every day after the sample was cooled down to RT. The vial was placed back into the sand bath immediately after pH measurement. The measurements were carried out until pH of the solution became stable, indicating complete degradation of the MXene, which was also evident visually. After that, the dispersions were centrifuged at 4500 rpm for 20 min to precipitate the solids. The sediment from degradation of each MXene was collected, rinsed with DI water, and analyzed with Raman spectroscopy. In addition, the supernatant from Ti_3CN degradation was collected and analyzed in liquid form by ATR FTIR. The initial concentrations of different batches of MXenes used in this experiment are shown in Figure S5 (Supporting Information).

For Experiment 3 (Figure S2c), 6 ml of each MXene solution were transferred into a 10 ml headspace vial, sealed, and placed upside down to prevent gas escape through the cap. These vials contained around half volume of ambient air in addition to MXene

colloidal solution. The vials were stored at 70, 80, and 90 ^{o}C, correspondingly, in an oven and Raman spectroscopy was used to analyze gas phase directly through the walls of the vials over time without opening them upon cooling to RT. After the measurement, the vials were immediately returned back to the oven at the corresponding temperature until the next measurement (typically on the following day except T_2C MXene that was measured every 2 h). The initial concentrations of different batches of MXenes used in this experiment are shown in Figure S8 and S9 (Supporting Information).

ASSOCIATED CONTENT

SUPPORTING INFORMATION

The supporting information is available free of charge on the ACS Publications website.

UV-vis spectra and photographs of MXene aqueous colloidal solutions; schematics of Experiments 1 - 3; bond length calculation from rotational Raman spectrum of the gas phase collected during transformation of Ti_2C in water; EDS and SEM of the solid degradation products from MXenes; pH values of MXene aqueous colloidal solutions kept at 70 ^{o}C; DLS data for MXene colloidal solutions; AFM images and line scan profiles for MXene flakes on Si wafers; degradation kinetics of MXenes in aqueous solutions at 70, 80, and 90 ^{o}C.

The authors declare no competing financial interests.

AUTHOR INFORMATION

CORRESPONDING AUTHOR

*Vadym N. Mochalin: mochalinv@mst.edu

ACKNOWLEDGEMENTS

The authors thank G. Hulliung (Missouri S&T) for help with MXene synthesis and pH measurements. This work was partially supported by the National Science Foundation under Grant No. MoMS 1930881.

SUPPORTING INFORMATION

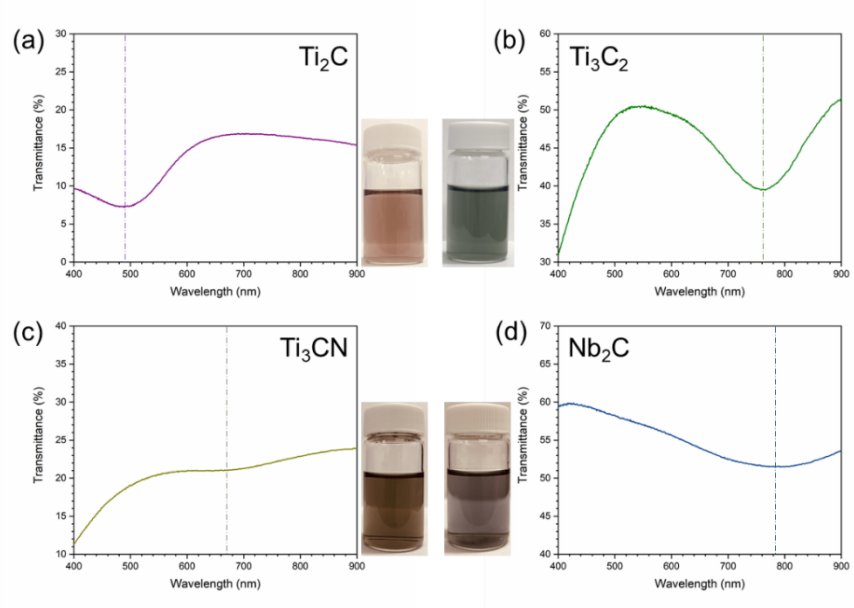

Figure S1. UV-vis spectra and optical photographs of diluted (a) Ti_2C, (b) Ti_3C_2, (c) Ti_3CN, and (d) Nb_2C aqueous colloidal solutions. Vertical lines mark positions of the corresponding plasmon resonance peaks that determine color of the colloidal solutions.

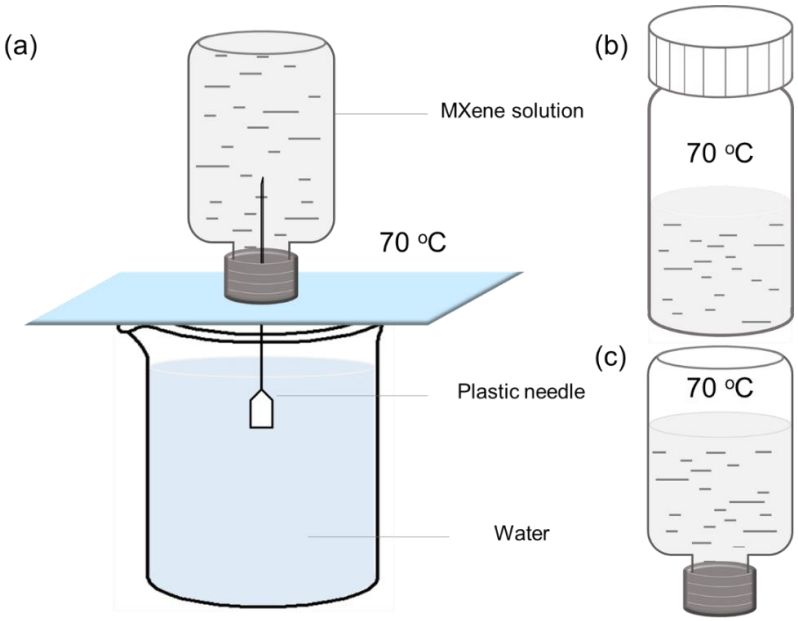

Figure S2. Schematics of (a) Experiment 1, (b) Experiment 2 and (c) Experiment 3.

CHARACTERIZATION

Gas collected due to transformations of Ti_2C, Ti_3C_2, Ti_3CN, and Nb_2C MXenes in water from Experiment 1 was analyzed with a Thermal Scientific Trace-1300 gas chromatograph equipped with a fused silica capillary column (Carboxen 1006 PLOT, length 30 m, diameter 0.53 mm and 30 µm thickness) and a thermal conductivity detector (TCD). Helium was used as the carrier and reference gas, with the flow rate 4 and 4.3 ml/min, respectively. Other parameters of GC analysis: purge flow 5 ml/min, oven, TCD detector, and TCD filament temperatures 35, 230, and 280 ^{o}C, respectively. For each measurement, 0.1 ml of gas was manually injected with 1 ml gastight syringe (Hamilton).

Raman spectroscopy was performed to analyze the gas phase composition in the vials in Experiment 1 and 3 without opening the vials. Renishaw InVia confocal Raman micro-spectrometer with 532 nm laser and a 1200 l mm^{-1} grating was used for spectra acquisition. 20x objective was employed to record spectra for Experiment 1 and 5x

objective for Experiment 3. The laser beam travelling through the glass wall of the vial was carefully focused inside the gas bubble using confocal microscope. The Raman spectra of the gas were acquired with 20 s exposure time, 100% of laser power and 10 accumulations. The Raman spectra of solid products collected from Experiment 2 were recorded with 532 nm laser, 100x objective and a 1200 l mm^{-1} grating. The spectra of the solid products were acquired with 10 s exposure time, 5% of laser power (to minimize their laser induced damage) and 20 accumulations.

UV−vis spectra of Ti_2C, Ti_3C_2, Ti_3CN, and Nb_2C MXene colloidal solutions were recorded in a quartz cuvette (1 cm optical path length) in the wavelength range of 400−900 nm using a fiber optics QE Pro UV−vis spectrometer (Ocean Optics).

Elemental maps of the MXene solid degradation products were produced using SEM-EDS. The SEM images and EDS maps were acquired with an FEI Helios Nanolab Dual-beam microscope at 20 kV accelerating voltage and 5-8 mm working distance.

Attenuated total reflection (ATR) FTIR spectrum of dissolved degradation products of Ti_3CN MXene was recorded in the range 500-4000 cm^{-1} from a drop of solution directly applied on the surface of the ATR crystal using Nicolet iS50 FT-IR spectrum analyzer.

pH measurements were conducted using a METTLER TOLEDO S30 SevenEasy pH meter equipped with a Fisher Scientific accumet (Catalog No. 13-620-631) electrode.

BOND LENGTH CALCULATION FROM ROTATIONAL RAMAN SPRCTRUM OF GAS PHASE

The bond length of CH_4 was calculated from Raman rotational spectrum (Figure S3) using the moment of inertia of a spherical rotor and mass of H atom according to the equation [35]:

$$I = \frac{8}{3} m_H R^2 \quad (1)$$

where m_H is the mass of H atom in kg, R is the bond length of CH_4 in m, I is the moment of inertia of a spherical rigid rotor representing CH_4, which can be calculated using the equation:

$$B = \frac{h}{8\pi^2 cI} \quad (2)$$

where B is the rotational constant in m^{-1} that is measured directly from the experimental rotational spectrum where the peaks are spaced by the amount equal $4B$, as shown in Figure S3,[36] h is the Planck constant, and c is the speed of light.

Using this procedure, the calculated bond length is $1.09 \times 10^{-10}\, m$, perfectly matching the known C-H bond length in methane.[37]

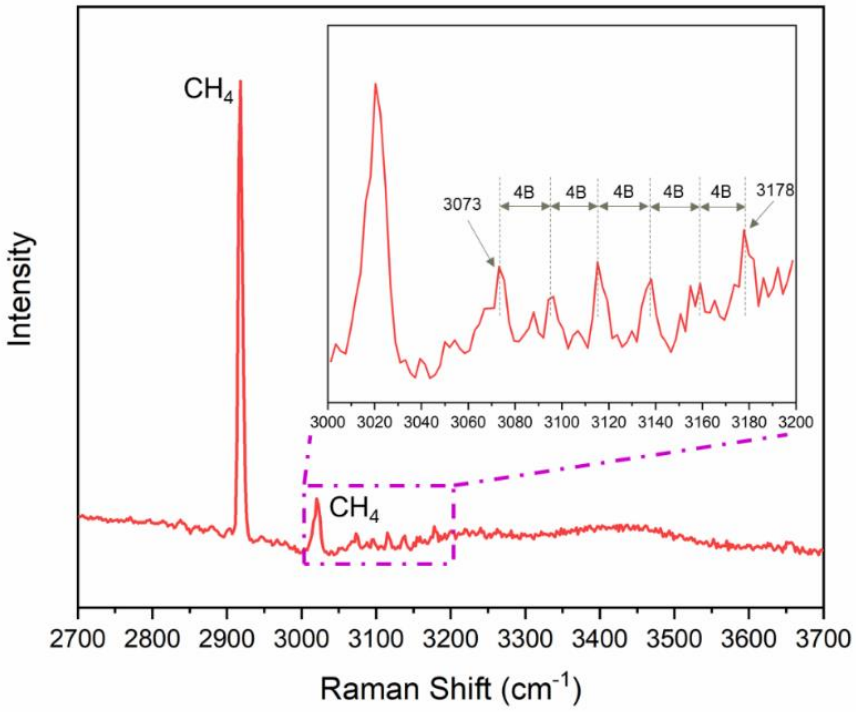

Figure S3. Raman spectrum of the gas phase collected from Ti_2C colloidal solution in water.

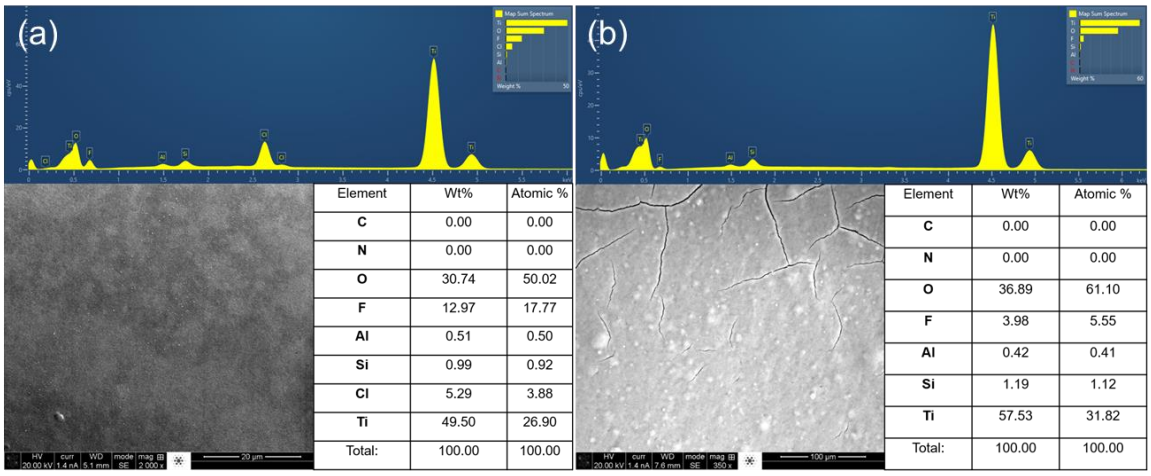

Element	Wt%	Atomic %
C	0.00	0.00
N	0.00	0.00
O	30.74	50.02
F	12.97	17.77
Al	0.51	0.50
Si	0.99	0.92
Cl	5.29	3.88
Ti	49.50	26.90
Total:	100.00	100.00

Element	Wt%	Atomic %
C	0.00	0.00
N	0.00	0.00
O	36.89	61.10
F	3.98	5.55
Al	0.42	0.41
Si	1.19	1.12
Ti	57.53	31.82
Total:	100.00	100.00

Figure S4. EDS and SEM of solid degradation products collected from (a) Ti_2C and (b) Ti_3CN aqueous colloidal solutions upon complete MXene degradation.

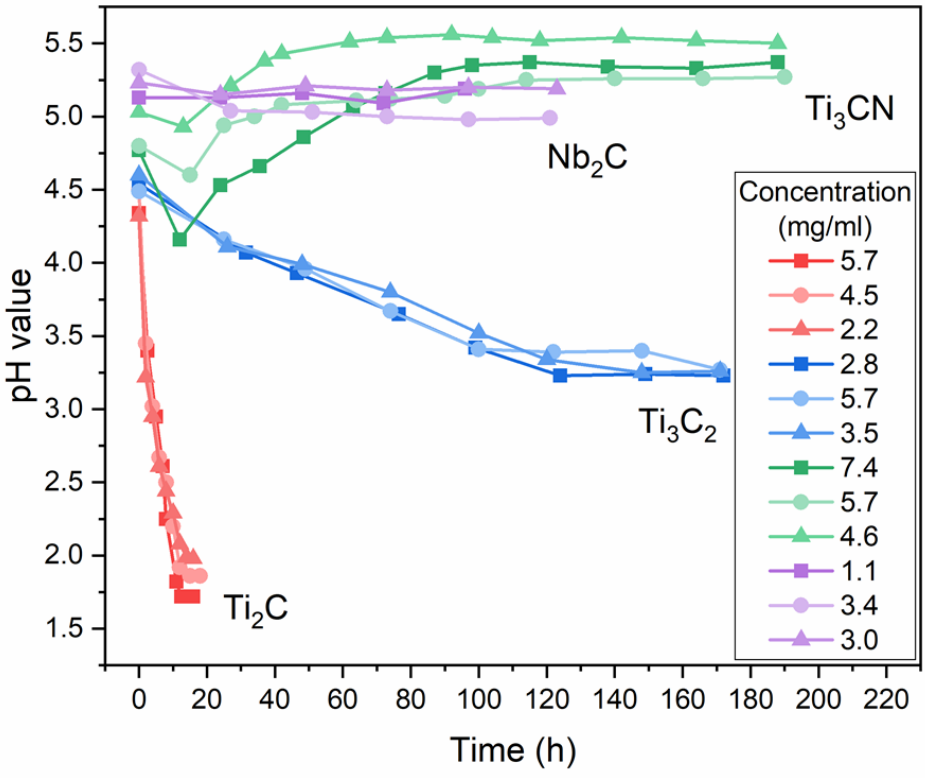

Figure S5. pH values of Ti_2C, Ti_3C_2, Ti_3CN, and Nb_2C aqueous colloidal solutions kept at 70 ^oC over time. Initial concentrations of MXene solutions are indicated for each experiment.

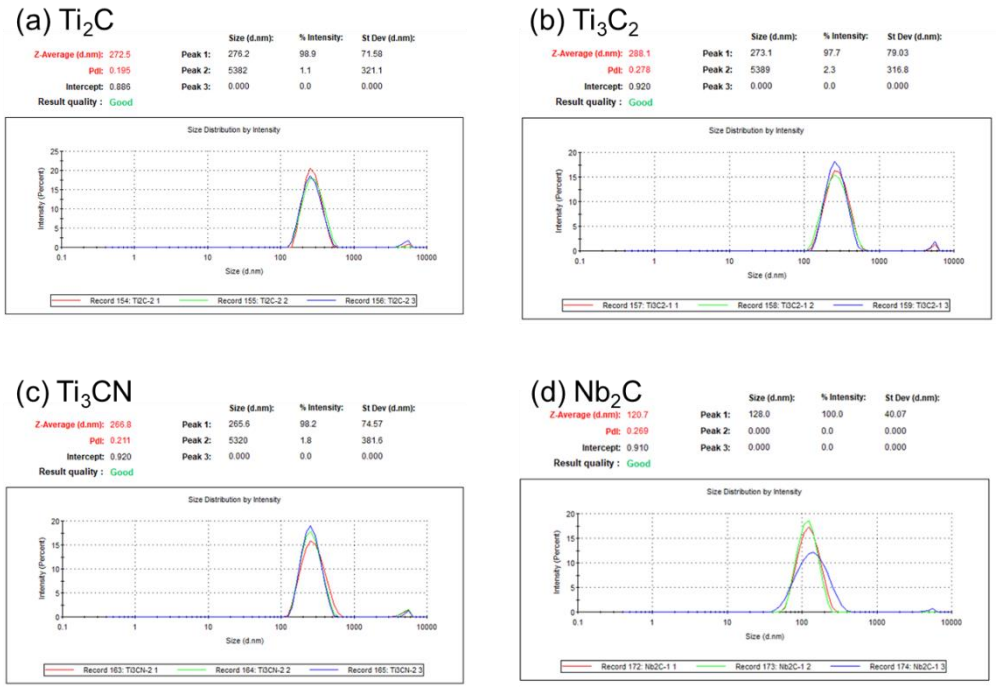

Figure S6. DLS particle size (diameter) in (a) Ti_2C, (b) Ti_3C_2, (c) Ti_3CN, and (d) Nb_2C aqueous colloidal solutions.

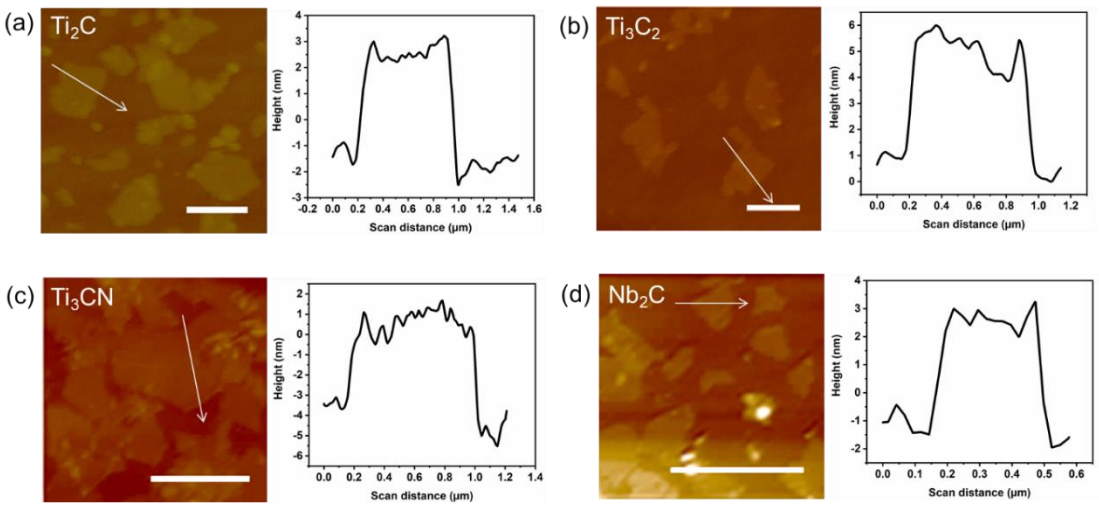

Figure S7. AFM images and line scan profiles for (a) Ti_2C, (b) Ti_3C_2, (c)Ti_3CN, and (d) Nb_2C flakes deposited from their freshly prepared aqueous colloidal solutions deposited and dried on Si wafers. Scale bars are 1 μm.

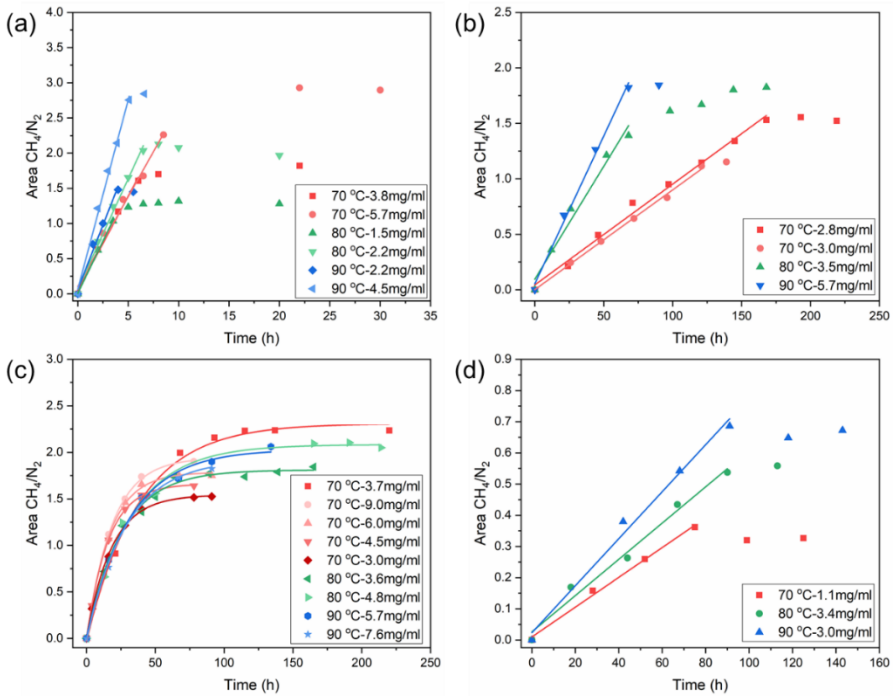

Figure S8. Degradation kinetics of (a) Ti_2C, (b) Ti_3C_2, (c) Ti_3CN, and (d) Nb_2C MXenes in aqueous solutions at 70, 80, and 90 °C. Solid lines represent fits according to the corresponding linear or exponential fits. Initial concentrations of MXene solutions are indicated for each experiment.

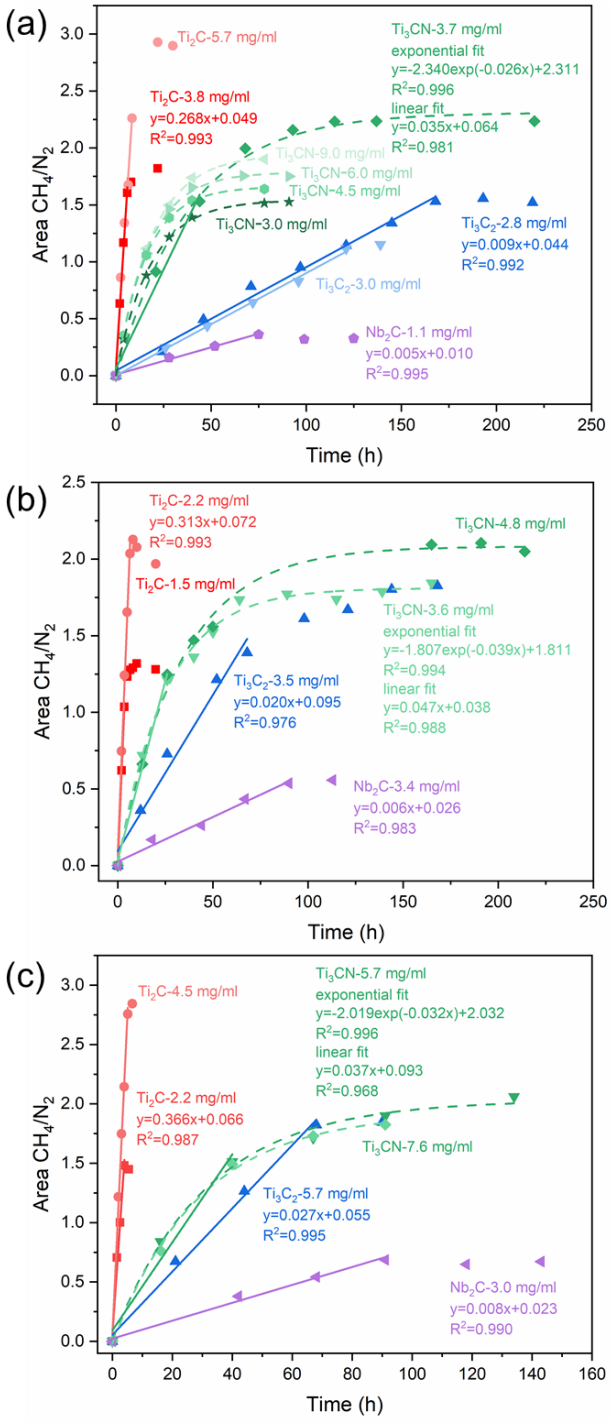

Figure S9. Degradation kinetics of Ti_2C, Ti_3C_2, Ti_3CN, and Nb_2C MXenes in aqueous solutions at (a) 70 ^oC, (b) 80 ^oC, and (c) 90 ^oC. Solid and dash lines represent the corresponding color coded linear (all MXenes) or non-linear (in case of Ti_3CN) fits. Initial concentrations of MXene solutions are indicated for each experiment.

REFERENCES

[1] M. Naguib, M. Kurtoglu, V. Presser, J. Lu, J.J. Niu, M. Heon, L. Hultman, Y. Gogotsi, M.W. Barsoum, Two-dimensional nanocrystals produced by exfoliation of Ti_3AlC_2, *Advanced Materials*, 23 (**2011**) 4248-4253.

[2] M. Naguib, V.N. Mochalin, M.W. Barsoum, Y. Gogotsi, 25th anniversary article: MXenes: A new family of two‐dimensional materials, *Advanced Materials*, 26 (**2014**) 992-1005.

[3] M. Alhabeb, K. Maleski, B. Anasori, P. Lelyukh, L. Clark, S. Sin, Y. Gogotsi, Guidelines for synthesis and processing of two-dimensional titanium carbide ($Ti_3C_2T_x$ MXene), *Chemistry of Materials*, 29 (**2017**) 7633-7644.

[4] M. Naguib, O. Mashtalir, J. Carle, V. Presser, J. Lu, L. Hultman, Y. Gogotsi, M.W. Barsoum, Two-dimensional transition metal carbides, *ACS Nano*, 6 (**2012**) 1322-1331.

[5] Y. Dong, S. Chertopalov, K. Maleski, B. Anasori, L. Hu, S. Bhattacharya, A.M. Rao, Y. Gogotsi, V.N. Mochalin, R. Podila, Saturable absorption in 2D Ti_3C_2 MXene thin films for passive photonic diodes, *Advanced Materials*, 30 (**2018**) 1705714.

[6] J. Yi, L. Du, J. Li, L. Yang, L. Hu, S. Huang, Y. Dong, L. Miao, S. Wen, V.N. Mochalin, Unleashing the potential of Ti_2CT_x MXene as a pulse modulator for mid-infrared fiber lasers, *2D Materials*, 6 (**2019**) 045038.

[7] S. Chertopalov, V.N. Mochalin, Environment sensitive photoresponse of spontaneously partially oxidized $Ti_3C_2T_x$ MXene thin films, *ACS Nano*, 12 (**2018**) 6109-6116.

[8] S. Xu, Y. Dall'Agnese, G. Wei, C. Zhang, Y. Gogotsi, W. Han, Screen-printable microscale hybrid device based on MXene and layered double hydroxide electrodes for powering force sensors, *Nano Energy*, 50 (**2018**) 479-488.

[9] S.J. Kim, H.J. Koh, C.E. Ren, O. Kwon, K. Maleski, S.Y. Cho, B. Anasori, C.K. Kim, Y.K. Choi, J. Kim, Y. Gogotsi, H.T. Jung, Metallic $Ti_3C_2T_x$ MXene gas sensors with ultrahigh signal-to-noise ratio, *ACS Nano*, 12 (**2018**) 986-993.

[10] G. Li, K. Kushnir, Y. Dong, S. Chertopalov, A.M. Rao, V.N. Mochalin, R. Podila, L.V. Titova, Equilibrium and non-equilibrium free carrier dynamics in 2D $Ti_3C_2T_x$ MXenes: THz spectroscopy study, *2D Materials*, 5 (**2018**) 035043.

[11] G. Li, N. Amer, H. Hafez, S. Huang, D. Turchinovich, V.N. Mochalin, F.A. Hegmann, L.V. Titova, Dynamical control over terahertz electromagnetic interference shielding with 2D $Ti_3C_2T_y$ MXene by ultrafast optical pulses, *Nano Letters*, 20 (**2019**) 636-643.

[12] C. Zhang, S. Pinilla, N. McEvoy, C.P. Cullen, B. Anasori, E. Long, S.H. Park, A. Seral-Ascaso, A. Shmeliov, D. Krishnan, Oxidation stability of colloidal 2D titanium carbides (MXenes), *Chemistry of Materials*, 29 (**2017**) 4848-4856.

[13] A. Lipatov, M. Alhabeb, M.R. Lukatskaya, A. Boson, Y. Gogotsi, A. Sinitskii, Effect of synthesis on quality, electronic properties and environmental stability of individual monolayer Ti_3C_2 MXene flakes, *Advanced Electronic Materials*, 2 (**2016**) 1600255.

[14] T. Habib, X. Zhao, S.A. Shah, Y. Chen, W. Sun, H. An, J.L. Lutkenhaus, M. Radovic, M.J. Green, Oxidation stability of $Ti_3C_2T_x$ MXene nanosheets in solvents and composite films, *npj 2D Materials and Applications*, 3 (**2019**) 8.

[15] G. Li, K. Jiang, S. Zaman, J. Xuan, Z. Wang, F. Geng, Ti_3C_2 sheets with an adjustable surface and feature sizes to regulate the chemical stability, *Inorganic Chemistry*, 58 (**2019**) 9397-9403.

[16] V. Natu, J.L. Hart, M. Sokol, H. Chiang, M.L. Taheri, M.W. Barsoum, Edge capping of 2D ‐ MXene sheets with polyanionic salts to mitigate oxidation in aqueous colloidal suspensions, *Angewandte Chemie International Edition*, 58 (**2019**) 12655-12660.

[17] X. Zhao, A. Vashisth, E. Prehn, W. Sun, S.A. Shah, T. Habib, Y. Chen, Z. Tan, J.L. Lutkenhaus, M. Radovic, Antioxidants unlock shelf-stable $Ti_3C_2T_x$ (MXene) nanosheet dispersions, *Matter*, 1 (**2019**) 513-526.

[18] O. Mashtalir, K.M. Cook, V.N. Mochalin, M. Crowe, M.W. Barsoum, Y. Gogotsi, Dye adsorption and decomposition on two-dimensional titanium carbide in aqueous media, *Journal of Materials Chemistry A*, 2 (**2014**) 14334-14338.

[19] M. Naguib, O. Mashtalir, M.R. Lukatskaya, B. Dyatkin, C. Zhang, V. Presser, Y. Gogotsi, M.W. Barsoum, One-step synthesis of nanocrystalline transition metal oxides on thin sheets of disordered graphitic carbon by oxidation of MXenes, *Chem Communications*, 50 (**2014**) 7420-7423.

[20] Y. Lee, S.J. Kim, Y.J. Kim, Y. Lim, Y. Chae, B.J. Lee, Y.T. Kim, H. Han, Y. Gogotsi, C.W. Ahn, Oxidation-resistant titanium carbide MXene films, *Journal of Materials Chemistry A*, 8 (**2020**) 573-581.

[21] S. Huang, V.N. Mochalin, Hydrolysis of 2D transition-metal carbides (MXenes) in colloidal solutions, *Inorganic Chemistry*, 58 (**2019**) 1958-1966.

[22] W.H. Philipp, Chemical Reactions of Carbides, Nitrides, and Diborides of Titanium and Zirconium and Chemical Bonding in These Compounds, in, NASA Lewis Research Center, Washington, **1966**, pp. 1-20.

[23] M.C. Sneed, Comprehensive Inorganic Chemistry, Van Nostrand, New York, **1953**.

[24] H. Remy, Treatise on Inorganic Chemistry, 11th ed., Elsevier Pub. Co., Amsterdam, **1956**.

[25] A.I. Avgustinik, G.V. Drozdetskaya, S.S. Ordan'yan, Reaction of titanium carbide with water, *Powder Metall Met Ceram*, 6 (**1967**) 470-473.

[26] C. Wang, Y.L. Pan, S.C. Hill, B. Redding, Photophoretic trapping-Raman spectroscopy for single pollens and fungal spores trapped in air, *Journal of Quantitative Spectroscopy and Radiative Transfer*, 153 (**2015**) 4-12.

[27] Z. Du, X. Zhang, S. Xi, L. Li, Z. Luan, C. Lian, B. Wang, J. Yan, *In situ* Raman spectroscopy study of synthetic gas hydrate formed by cold seep flow in the South China Sea, *Journal of Asian Earth Sciences*, 168 (**2018**) 197-206.

[28] T. Su, R. Peng, Z.D. Hood, M. Naguib, I.N. Ivanov, J.K. Keum, Z. Qin, Z. Guo, Z. Wu, One‐step synthesis of Nb_2O_5/C/Nb_2C (MXene) composites and their use as photocatalysts for hydrogen evolution, *ChemSusChem*, 11 (**2018**) 688-699.

[29] M. Seredych, C.E. Shuck, D. Pinto, M. Alhabeb, E. Precetti, G. Deysher, B. Anasori, N. Kurra, Y. Gogotsi, High-temperature behavior and surface chemistry of carbide MXenes studied by thermal analysis, *Chemistry of Materials*, 31 (**2019**) 3324-3332.

[30] C. Sun, D. Xu, D. Xue, Direct *in situ* ATR-IR spectroscopy of structural dynamics of $NH_4H_2PO_4$ in aqueous solution, *CrystEngComm*, 15 (**2013**) 7783-7791.

[31] M. Thämer, L. De Marco, K. Ramasesha, A. Mandal, A. Tokmakoff, Ultrafast 2D IR spectroscopy of the excess proton in liquid water, *Science*, 350 (**2015**) 78-82.

[32] Y. Li, S. Huang, C. Wei, C. Wu, V.N. Mochalin, Adhesion of two-dimensional titanium carbides (MXenes) and graphene to silicon, *Nature Communications*, 10 (**2019**) 1-8.

[33] F. Du, H. Tang, L. Pan, T. Zhang, H. Lu, J. Xiong, J. Yang, C.J. Zhang, Environmental friendly scalable production of colloidal 2D titanium carbonitride MXene with minimized nanosheets restacking for excellent cycle life lithium-ion batteries, *Electrochimica Acta*, 235 (**2017**) 690-699.

[34] J.L. Hart, K. Hantanasirisakul, A.C. Lang, B. Anasori, D. Pinto, Y. Pivak, J.T. van Omme, S.J. May, Y. Gogotsi, M.L. Taheri, Control of MXenes' electronic properties through termination and intercalation, *Nature Communications*, 10 (**2019**) 1-10.

[35] P.W. Atkins, J. De Paula, J. Keeler, Atkins' Physical Chemistry, 8th ed., Oxford University Press, New York, **2018**.

[36] P.F. Bernath, Spectra of Atoms and Molecules, 4th ed., Oxford University Press, New York, **2020**.

[37] M. Silberberg, Chemistry: The Molecular Nature of Matter and Change, 8th ed., McGraw-Hill, Boston, **2018**.

III. ADHESION OF TWO-DIMENSIONAL TITANIUM CARBIDES (MXENES) AND GRAPHENE TO SILICON

Yanxiao Li[1‡], Shuohan Huang[2‡], Congjie Wei[1], Chenglin Wu[1*], Vadym N. Mochalin[2,3*]
[1]Department of Civil, Architectural, and Environmental Engineering, Missouri University of Science and Technology, Rolla, MO 65409, USA
[2]Department of Chemistry, Missouri University of Science and Technology, Rolla, MO 65409, USA
[3]Department of Materials Science and Engineering, Missouri University of Science and Technology, Rolla, MO 65409, USA
[‡] These authors contributed equally to the study
* Corresponding author E-mail: wuch@mst.edu, mochalinv@mst.edu

ABSTRACT

Two-dimensional transition metal carbides (MXenes) have attracted a great interest of the research community as a relatively recently discovered large class of materials with unique electronic and optical properties. Understanding of adhesion between MXenes and various substrates is critically important for MXene device fabrication and performance. We report results of direct atomic force microscopy (AFM) measurements of adhesion of two MXenes ($Ti_3C_2T_x$ and Ti_2CT_x) with a SiO_2 coated Si spherical tip. The Maugis-Dugdale theory was applied to convert the AFM measured adhesion force to adhesion energy, while taking into account surface roughness. The obtained adhesion energies were compared with those for mono-, bi-, and tri-layer graphene, as well as SiO_2 substrates. The average adhesion energies for the MXenes are 0.90 ± 0.03 J m^{-}2 and 0.40 ± 0.02 J m^{-2} for thicker $Ti_3C_2T_x$ and thinner Ti_2CT_x, respectively, which is of the same order of magnitude as that between graphene and silica tip.

1. INTRODUCTION

A large family of two-dimensional (2D) transition metal carbides and nitrides (MXenes) have emerged over the past few years as a class of materials with superior and highly tunable electronic and optical properties [1, 2]. These properties render MXenes prospective materials for supercapacitors [3, 4], Li-ion and beyond Li-ion batteries [5, 6], triboelectric generators [7], photonic diodes and Q-switched lasers [8], sensors [9, 10], composites [11, 12], etc. More than 20 different MXenes have been synthesized by selective A element extraction with fluorine-containing etchants from bulk ternary compounds known as MAX phases [1, 13]. MXenes have a general formula $M_{n+1}X_nT_x$, where M represents an early transition metal (Ti, Zr, V, Nb, Ta, Cr, Mo, Sc, etc.), X is carbon or nitrogen, and n is an integer. T denotes the terminating functional groups (fluorine, hydroxyl, and other oxygen-containing groups) attached to MXene basal surfaces during synthesis [14-16]. Among experimentally available MXenes, $Ti_3C_2T_x$ and Ti_2CT_x are some of the most widely investigated. MXenes are intrinsically hydrophilic and yet, they have demonstrated higher electrical conductivity than solution processed graphene [17]. In addition, their exceptional electrochemical properties show great promise for flexible electronics and planar devices [18]. There are studies on MXene dispersions in organic solvents for incorporation into polymers, inks, etc [19]. As researchers move closer to device fabrication, adhesion to different materials, as well as other mechanical properties of MXenes become of greater importance. There is a handful of published data on the mechanical behavior of MXenes. Theoretical calculations using molecular dynamics (MD) have predicted the Young's modulus of 597 GPa for bare Ti_2C and 502 GPa for bare Ti_3C_2

MXenes [20], whereas a recent experimental AFM indentation study of a single suspended $Ti_3C_2T_x$ MXene flake reported the value of 333 ± 30 GPa [21]. Although no other experimental data for $Ti_3C_2T_x$ or Ti_2CT_x are available for comparison, the agreement between MD derived and experimental Young's modulus is fairly good, taking into account the defective structure and surface terminations in real MXene samples that have not been captured in the simulations. MD modeling has also predicted a high bending rigidity of MXenes compared to single atomic layer 2D materials like graphene and hexagonal BN [22], an important result for the development of sensing applications of 2D materials. However, to our knowledge, no theoretical or experimental studies of adhesive properties of MXenes have been reported to date.

Nanoindentation has been widely used to characterize adhesion of thin films [23-25]. In recent years, the adhesive interactions of monolayer and a few layer 2D materials have been intensively investigated. One of the important questions is to understand how the properties, in particular adhesive strength, change when transitioning from bulk to 2D form of a material. Answering this fundamental question will require systematic studies of the property (e.g., adhesive strength) while varying the thickness of a material without changing its atomic composition or type of bonding within the material. From this standpoint, the MXenes family represents another unique and still widely underutilized advantage, allowing to systematically change the thickness of the monolayer without changing the type of bonding or elemental composition of the material (e.g., going from Ti_2C to Ti_3C_2 to Ti_4C_3, etc. within the same family of titanium carbide MXenes). Other 2D materials have fixed monolayer thickness and thus would not allow the systematic study

of a property as a function of their monolayer thickness disentangled from other variables, such as elemental composition, chemical bonding, etc.

In this work, AFM was used to measure the adhesive properties of two MXenes ($Ti_3C_2T_x$, Ti_2CT_x), as well as the mono-layer, bi-layer, and tri-layer graphene interacting with the oxidized silicon tip. The force-displacement responses were evaluated and compared. The measured adhesion force was converted into the adhesion energy using the Maugis-Dugdale [26] theory and taking surface roughness into consideration. The experimentally measured adhesion energy between $Ti_3C_2T_x$ and SiO_2 is 0.90 ± 0.03 J m^{-2}, which is higher than that of Ti_2CT_x (0.40 ± 0.02 J m^{-2}), thus the monolayer thickness was found to have a significant effect on the adhesion energy. However, in contrast to our experimental data for graphene, the number of MXene monolayers in a stacked MXene structure was found to have little impact on the adhesion energy.

2. RESULTS

2.1. SURFACE PROFILE

The surface roughness of the two types of MXene flakes was characterized using AFM scans in tapping mode with a 3 nm radius tip as shown in Figure.1a. The RMS values for the MXene flake (Figure. 1b) are almost same as for SiO_2 surface, indicating that MXene flakes are very thin and conform closely to the substrate.

Typical line scans for MXene films of different thicknesses are shown in Figure. 2a for $Ti_3C_2T_x$ and Figure 2b for Ti_2CT_x. The sharp changes in height at both sides of the line scans indicate the edges of the flakes. The horizontal length of the curves' plateaus

gives the average size of the MXene flakes between the two edges. The average RMS values for $Ti_3C_2T_x$ and Ti_2CT_x films (excluding the potentially oxidized edges) with different thicknesses were calculated and presented in Figure 2c, d, respectively. Compared with the corresponding average thickness, the RMS values are relatively low (59–70 pm for $Ti_3C_2T_x$, 69–87 pm for Ti_2CT_x) and within 5% of the corresponding thickness (compare top and bottom panels in Figure 2), indicating relatively flat MXene surfaces. As follows from Figure 2c, d, no clear thickness (i.e., the number of MXene monolayers) dependency was observed for the measured RMS values of the MXene films. The average RMS values were used in calculating the adhesion energies (below).

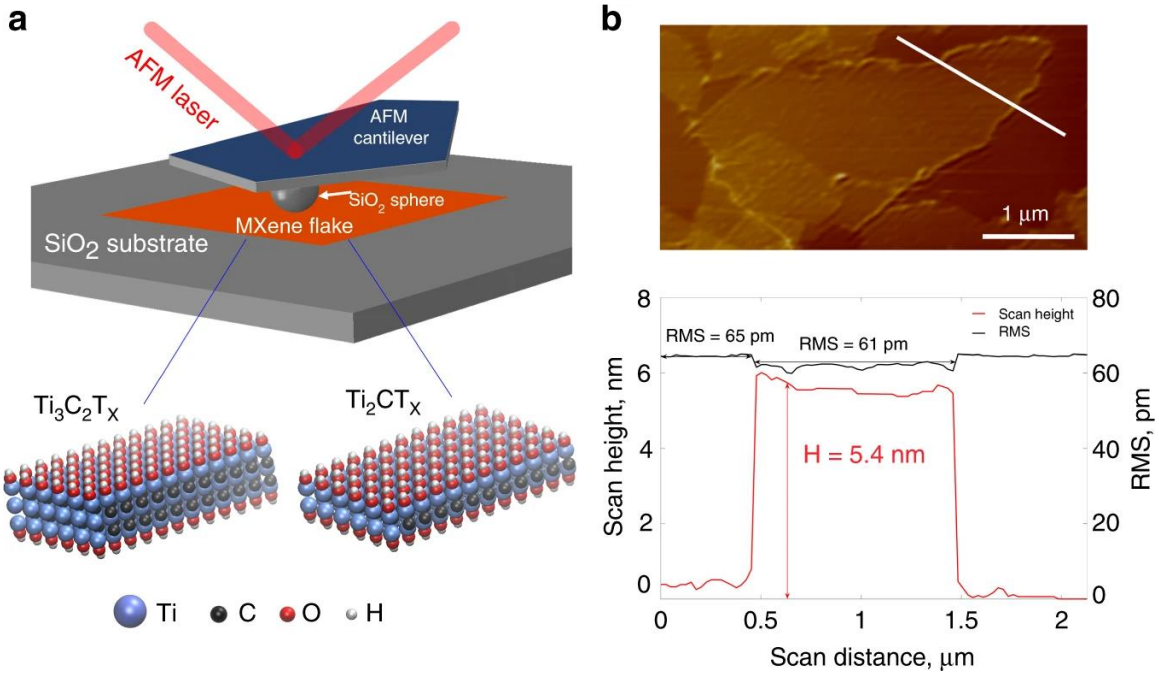

Figure 1. (a) Schematic representation of AFM indentation experiment, (b) AFM image and surface profile along the white line across the $Ti_3C_2T_x$ flake deposited on SiO_2 coated Si substrate.

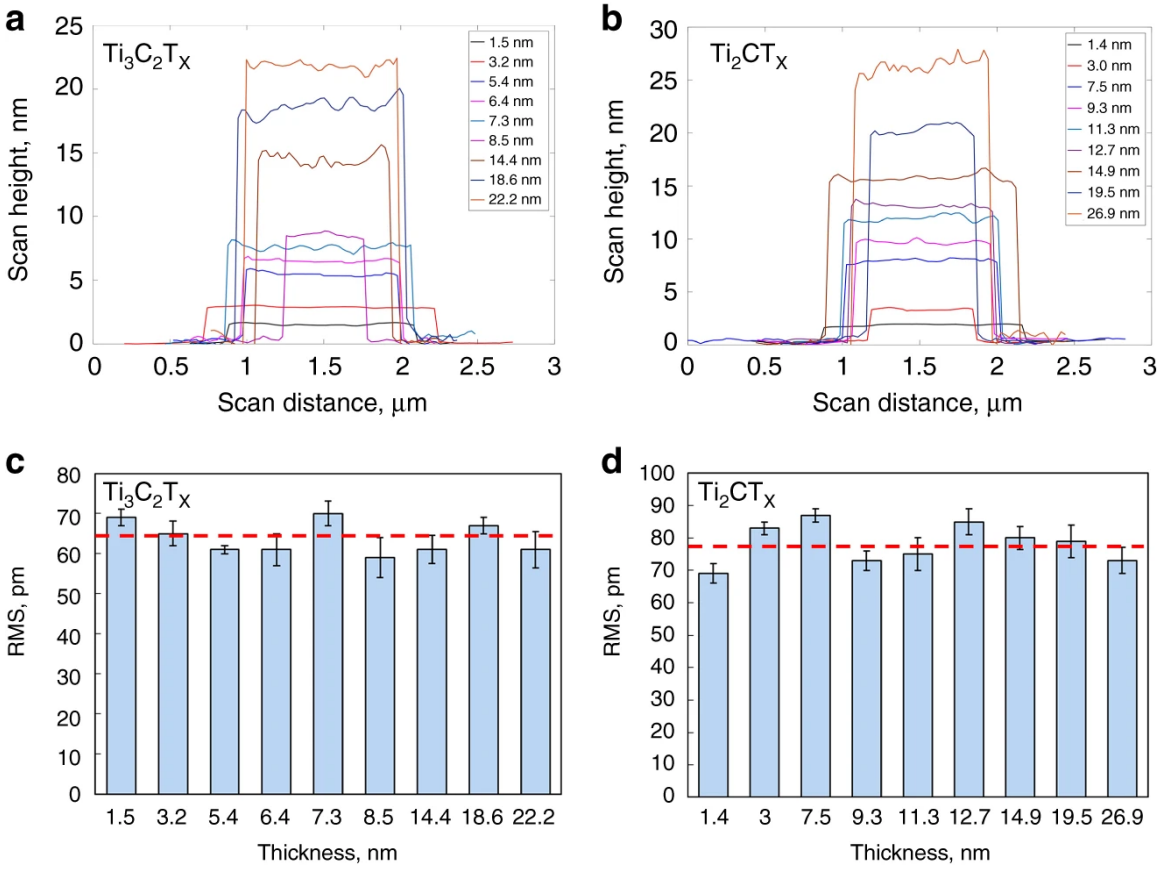

Figure 2. AFM line scans (a, b) and corresponding RMS values (c, d) for $Ti_3C_2T_x$ and Ti_2CT_x films of different thicknesses. Horizontal dash lines in bottom panels represent the average RMS for $Ti_3C_2T_x$ and Ti_2CT_x, which were used in adhesion energy calculations. Error bars represent standard deviations in RMS values.

2.2. FORCE-DISPLACEMENT RESPONSE

A typical force versus displacement response for tip approach and withdrawal measured on 5-monolayer $Ti_3C_2T_x$ sample is shown in Figure 3a. At the start of the experiment, the AFM tip was at a large distance from the sample surface. As the tip approached the sample surface (I) (indicated by the black line starting from the left side of the graph), a slowly increasing negative force (adhesion) was measured. At a certain displacement value (II), the "jump-in" phenomenon was observed resulting from sudden

bending of the AFM cantilever towards the sample surface as the adhesion reached its local maximum. After this, the AFM cantilever bending reduced with the continued displacement of the cantilever towards the sample until there was no negative load on the cantilever (at this point the cantilever is not bent) and the tip was in firm contact with the surface—this corresponds to the zero-displacement point (III); from here the indentation process begins upon further increase of displacement (IV). During the indentation stage, the tip experienced a positive force on it since the cantilever bends out of the sample surface (compare cartoons IV and II).

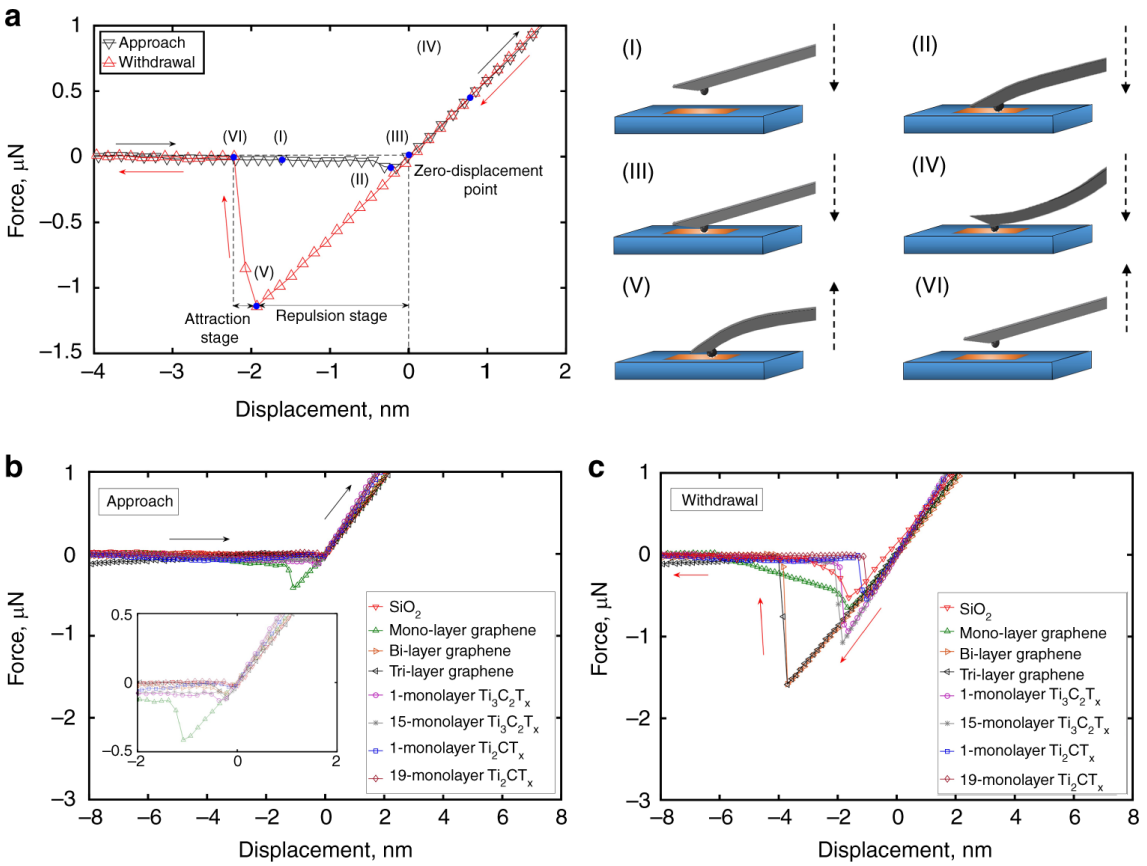

Figure 3. Force versus displacement graphs: (a) approach and withdrawal for 5-monolayer $Ti_3C_2T_x$ sample and cartoons illustrating relative positions of the tip and the sample during different key stages of the AFM indentation process, (b) approach, (c) withdrawal for different samples.

In the withdrawal process starting from the rightmost part of the graph in Figure 3a (indicated by the red line), the force on the tip reduced during the tip retraction. At 0 nm displacement (i.e., zero-displacement point), there is now a pulling force acting on the tip, which is balanced by its adhesion to the sample. When the displacement becomes slightly negative upon further withdrawal, the tip still adheres to the sample, resulting in cantilever bending towards the sample again (V). As the tip withdrawal continues, adhesion force approaches its maximum value before the tip "jumps-off" the sample surface (V to VI), turning the force acting on the cantilever into zero. The maximum adhesion force measured in point V (−1.11 μN in Figure 3a) was then used to calculate the adhesion energy between the tip and sample surface.

For all samples, the adhesion forces measured during the tip approach (−0.02 to −0.42 μN, Figure 3b) are generally lower than those recorded in the withdrawal stage (−0.5 to −1.56 μN, Figure 3c). The maximum adhesion force measured between the tip and monolayer graphene is much lower than that for bi-layer or tri-layer graphene (Figure 3c). However, in contrast to graphene adhesion, no number-of-monolayer dependency of the maximum adhesion force was found for the MXene films. The maximum values of adhesion force are higher for $Ti_3C_2T_x$ (1.07 μN) than those for Ti_2CT_x (0.53 μN). The "jump-off" (V to VI) observed for graphene, as well as MXene samples describes adhesion with a large interaction range, which may be a sign of the capillary force effect. Similar findings were reported in the nanoindentation experiments conducted on the surface of graphene [27]. The jump-off instability is worth mentioning at this conjunction as it might affect the accuracy of the measurements. However, this concern was eliminated by an accuracy analysis comparing the cantilever stiffness with the adhesion gradient during the

experiment (Supplementary Note 1 and Supplementary Figure 1). More force versus displacement data are provided in Supplementary Figure 2. The average adhesion forces along with standard deviations for all samples are plotted in Supplementary Figure 3a.

2.3. ADHESION ENERGY

The adhesion energy was calculated from the measured "jump-off" (or maximum adhesion) force using the Maugis–Dugdale theory [28],

$$W_{\mathrm{adh}}=\frac{F_{\mathrm{adh}}}{\lambda\pi R_{\mathrm{tip}}} \tag{1}$$

where W_{adh} is the adhesion energy per unit area, F_{adh} is the maximum adhesion force measured during the withdrawal stage, $R_{\mathrm{tip}}$is the tip radius and λ is an effective coefficient that depends on the model and data used (λ=1.613 for SiO_2, λ=1.587, 1.543, 1.543 for mono-, bi-, and tri-layer graphene, correspondingly, λ=1.560, 1.558 for 1-monolayer and 15-monolayer $Ti_3C_2T_x$, and λ=1.602, 1.602 for 1-monolayer and 19-monolayer Ti_2CT_x, correspondingly, see Supplementary Note 2). To account for the roughness effect, the tip roughness (RMS ≈ 180 pm provided by the vendor, Novascan, Inc.) and the average surface roughness of SiO_2 (65 pm), graphene (58 pm, 60 pm and 63 pm for mono-, bi- and tri-layer graphene, respectively) and MXenes (64 pm and 78 pm for $Ti_3C_2T_x$ and Ti_2CT_x, respectively), all shown in Supplementary Figure 3b, were employed using the modified Rumpf model [28, 29]. The actual adhesion energy is:

$$W_{\mathrm{adh}}=\left(\frac{F_{\mathrm{adh}}}{\lambda\pi R_{\mathrm{tip}}}\right)\left(\frac{\left(1+\frac{R_{\mathrm{tip}}}{1.48R_{\mathrm{film}}}\right)^{-1}+\left(1+\frac{1.48R_{\mathrm{film}}}{Z_0}\right)^{-2}}{\left(1+\frac{R_{\mathrm{tip}}}{1.48R_{\mathrm{tip\text{-}RMS}}}\right)^{-1}+\left(1+\frac{1.48R_{\mathrm{tip\text{-}RMS}}}{Z_0}\right)^{-2}}\right) \tag{2}$$

where R_{film} is the RMS value for the sample surface, $R_{tip\text{-}RMS}$ is the RMS value for the tip and Z_0 is the equilibrium separation of two surfaces. In our experiments, the equilibrium separation Z_0 is defined as zero-force distance between the surface of SiO_2 tip and the sample surface, which was estimated to be 0.3 nm [30]. All adhesion energies in this work were calculated according to Eq. (2). The histograms of the adhesion energy between all sample surfaces including SiO_2/SiO_2, graphene/SiO_2, $Ti_3C_2T_x/SiO_2$, and Ti_2CT_x/SiO_2 are presented in Figure 4. Gaussian fitting was applied to obtain the average adhesion energy and standard deviations for each specimen.

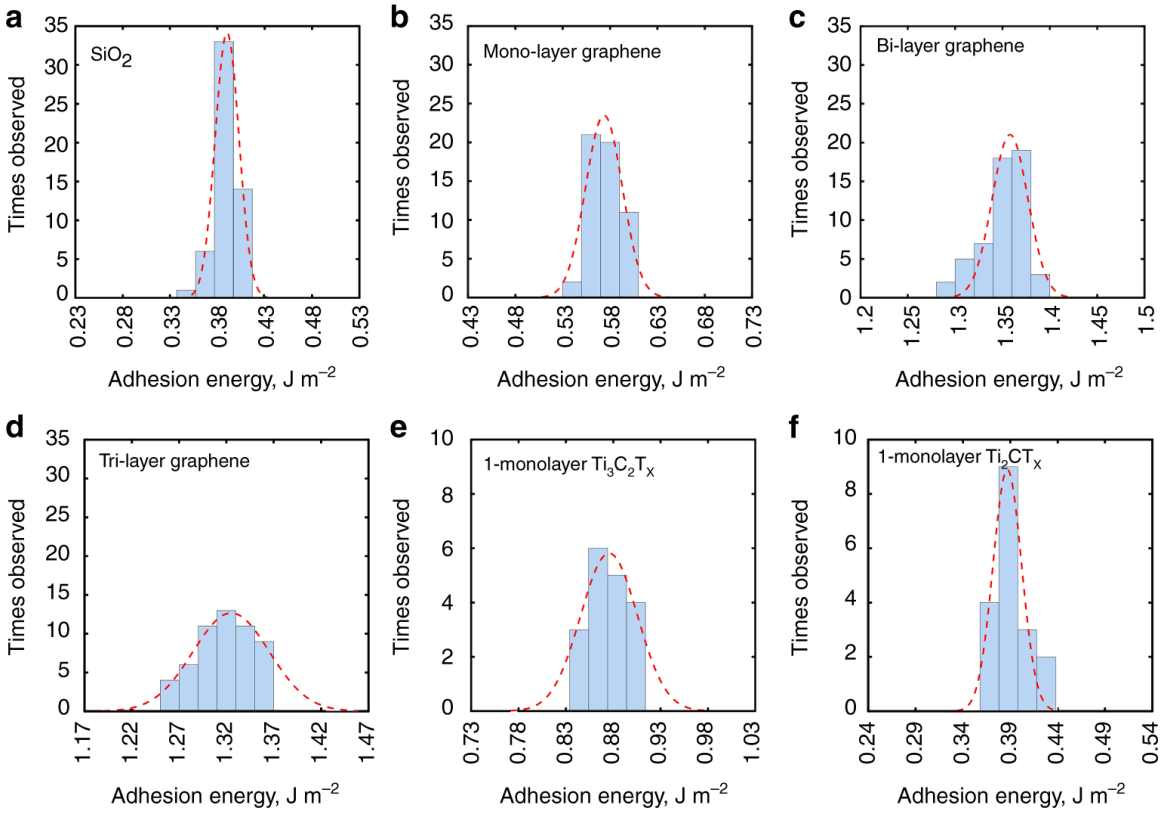

Figure 4. Histograms of calculated adhesion energies for: (a) SiO_2/SiO_2, (b) mono-layer graphene/SiO_2, (c) bi-layer graphene/SiO_2, (d) tri-layer graphene/SiO_2, (e) 1-monolayer $Ti_3C_2T_x/SiO_2$, and (f) 1-monolayer Ti_2CT_x/SiO_2. (The total count is 54 for SiO_2 and graphene and 18 for MXene).

We compare all measurements and plot the average adhesion for each type of interactions in Figure 5. The average adhesion energy for SiO_2/SiO_2 (0.40 ± 0.01 J m^{-2}) is fairly close to the value obtained for piranha solution treated Si wafer by Na, et al. (0.33 ± 0.01 J m^{-2}) [30].

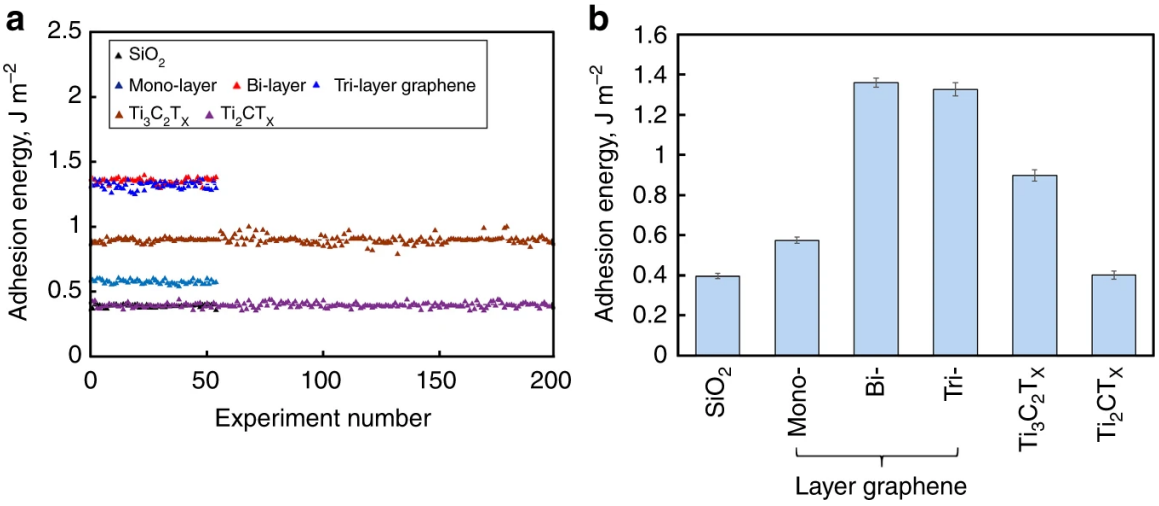

Figure 5. (a) Adhesion energy for all measured samples (since adhesion energy of $Ti_3C_2T_x$ and Ti_2CT_x thin films is independent of the film thickness, MXene films with different number of monolayers are represented by one symbol in the graph), (b) average adhesion energies with error bars indicating standard deviations.

The adhesion energies of SiO_2 with mono-layer, bi-layer, and tri-layer graphene are 0.58 ± 0.02, 1.36 ± 0.02, and 1.33 ± 0.03 J m^{-2}, respectively, indicating the number-of-monolayer dependence. This experimental dependence shows that adhesion energy of graphene with SiO_2 initially increases when going from mono-layer to bi-layer graphene and then stays constant when the number of graphene monolayers in the stack is increased to three. Similarly, a small increase in normal pull-off force that was more pronounced when going from 1 to 2 stacked graphene layers and less pronounced for a larger number

of layers, has been predicted by modeling [31]. However, this trend was “not observed in experiments possibly due to the experimental uncertainty” [31]. Another relevant paper on the number-of-layer effect on adhesion of graphene [32] mentions the opposite trend (measured by blister method), which also ceases when the number of graphene layers exceeds 2. There are also studies mentioning no number-of-layer effect on the pull-off force of graphene [33]. This broad spectrum of literature results may indicate the challenges associated with experimental measurements, as well as the differences between the measurement techniques (for example, the blister method inevitably measures the effect of shear force between the material and substrate along with adhesion), and differences in graphene sample preparation (mechanically exfoliated versus CVD graphene) [32]. However, for the purposes of our study it is important that: (i) modeling predicts a slight increase in the adhesion with a number of graphene monolayers [31], while it is not easy to explain the trend in opposite direction [32]; and (ii) both modeling and experiments (even those where oppositely directed trend was observed) converge on that the number-of-layer trend for graphene ceases when this number exceeds 2–3, i.e., when the distance between the top-most and the bottom-most graphene layers is ~0.7–1 nm.

The average adhesion energy of the monolayer graphene measured in this work ($0.58 \pm 0.02\ \mathrm{J\,m^{-2}}$) is close to the results of Jiang and Zhu ($0.46 \pm 0.02\ \mathrm{J\,m^{-2}}$) [23] and Torres et al. ($0.57\ \mathrm{J\,m^{-2}}$) [34]. The small differences between these results are possibly due to different methods of graphene synthesis or different measurement methods. Jiang and Zhu measured graphene sample prepared by mechanical exfoliation, while CVD graphene was used by Torres et al. Here, we use an AFM experiment similar to Jiang and Zhu [23], while Torres et al. [34] measured using the nanoparticles method. Due to differences in

sample preparation approaches, as well as adhesion energy measurement techniques, the authors could not provide explicit or definite reasons for the slightly higher adhesion measured in this work as compared to different literature data.

The average adhesion energy measured between SiO_2 and 1-monolayer $Ti_3C_2T_x$ is $0.90 \pm 0.03\ J\ m^{-2}$, which is about twice that between SiO_2 and 1-monolayer Ti_2CT_x ($0.40 \pm 0.02\ J\ m^{-2}$), and larger than that between SiO_2 and monolayer graphene. At the same time, the average adhesion energy between SiO_2 and 1-monolayer Ti_2CT_x is less than between SiO_2 and monolayer graphene (Figure 5). Since surface chemistry of $Ti_3C_2T_x$ and Ti_2CT_x is very similar as verified by the X-Ray photoelectron spectroscopy (XPS) (Supplementary Note 3 and Supplementary Figure 4), we ascribe this result as mostly due to the monolayer thickness differences between the two MXenes (0.94 nm for $Ti_3C_2T_x$ and 0.67 nm for Ti_2CT_x, respectively, calculated from X-Ray diffraction (XRD) data in Supplementary Figure 5 and density functional theory optimized geometries in Supplementary Figure 6). Although there was a clear monolayer thickness dependence of adhesion between each of the two MXenes and SiO_2, we did not observe any number-of-monolayer (or sample thickness) dependency (Figure 3b, c, Figure 5a and Supplementary Figure 2c, d). Details of the variation of measured adhesion energies among MXenes with different thickness and from different batches can be found in Supplementary Note 4, Supplementary Table 1, Supplementary Figure 7, and Source Data. We hypothesize that the absence of the number-of-monolayer dependence for MXene stacks may be due to a large interlayer spacing (Supplementary Figure 5, 6), which is several times more than the interlayer spacing in stacks of graphene. This large interlayer spacing in MXenes limits the experimentally measured adhesion by only the topmost (closest to the tip) layer

contribution, preventing adhesive interactions between the underlying MXene layers and the tip. Referring to the above discussion on a number-of-monolayer dependence of adhesion for graphene, which ceases after 2–3 graphene monolayers in the stack (see also our experimental data in Figure 5), we find that the distance at which this dependence ceases in case of stacked graphene is close to the thickness of either $Ti_3C_2T_x$ or Ti_2CT_x monolayers. It is, therefore, not surprising that no number-of-monolayer trend was observed here for the MXene samples, since their monolayer thickness and interlayer spacing are larger than those of graphene.

3. DISCUSSION

The adhesion energies between SiO_2 coated Si tip and two types of MXenes were measured for the first time using AFM with a spherical tip and compared to adhesion energies between the same tip and mono-layer, bi-layer, and tri-layer graphene. The measured values are 0.90 ± 0.03 J m^{-2} and 0.40 ± 0.02 J m^{-2} for $Ti_3C_2T_x$ and Ti_2CT_x, which are in the range of adhesion between SiO_2 and graphene monolayer. A higher adhesion energy between SiO_2 and $Ti_3C_2T_x$ can be attributed to a thicker monolayer of this MXene compared to that of Ti_2CT_x. This observation provides the first illustration of how MXenes can be used to study the fundamental effects of monolayer thickness, disentangled from other factors, on mechanical properties of 2D materials. In contrast to graphene, no number-of-monolayers dependency was observed in this study for adhesion energy of multilayer MXene stacks, which we ascribe due to a larger interlayer spacing and monolayer thickness of the MXenes. The role of surface chemistry in adhesion interactions

of MXenes with SiO_2 and other substrates still remains unclear, but potentially it can be used to control the adhesion in the future, provided we could better understand MXene chemistry and tailor the functional groups terminating MXene surfaces.

4. METHODS

4.1. ATOMIC FORCE MICROSCOPY (AFM)

AFM (Digital Instruments Nanoscope IIIA) was conducted under the ambient conditions as illustrated in Figure 1a. Thin films of graphene and MXene were mounted on the silicon substrate with a thin (~300 nm) layer of spontaneously formed silicon oxide. Surface profiles were measured using the tapping mode with a 3-nm radius silicon tip. The static eliminator (Static Sensing Ionizer, Keyence®) was used to neutralize any interfering electrostatic charges on the sample and/or AFM tip [35]. A 500-nm radius colloidal silicon tip with silicon dioxide (SiO_2) surface was used to measure adhesive behavior of the samples. SEM images of the microsphere AFM tip are provided in Supplementary Figure 8. The probe was calibrated before and after each experiment using the AFM grating to ensure that no damage to the probe occurred during the experiment. For each MXene flake, three measurements were conducted on the grid areas as illustrated in Supplementary Figure 9a. As for graphene, nine measurements were performed on one flake due to a larger area of graphene flakes compared to MXene flakes. For further details and discussion of between the samples variations see Supplementary Note 4, Supplementary Table 2, and Source Data. The cantilever stiffness provided by the supplier (Novascan, Inc.) was

~2 N m^{-1}. The force-displacement responses for the approach and withdrawal stages were recorded and analyzed.

The typical adhesive interaction of thin films involves the van der Waals, capillary, and electrostatic forces [36]. The capillary force is usually induced by water bridging the sample and tip surfaces [37, 38]. We did check the effect of moisture by conducting AFM experiments with $Ti_3C_2T_x$ while varying the relative humidity (RH, Supplementary Figure 10). The maximum fluctuation of the adhesion force is within 5% of the average value for $Ti_3C_2T_x$. These results show no significant humidity effect when RH is lower than 24%. We have also checked adhesion force versus time in air at room temperature to investigate the effect of sample oxidation. Supplementary Figure 11a shows that the adhesion force stays constant within the first 48 h. The corresponding AFM images (Supplementary Figure 11b) do not show any changes in the MXene surface morphology. After 48 h, the measured adhesion force drops dramatically accompanied by the visible changes in the AFM images, demonstrating signs of MXene oxidation (formation of TiO_2 etc.). This indicates that the drop in adhesion force for $Ti_3C_2T_x$ after 48 h exposure to ambient air is due to chemical changes of the MXene, emphasizing the need to work with freshly prepared MXene samples, which was always properly taken care of in this study: all MXene samples were measured within no more than 12 h from their preparation and drying.

4.2. SYNTHESIS OF GRAPHENE AND PREPARATION OF GRAPHENE SAMPLES ON SILICON WAFERS

Large-area monolayer graphene was grown by chemical vapor deposition (CVD) on 2 × 10 cm copper foils (Alfa Aesar, CAS: 7440-50-8, LOT No. P17D009). During this process, gas species were fed into the reactor flow over the 25 μm thick piece of copper foil, where hydrocarbon precursors decomposed to carbon radicals at the copper surface and then formed monolayer graphene [39].

To prepare the multilayer graphene, a copper foil with graphene on top was spin-coated with a layer of polymethyl methacrylate (PMMA) (3000 rpm for 30 s) [40]. The foil was then etched away in 0.2 mol L^{-1} $FeCl_3$ and 0.2 mol L^{-1} $(NH_4)_2S_2O_8$ for 2 h [41]. The remaining graphene/PMMA was cleaned with deionized water, transferred onto freshly synthesized graphene on copper foil and heated at 50 °C in dry air to remove water. After another copper foil etching process, the graphene/graphene/PMMA sample was obtained. The tri-layer graphene was prepared by repeating this procedure. The graphene/PMMA, graphene/graphene/PMMA and graphene/graphene/graphene/PMMA samples were then transferred onto target Si (111)/SiO_2 substrates and baked at 120 °C for 15 min. Prior to transfer, Si substrates were cleaned by 30 min bath sonication in acetone and hydrophilized in piranha solution (3 mL 30% H_2O_2 slowly added to 9 mL 98% H_2SO_4) for 24 h, followed by thorough rinsing with deionized water. Finally, PMMA was removed using acetone solution, yielding a sample of graphene on the Si/SiO_2 substrate. The residue of polymer film was etched away at 400 °C in hydrogen [27].

4.3. SYNTHESIS OF MAX PHASES

Ti_3AlC_2 was prepared by pressureless synthesis method [42]. The initial powders of titanium (-325 mesh, 99%, Alfa Aesar), aluminum (-325 mesh, 99.5%, Alfa Aesar), and graphite (-325 mesh, 99%, Alfa Aesar) were ball-milled in 3:1.1:1.88 molar ratio in a polyethylene jar for 12 h at 100 rpm. Afterwards, the mixture was sintered at 1550 ^oC for 2 h in Ar flow in an alumina boat using a tube furnace (GSL-1800X -KS60-UL, MTI Corporation). For Ti_2AlC synthesis, the initial powders of titanium carbide (typically 2-micron size, 99.5%, Alfa Aesar), titanium (-325 mesh, 99%, Alfa Aesar), and aluminum (-325 mesh, 99.5%, Alfa Aesar) were ball-milled in a molar ratio of 0.85:1.15:1.05. The mixture was then heated at 1400 ^oC for 4 h under Ar flow in an alumina boat. The resulting ceramics were manually crushed into powders using mortar and pestle.

4.4. PREPARATION OF MXENE THIN FILMS ON SILICON WAFERS

$Ti_3C_2T_x$ MXene was synthesized by selective etching of Al from Ti_3AlC_2 [43]. The etching was done by slowly mixing 0.3 g of Ti_3AlC_2 (-325 mesh, particle size $\leq$ 45 μm) to the etchant, prepared by dissolving 0.3 g LiF in 6 mL of 6 M HCl in a 50 mL plastic centrifuge tube. The mix was stirred for 24 h at room temperature, followed by repeated washing with deionized water and centrifugation until the pH of supernatant reached 5.5–6.0.

$Ti_3C_2T_x$ aqueous colloidal solution was obtained via 5 min hand-shaking followed by 1 h centrifugation at 3500 rpm. $Ti_3C_2T_x$ thin films on Si were prepared from the concentrated $Ti_3C_2T_x$ colloidal solutions via interfacial film deposition method [8]. In order to prepare MXene thin films, 50–300 μL of $Ti_3C_2T_x$ colloidal solution was mixed in 50 mL

DI water together with 3–6 mL toluene added during 15 min of vigorous stirring. The dispersion was then poured directly into a beaker filled with 400 mL DI water and with a few pieces of pre-cleaned Si wafers placed at the bottom. After ~20 min standing still, the $Ti_3C_2T_x$ film was self-assembled at the interface between water and toluene, and then the pieces of Si wafers were slowly lifted up from the solution through the interface, catching the interfacial MXene film. Finally, the MXene coated Si wafers were dried for 12 h in Ar flow at room temperature to avoid oxidation. Ti_2CT_x colloidal solutions, as well as thin films were obtained using same methods, except the MAX phase in this case was Ti_2AlC (-325 mesh, particle size $\leq$ 45 μm) and the MXene (Ti_2CT_x) film drying time was 4 h in Ar flow at room temperature.

By adjusting the concentration of MXene colloidal solution during sample preparation, MXene films with different thicknesses were deposited ranging between 1.4 to 26.9 nm. The adhesion measurements were carried out immediately after the films were dried.

4.5. MOISTURE AND OXIDATION EFFECTS

To investigate the moisture effect on adhesion measurements, three $Ti_3C_2T_x$ samples after initial drying (12 h in dry Ar flow) were placed into a closed chamber with P_2O_5, where RH was monitored with CECOMINOD046940 monitor (Hyelec). The samples were removed for adhesion measurements when RH reached 24%, 21%, 18%, 15%, 12%, 9%, and 6% (Supplementary Figure 10). To investigate the effect of oxidation on adhesion measurements, adhesion forces and AFM images were obtained for three $Ti_3C_2T_x$ samples exposed to air for 24–96 h (Supplementary Figure 11).

4.6. RAMAN SPECTROSCOPY CHARACTERIZATION

Raman spectroscopy was conducted using a Horiba LabRAM ARAMIS spectrometer with 632.8 nm laser. Supplementary Figure 9b, c show Raman spectra of $Ti_3C_2T_x$ and Ti_2CT_x MXenes on Si and on cover glass. The peaks at 520 cm^{-1} recorded from MXenes deposited on Si wafer belong to Si. The MXene samples show characteristic Raman peaks of $Ti_3C_2T_x$ at 206, 270, 374, 605, and 718 cm^{-1} [44-46], and of Ti_2CT_x at 200, 300, 409, and 608 cm^{-1} [47], respectively. All the peaks originate from Ti–C bond vibrations that are also present in the Raman spectra of respective parent MAX phases published in literature [48].

Graphene is usually characterized by G band at ~1600 cm^{-1} and 2D band at ~2650 cm^{-1}. Raman spectra of our graphene transferred samples exhibited typical characteristics of high-quality graphene: for monolayer graphene the 2D/G intensity ratio is ~2.21 and a full-width at half maximum (FWHM) of 2D band is ~27 cm^{-1} [49]. The 2D/G ratio and FWHM for the bi-layer graphene are 1 and 52 cm^{-1}, and for the tri-layer graphene, these values are 0.5 and 63 cm^{-1} [50] (Supplementary Figure 9d).

4.7. X-RAY DIFFRACTION CHARACTERIZATION

The structures of $Ti_3C_2T_x$ and Ti_2CT_x MXene thin films were characterized using X-Ray Diffraction (XRD, PANalytical, Phillips MPD) with Cu K<α> radiation (λ=1.5406 Å) at U=45 kV, I=40 mA.

4.8. X-RAY PHOTOELECTRON SPECTROSCOPY CHARACTERIZATION

X-Ray photoelectron spectroscopy (XPS) measurements of $Ti_3C_2T_x$ and Ti_2CT_x MXene thin films were performed using a KRATOS AXIS 165 X-Ray photoelectron spectrometer with a monochromatic Al X-Ray source.

4.9. CALCULATION OF THE NUMBER OF MXENE MONOLAYERS

The local number of MXene monolayers in our samples was calculated from a combination of AFM and XRD data as follows. The (002) peaks for $Ti_3C_2T_x$ and Ti_2CT_x are at $2\theta=5.98^\circ 2\theta=5.98^\circ$, and $6.48^\circ 6.48^\circ$, respectively (Supplementary Figure 5). According to Bragg's Law $2d\sin\theta=n\lambda 2d\sin\theta=n\lambda$, the corresponding *d*-spacing values are 1.48 nm and 1.36 nm [51, 52], which are sums of the thickness of MXene monolayer and the interlayer spacing. Therefore, the number of MXene monolayers in different thin films can be calculated as the local AFM measured thickness of the films (Figure 2) divided by the corresponding *d*-spacing values (Supplementary Figure 6).

DATA AVAILABILITY

Data available on request from the authors.

ACKNOWLEDGEMENTS

The authors would like to thank Material Research Center at Missouri University of Science and Technology for financial support, as well as Dr. R. Brow (Missouri University of Science and Technology) for providing access to Raman spectrometer.

AUTHOR CONTRIBUTIONS

Y.X.L. and S.H.H. contributed equally to this work. C.L.W. and V.N.M. conceived and supervised the project, designed the experiments, and guided the team; Y.X.L. synthesized graphene, performed characterization, as well as adhesion measurements and data analysis; S.H.H. synthesized $Ti_3T_2T_x$ and Ti_2CT_x MXenes, participated in adhesion measurements, performed sample characterization, as well as the data analysis; C.J.W. carried out accuracy analysis of adhesion measurements. All the authors discussed results, wrote, and commented on the paper.

SUPPORTING INFORMATION

SUPPLEMENTARY NOTES

Supplementary Note 1: Accuracy Analysis of Adhesion Measurements. The jump-off instability has been the main concern when using AFM to measure adhesion forces. To avoid the unstable jump-off, the adhesive force gradient between the spherical tip and sample surface should be much greater than the spring stiffness of the AFM

cantilever [53]. Here, we calculated the force *versus* displacement and obtained the force gradients for each type of specimen approaching the maximum adhesion. These values were compared with the slope of the cantilever's spring constant (2 N m^{-1}) to demonstrate the accuracy of the adopted method.

The pairwise interaction energy between the atom on the tip and the atom on the sample surface was assumed in the form of Lennard-Jones potential:

$$W_{\mathrm{LJ}}(r) = -\frac{C_1}{r^6} + \frac{C_2}{r^{12}}. \tag{1}$$

Integration of Eq. (1) gives the interaction energy per unit area between the sample surface and the tip, E (see supporting information of reference 2) [23]:

$$E = -\gamma\left[\frac{3}{2}\left(\frac{Z_0}{Z}\right)^3 - \frac{1}{2}\left(\frac{Z_0}{Z}\right)^9\right], \tag{2}$$

where Z_0 is the separation between tip and sample surface, Z is the distance between the sample surface and the spherical tip and γ is the adhesion energy per unit area at Z_0. The corresponding adhesive traction (f) and force gradient (k_{vdW}) can be obtained by taking the negative first and second derivatives of E as follows:

$$f = -\frac{dE}{dZ} = -\frac{9\gamma}{2Z_0}\left[\left(\frac{Z_0}{Z}\right)^4 - \left(\frac{Z_0}{Z}\right)^{10}\right], \tag{3}$$

$$k_{\mathrm{vdW}} = -\frac{d^2E}{dZ^2} = -\frac{27\gamma}{Z_0^2}\left[-\frac{2}{3}\left(\frac{Z_0}{Z}\right)^5 + \frac{5}{3}\left(\frac{Z_0}{Z}\right)^{11}\right]. \tag{4}$$

The adhesion force (F) can then be obtained by:

$$F = \pi a^2 f, \tag{5}$$

where a is the contact radius at "jump-off" obtained using Carpick's solution [54] to the Maugis-Dugdale model as:

$$a = \left[1.54 + 0.279\left(\frac{2.28\mu^{1.3} - 1}{2.28\mu^{1.3} + 1}\right)\right]\left[\frac{0.98\left(1 - e^{-1.082\mu}\right)}{1 + 0.98\left(1 - e^{-1.082\mu}\right)}\right]^{2/3}\left(\frac{K}{\pi\gamma R^2}\right)^{-1/3}, \tag{6}$$

The parameter μ is defined as:

$$\mu=1.157\left(\frac{16R\gamma^2}{9K^2Z_0^3}\right)^{1/3}, \quad (7)$$

μ ranges between 0 and infinity, which correspond to the Derjaguin-Muller-Toporov (DMT) and Johnson-Kendall-Roberts (JKR) models, respectively. R is the tip radius, γ and Z_0 are defined in Eq. (2), and K is the reduced elastic modulus:

$$K=\frac{4}{3}\frac{1}{(1-\nu_1^2)/E_1+(1-\nu_2^2)/E_2}. \quad (8)$$

where E_1, ν_1 and E_2, ν_2 are the elastic moduli and the Poisson's ratios for the tip and specimen, respectively. Since the specimen thickness is low, the elastic properties of amorphous silicon dioxide (SiO_2) were used in the analysis. The elastic properties for SiO_2 were taken as E_{SiO_2}=70 GPa, ν_{SiO_2}=0.3 (See supporting information in reference 2) [23]. The equilibrium separation of the surface Z_0 was set as 0.30 nm based on the interaction between graphene and SiO_2 [55], same value was assumed for MXene as well. The maximum adhesive force can then be obtained at k_{vdW}=0. The maximum force gradients (F_k) for SiO_2, graphene, and MXene are 68750N m^{-1}, 28640N m^{-1}, and 13624N m^{-1}, respectively, with $\pm$10% error. For comparison, the dashed straight lines with the slope of the cantilever's spring stiffness were plotted tangential to the curves at the maximum adhesive force points in Supplementary Figure 1. These results demonstrate that the measured adhesion is the maximum adhesion of the sample surfaces.

Supplementary Note 2: Determination of λ in Maugis-Dugdale Theory for this Experiment. For Eq. (1) in the main text, λ is the coefficient ranging between 1.5 and 2. The JKR theory and DMT theory describe two extreme contacts between spherical particle and flat surface when λ=1.5, and λ=2, respectively.

An empirical fitting equation often used [54] to solve for the coefficient λ is employed:

$$\lambda = \left| -\frac{7}{4} + \frac{1}{4}\left(\frac{4.04\mu^{1.4}-1}{4.04\mu^{1.4}+1}\right)\right| . \quad (9)$$

where μ is defined in Eq. (7). The solved λ varies for each case, depending on the jump-off adhesion force. From the calculations, λ=1.613 for SiO_2, λ=1.587, 1.543, 1.543 for mono-, bi-, and tri-layer graphene, λ=1.560 and 1.558 for 1- and 15-monolayer $Ti_3C_2T_x$, and 1.602 and 1.602 for 1- and 19-monolayer Ti_2CT_x, respectively.

Supplementary Note 3: XPS Analysis of $Ti_3C_2T_x$ and Ti_2CT_x MXene Samples. We examined MXene surface chemistry by XPS. The commonly anticipated functional groups on MXene flakes are -OH, -O- and -F. XPS survey for $Ti_3C_2T_x$ MXene film shows F/O atomic ratio 0.37 (Supplementary Figure 4), while for Ti_2CT_x MXene film it is 0.32 (Supplementary Figure 4). Thus, the results indicate almost same F/O ratio for both MXenes (as expected). Hence, we conclude that surface chemistry is more or less same for both $Ti_3C_2T_x$ and Ti_2CT_x MXenes. According to nuclear magnetic resonance studies [16], the majority of O atoms for MXene samples produced by MILD method belong to bridging Ti-O-Ti groups.

Supplementary Note 4: Statistical Variation in Measured Adhesion Energy. The measured adhesion energy variation among different flakes can be found in Figure 5a. For MXene flakes, experiment numbers 1-81 are from batch 1 (total of 9 different thickness). Experiment numbers 1-9 are for thickness #1, 10-18 for thickness #2, 19-27 for thickness #3, 28-36 for thickness #4 37-45 for thickness #5, 46-54 for thickness #6, 55-63 for thickness #7, 64-72 for thickness #8, 73-81 for thickness #9. Experiment numbers 82-90 and 91-99 are from batch 2 and 3 individually. Experiment numbers 100-180 are from

batch 4 (total of 9 thicknesses) and the numbers have same meaning as for batch 1. Experiment numbers 181-189 and 190-199 are from batches 5 and 6 individually. For each type of graphene flake (mono-, bi-, or tri-layer), experiment numbers 1-27 are from batch 1. 1-9 represent measurements for #1 graphene flake, 10-18 for #2, and 19-27 for #3 graphene flake. Experiment numbers 28-54 are from batch 2. 28-36 represent measurements for #4 graphene flake, 37-45 for #5, and 46-54 for #6 graphene flake. The maximum fluctuations of measured adhesion energy over the corresponding average values for MXene samples are shown in Supplementary Table 1. The maximum fluctuation for adhesion energy measured for $Ti_3C_2T_x$ and Ti_2CT_x is within 12% of the average. Therefore, there is no thickness dependency observed. The maximum fluctuations of measured adhesion energy over the corresponding average values for graphene samples are shown in Supplementary Table 2.

All adhesion measurements were performed using the same AFM tip. The tip was found to be intact after each experiment under SEM and was calibrated before and after each experiment. For each number of layers of graphene (mono-, bi-, and tri- graphene samples), 6 flakes were chosen. 9 measurements were conducted on each flake. For each thickness of $Ti_3C_2T_x$ or Ti_2CT_x flake, 6 flakes were selected and 3 measurement were conducted on the grid areas as illustrated in the Supplementary Figure 9a.

Samples from three separate batches were tested. The batch-to-batch variations in measured adhesion energies are small: within 7% and 8% of the average values for $Ti_3C_2T_x$ and Ti_2CT_x, respectively. The details of these measurements and comparisons are provided in Supplementary Figure 7.

The calculation data on adhesion energies from all measurements are provided in Source Data.

Table S1. Statistical variation of adhesion energy measurements for MXene

Adhesion Energy, J m^{-2}	Sample	Experiment Number				
		1-9 (batch 1, thickness #1)	10-18 (batch 1, thickness #2)	19-27 (batch 1, thickness #3)	28-36 (batch 1, thickness #4)	37-45 (batch 1, thickness #5)
Maximum fluctuation/ Average value, %	$Ti_3C_2T_x$	3.94	4.55	5.48	2.70	1.67
	Ti_2CT_x	7.68	9.47	6.15	4.68	8.97
Adhesion Energy, J m^{-2}	Sample	46-54 (batch 1, thickness #6)	55-63 (batch 1, thickness #7)	64-72 (batch 1, thickness #8)	73-81 (batch 1, thickness #9)	82-90 (batch 2)
Maximum fluctuation/ Average value, %	$Ti_3C_2T_x$	0.73	7.38	11.21	8.31	1.78
	Ti_2CT_x	9.47	5.46	11.68	9.15	6.00
Adhesion Energy, J m^{-2}	Sample	91-99 (batch 3)	100-108 (batch 4, thickness #1)	109-117 (batch 4, thickness #2)	118-126 (batch 4, thickness #3)	127-135 (batch 4, thickness #4)
Maximum fluctuation/ Average value, %	$Ti_3C_2T_x$	4.23	5.91	8.12	8.90	11.98
	Ti_2CT_x	6.21	7.68	9.47	6.15	4.68
Adhesion Energy, J m^{-2}	Sample	136-144 (batch 4, thickness #5)	145-153 (batch 4, thickness #6)	154-162 (batch 4, thickness #7)	163-171 (batch 4, thickness #8)	172-180 (batch 4, thickness #9)
Maximum fluctuation/ Average value, %	$Ti_3C_2T_x$	5.16	8.22	0.92	10.18	11.21
	Ti_2CT_x	8.97	9.47	5.46	11.13	9.15

Table S1. Statistical variation of adhesion energy measurements for MXene (Cont.)

Adhesion Energy, J m^{-2}	Sample	181-189 (batch 5)	190-198 (batch 6)			
Maximum fluctuation/ Average value, %	$Ti_3C_2T_x$	10.02	3.34			
	Ti_2CT_x	8.00	7.75			

Table S2. Statistical variation of adhesion energy measurements for graphene

Adhesion Energy, J m^{-2}	Sample	Experiment Number		
		1-9 (batch 1, flake #1)	10-18 (batch 1, flake #2)	19-27 (batch 1, flake #3)
Maximum fluctuation/ Average value, %	Mono-layer	4.67	4.81	4.67
	Bi-layer	3.20	1.50	2.72
	Tri-layer	4.96	5.03	5.80
Adhesion Energy, J m^{-2}	Sample	28-36 (batch 2, flake #4)	37-45 (batch 2, flake #5)	46-54 (batch 2, flake #6)
Maximum fluctuation/ Average value, %	Mono-layer	5.09	5.99	4.67
	Bi-layer	4.55	4.68	4.30
	Tri-layer	2.00	3.03	3.29

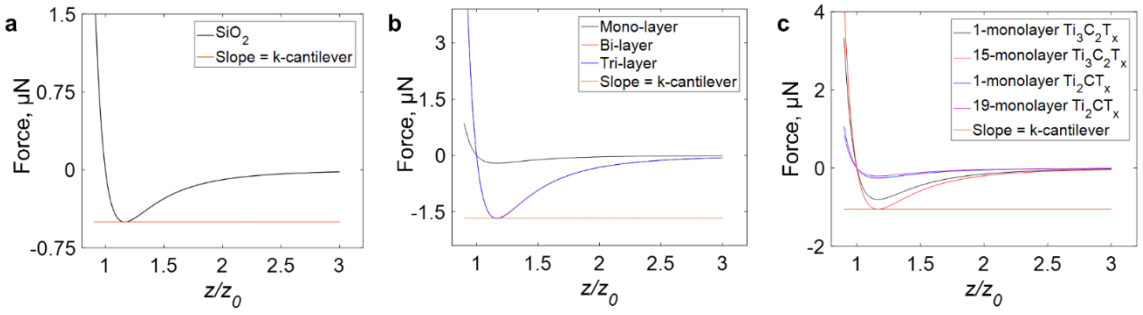

Figure S1. Force curves for different samples used in this study. (a) SiO_2/SiO_2, (b) SiO_2/graphene and (c) SiO_2/MXene.

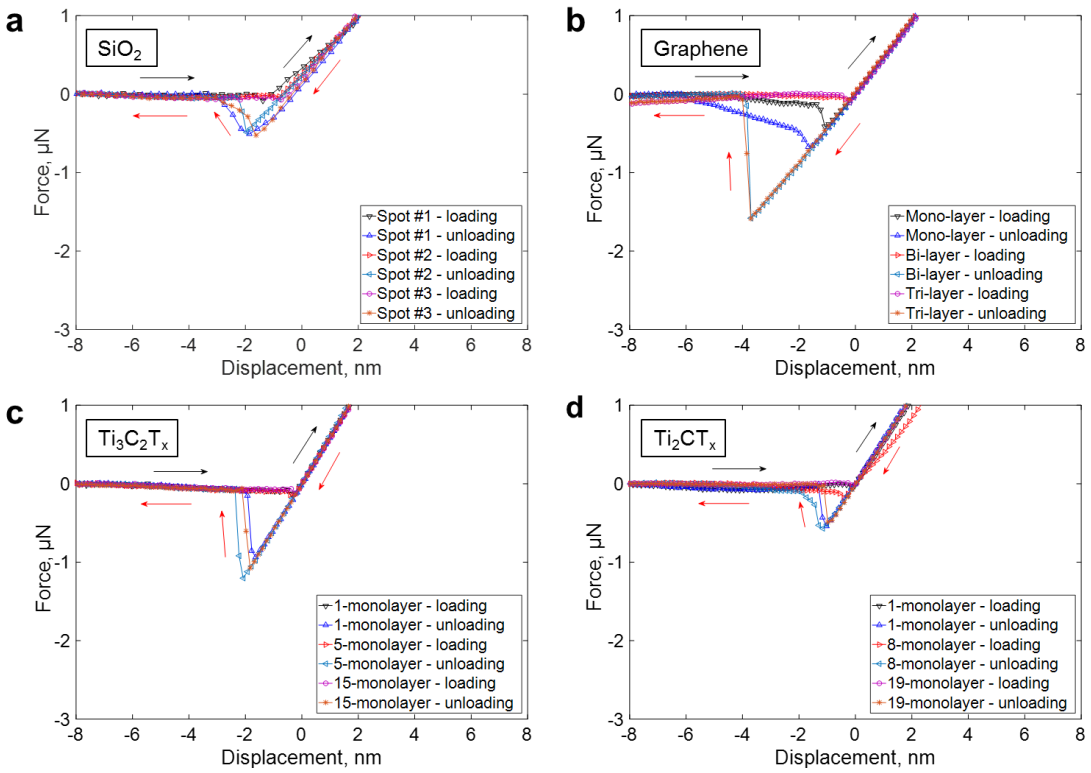

Figure S2. Force *versus* displacement responses for different interfacial interactions. (a) SiO_2/SiO_2, (b) SiO_2/graphene, (c) $SiO_2/Ti_3C_2T_x$, (d) SiO_2/Ti_2CT_x.

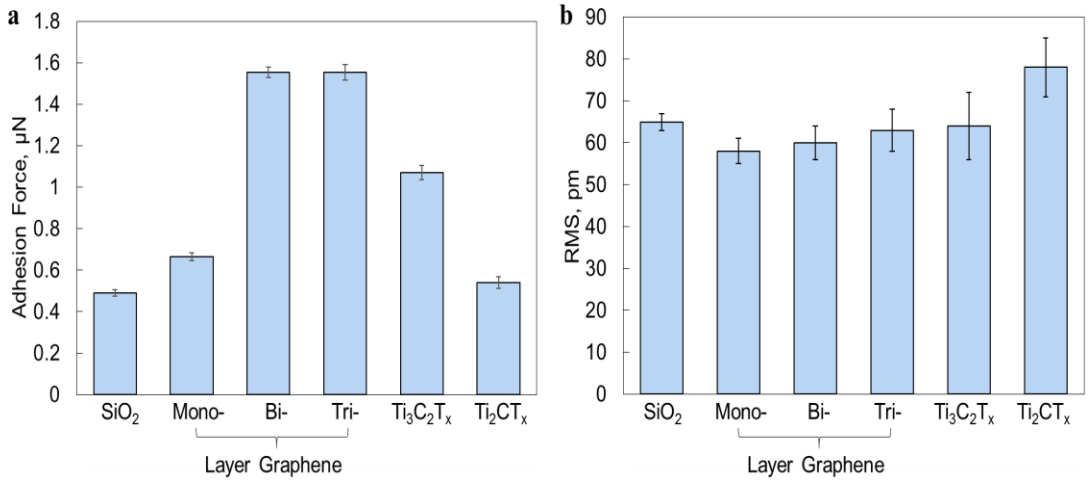

Figure S3. Average measured (a) adhesion forces and (b) RMS values with error bars indicating standard deviations.

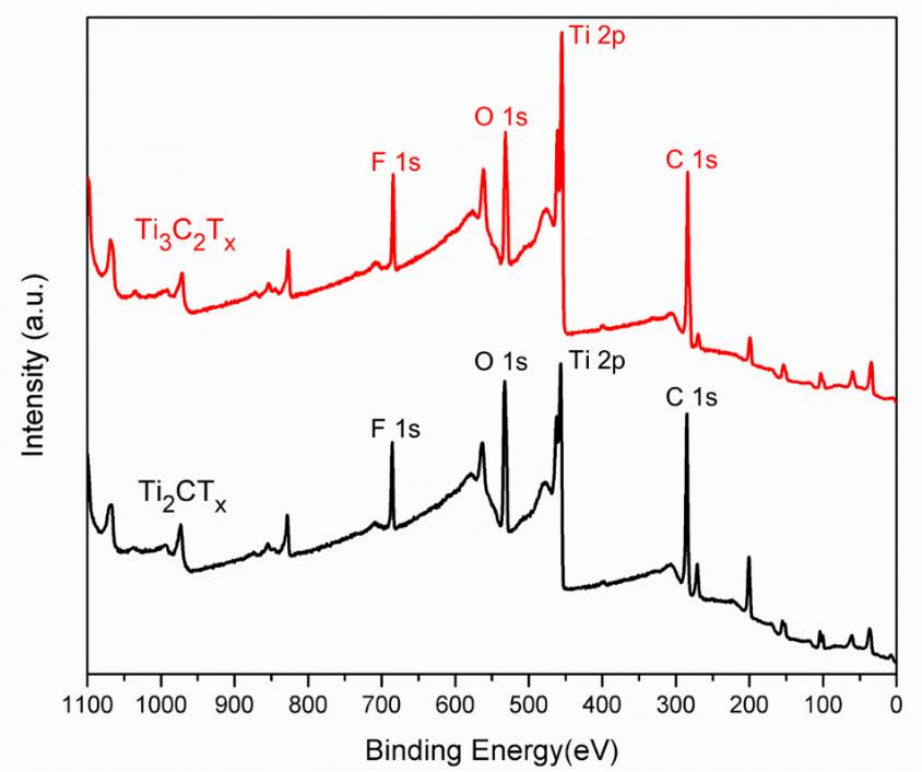

Figure S4. XPS survey spectra of $Ti_3C_2T_x$ and Ti_2CT_x MXene films.

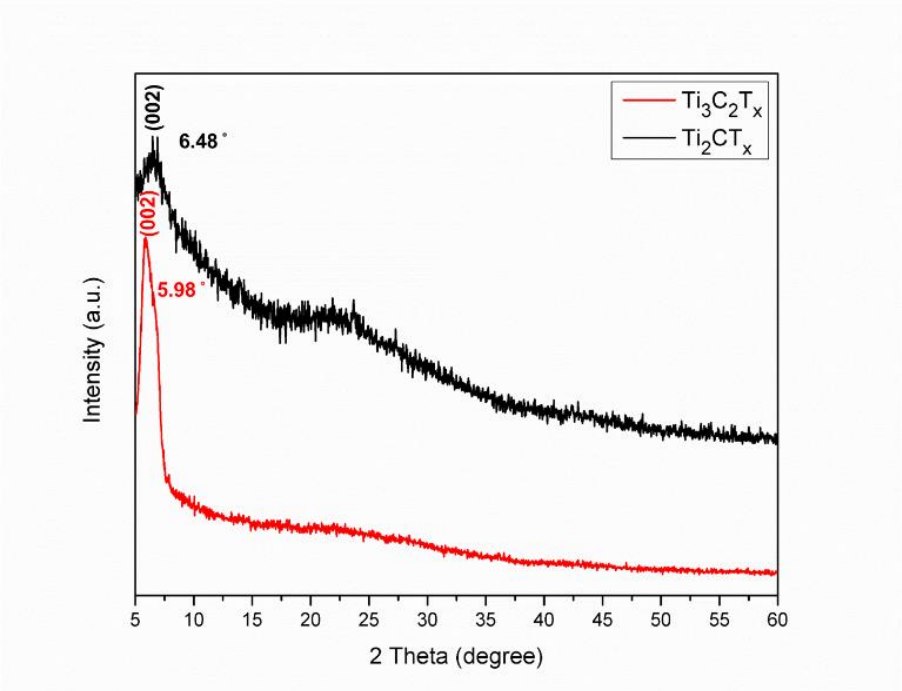

Figure S5. XRD patterns of $Ti_3C_2T_x$ and Ti_2CT_x MXene thin films.

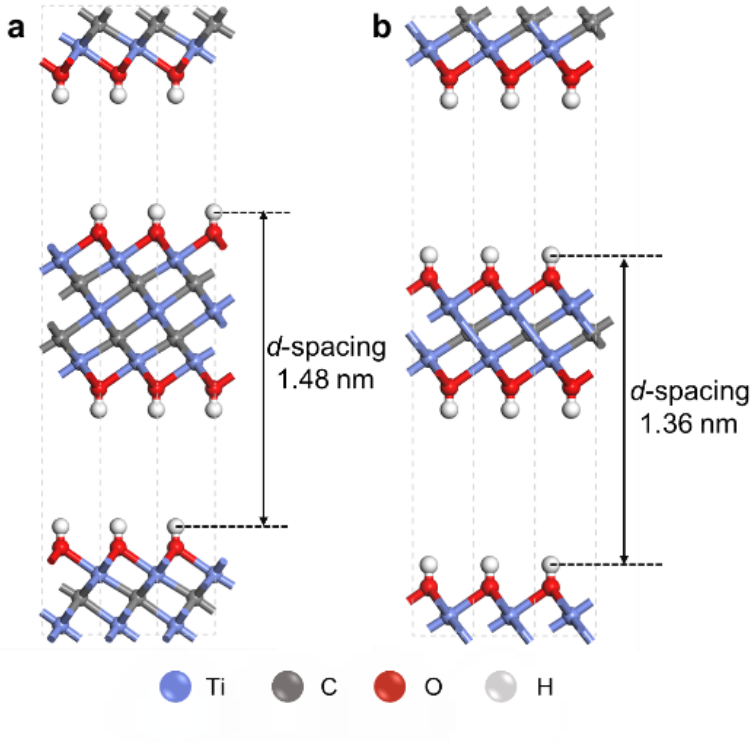

Figure S6. Atomic structures of (a) $Ti_3C_2T_x$, (b) Ti_2CT_x MXenes and their corresponding d −spacing values calculated from XRD (Supplementary Figure 5). The number of MXene monolayers in a thin film was calculated as

$$\text{Number of monolayers} = \frac{\text{Film thickness (from AFM)}}{d\text{-spacing}}.$$

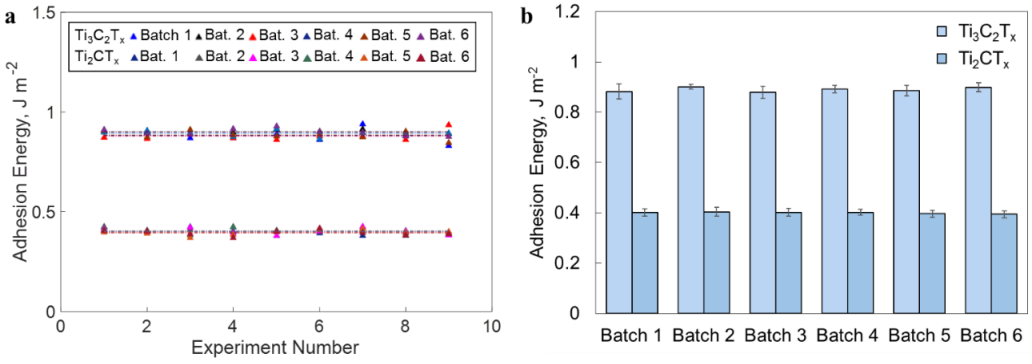

Figure S7. (a) Batch-to-batch variations of adhesion energy, (b) average adhesion energies with error bars indicating standard deviations.

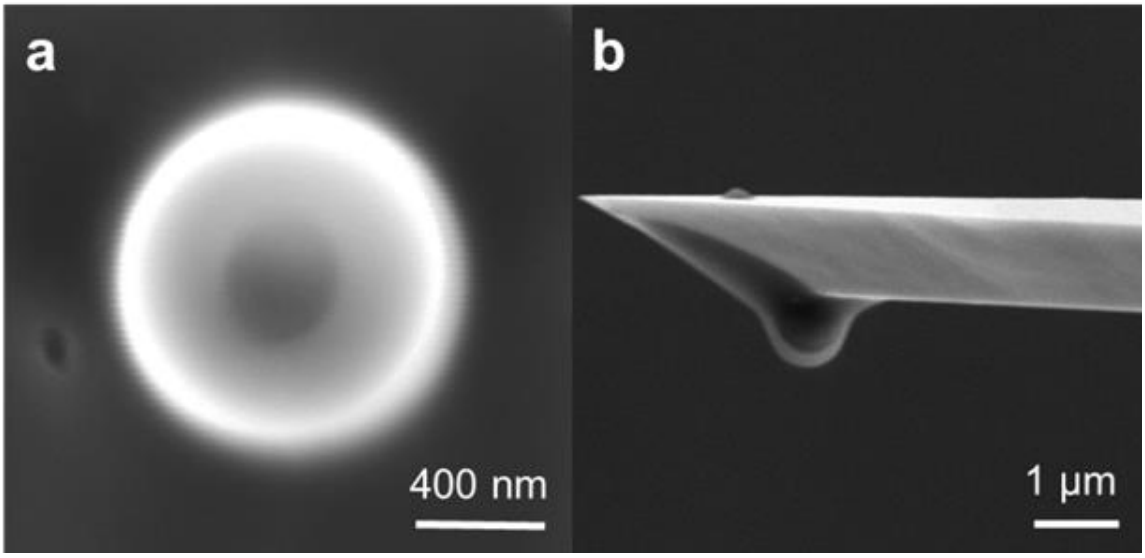

Figure 8. SEM images of AFM SiO_2 microsphere tip. (a) Top and (b) side view of the microsphere tip attached to the cantilever.

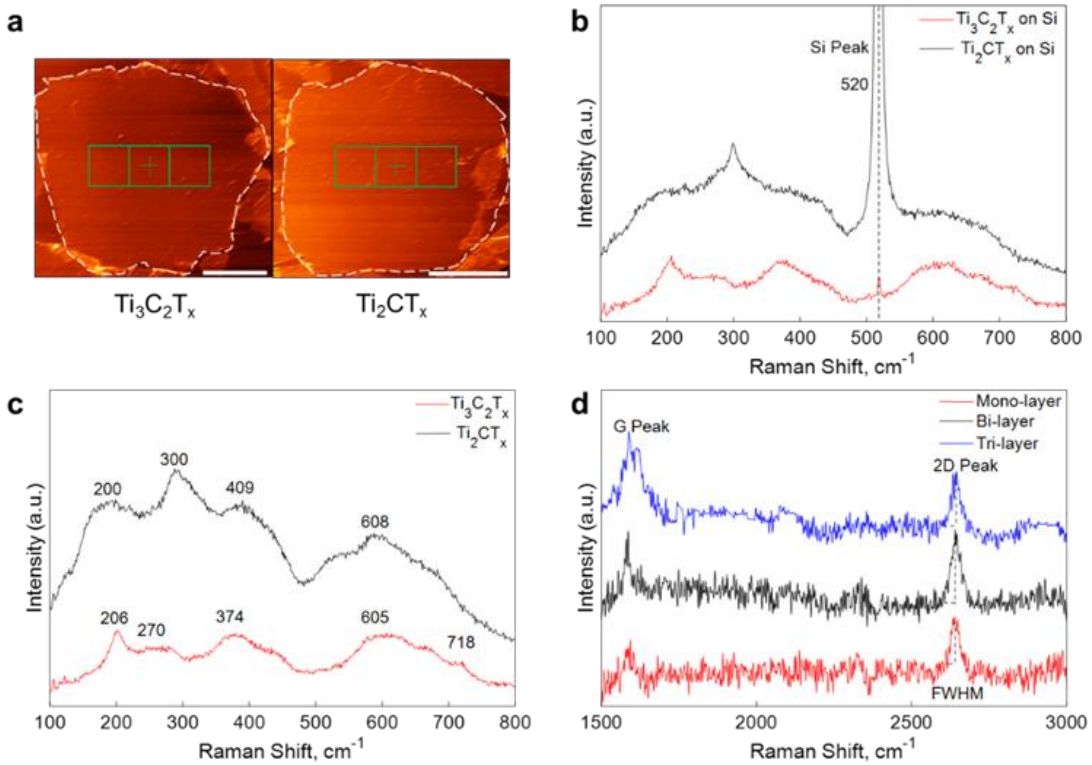

Figure S9. (a) AFM scans of representative MXene flakes (scale bar 1 µm), which were divided into 3 scanning areas individually. Raman spectra of (b) $Ti_3C_2T_x$ and Ti_2CT_x on Si, (c) $Ti_3C_2T_x$, Ti_2CT_x on the cover glass, and (d) mono-, bi-, and tri-layer graphene.

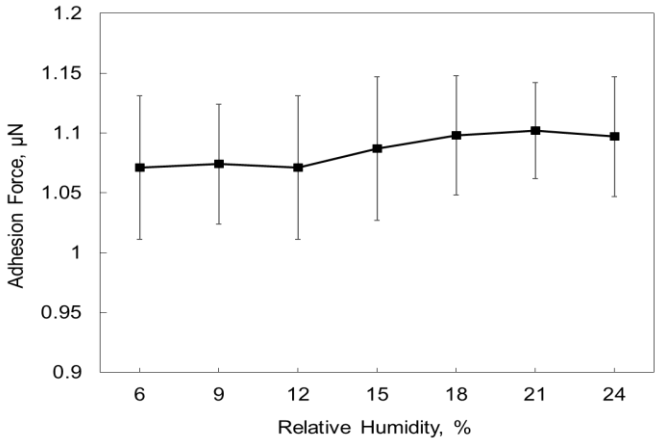

Figure S10. Adhesion force of MXene film ($Ti_3C_2T_x$) *vs* relative humidity.

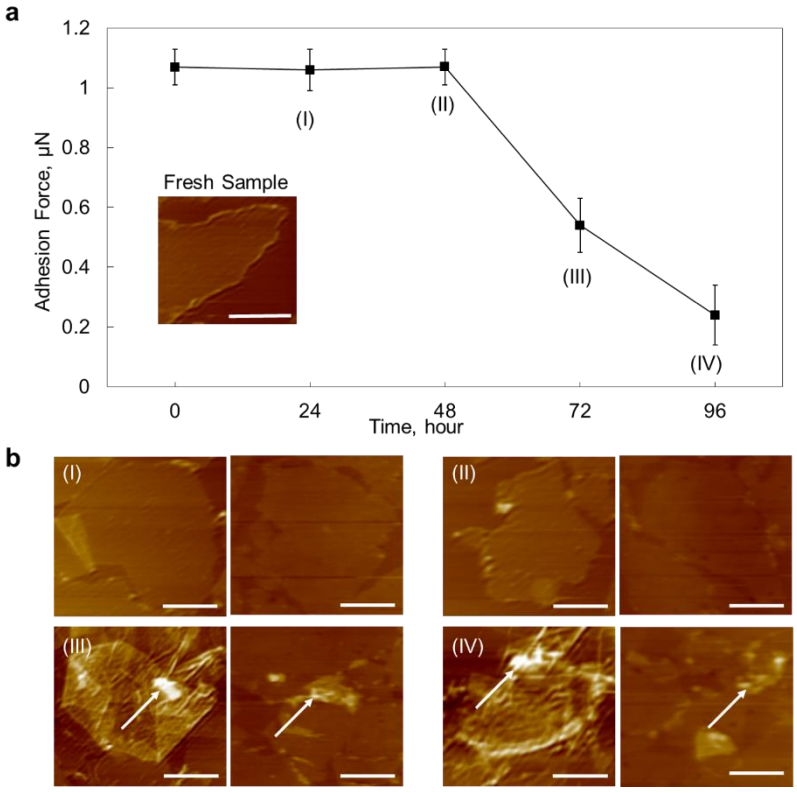

Figure S11. (a) Adhesion force *vs* time of exposure in air under room temperature for $Ti_3C_2T_x$ flakes and (b) AFM images of $Ti_3C_2T_x$ flakes taken at the time points indicated by roman numbers that correspond to the points in panel (a). All scale bars are 1 μm. The pairs of AFM images show results from two different experiments, which were also averaged in panel (a). Arrows indicate TiO_2 nanoparticles formed as result of MXene oxidation.

REFERENCES

[1] M. Naguib, V.N. Mochalin, M.W. Barsoum, Y. Gogotsi, 25th anniversary article: MXenes: A new family of two‐dimensional materials, *Advanced Materials*, 26 (**2014**) 992-1005.

[2] B. Anasori, M.R. Lukatskaya, Y. Gogotsi, 2D metal carbides and nitrides (MXenes) for energy storage, *Nature Reviews Materials*, 2 (**2017**) 16098.

[3] M. Ghidiu, M.R. Lukatskaya, M.Q. Zhao, Y. Gogotsi, M.W. Barsoum, Conductive two-dimensional titanium carbide 'clay' with high volumetric capacitance, *Nature*, 516 (**2014**) 78-81.

[4] M.R. Lukatskaya, S. Kota, Z. Lin, M.-Q. Zhao, N. Shpigel, M.D. Levi, J. Halim, P.-L. Taberna, M.W. Barsoum, P. Simon, Ultra-high-rate pseudocapacitive energy storage in two-dimensional transition metal carbides, *Nature Energy*, 2 (**2017**) 1-6.

[5] M. Naguib, J. Halim, J. Lu, K.M. Cook, L. Hultman, Y. Gogotsi, M.W. Barsoum, New two-dimensional niobium and vanadium carbides as promising materials for Li-ion batteries, *Journal of the American Chemical Society*, 135 (**2013**) 15966-15969.

[6] Y. Xie, M. Naguib, V.N. Mochalin, M.W. Barsoum, Y. Gogotsi, X. Yu, K.W. Nam, X.Q. Yang, A.I. Kolesnikov, P.R. Kent, Role of surface structure on Li-ion energy storage capacity of two-dimensional transition-metal carbides, *Journal of the American Chemical Society*, 136 (**2014**) 6385-6394.

[7] Y. Dong, S.S.K. Mallineni, K. Maleski, H. Behlow, V.N. Mochalin, A.M. Rao, Y. Gogotsi, R. Podila, Metallic MXenes: A new family of materials for flexible triboelectric nanogenerators, *Nano Energy*, 44 (**2018**) 103-110.

[8] Y. Dong, S. Chertopalov, K. Maleski, B. Anasori, L. Hu, S. Bhattacharya, A.M. Rao, Y. Gogotsi, V.N. Mochalin, R. Podila, Saturable absorption in 2D Ti_3C_2 MXene thin films for passive photonic diodes, *Advanced Materials*, 30 (**2018**) 1705714.

[9] E. Lee, A. VahidMohammadi, B.C. Prorok, Y.S. Yoon, M. Beidaghi, D.-J. Kim, Room temperature gas sensing of two-dimensional titanium carbide (MXene), *ACS Applied Materials & Interfaces*, 9 (**2017**) 37184-37190.

[10] S. Chertopalov, V.N. Mochalin, Environment sensitive photoresponse of spontaneously partially oxidized $Ti_3C_2T_x$ MXene thin films, *ACS Nano*, 12 (**2018**) 6109-6116.

[11] X. Wu, L. Hao, J. Zhang, X. Zhang, J. Wang, J. Liu, Polymer-$Ti_3C_2T_x$ composite membranes to overcome the trade-off in solvent resistant nanofiltration for alcohol-based system, *Journal of Membrane Science*, 515 (**2016**) 175-188.

[12] Y. Wu, P. Nie, L. Wu, H. Dou, X. Zhang, 2D MXene/SnS_2 composites as high-performance anodes for sodium ion batteries, *Chemical Engineering Journal*, 334 (**2018**) 932-938.

[13] M. Alhabeb, K. Maleski, B. Anasori, P. Lelyukh, L. Clark, S. Sin, Y. Gogotsi, Guidelines for synthesis and processing of two-dimensional titanium carbide ($Ti_3C_2T_x$ MXene), *Chemistry of Materials*, 29 (**2017**) 7633-7644.

[14] H.-W. Wang, M. Naguib, K. Page, D.J. Wesolowski, Y. Gogotsi, Resolving the structure of $Ti_3C_2T_x$ MXenes through multilevel structural modeling of the atomic pair distribution function, *Chemistry of Materials*, 28 (**2016**) 349-359.

[15] I. Persson, L.-Å. Näslund, J. Halim, M.W. Barsoum, V. Darakchieva, J. Palisaitis, J. Rosen, P.O.Å. Persson, On the organization and thermal behavior of functional groups on Ti_3C_2 MXene surfaces in vacuum, *2D Materials*, 5 (**2017**) 015002.

[16] M.A. Hope, A.C. Forse, K.J. Griffith, M.R. Lukatskaya, M. Ghidiu, Y. Gogotsi, C.P. Grey, NMR reveals the surface functionalization of Ti_3C_2 MXene, *Physical Chemistry Chemical Physics*, 18 (**2016**) 5099-5102.

[17] A.D. Dillon, M.J. Ghidiu, A.L. Krick, J. Griggs, S.J. May, Y. Gogotsi, M.W. Barsoum, A.T. Fafarman, Highly conductive optical quality solution‐processed films of 2D titanium carbide, *Advanced Functional Materials*, 26 (**2016**) 4162-4168.

[18] Z. Ling, C.E. Ren, M.-Q. Zhao, J. Yang, J.M. Giammarco, J. Qiu, M.W. Barsoum, Y. Gogotsi, Flexible and conductive MXene films and nanocomposites with high capacitance, *Proceedings of the National Academy of Sciences*, 111 (**2014**) 16676-16681.

[19] K. Maleski, V.N. Mochalin, Y. Gogotsi, Dispersions of two-dimensional titanium carbide MXene in organic solvents, *Chemistry of Materials*, 29 (**2017**) 1632-1640.

[20] V.N. Borysiuk, V.N. Mochalin, Y. Gogotsi, Molecular dynamic study of the mechanical properties of two-dimensional titanium carbides $Ti_{n+1}C_n$ (MXenes), *Nanotechnology*, 26 (**2015**) 265705.

[21] A. Lipatov, H. Lu, M. Alhabeb, B. Anasori, A. Gruverman, Y. Gogotsi, A. Sinitskii, Elastic properties of 2D $Ti_3C_2T_x$ MXene monolayers and bilayers, *Science Advances*, 4 (**2018**) eaat0491.

[22] V.N. Borysiuk, V.N. Mochalin, Y. Gogotsi, Bending rigidity of two-dimensional titanium carbide (MXene) nanoribbons: A molecular dynamics study, *Computational Materials Science*, 143 (**2018**) 418-424.

[23] T. Jiang, Y. Zhu, Measuring graphene adhesion using atomic force microscopy with a microsphere tip, *Nanoscale*, 7 (**2015**) 10760-10766.

[24] N.A. Burnham, D.D. Dominguez, R.L. Mowery, R.J. Colton, Probing the surface forces of monolayer films with an atomic-force microscope, *Physical review letters*, 64 (**1990**) 1931.

[25] H.-J. Butt, B. Cappella, M. Kappl, Force measurements with the atomic force microscope: Technique, interpretation and applications, *Surface Science Reports*, 59 (**2005**) 1-152.

[26] D. Maugis, Adhesion of spheres: the JKR-DMT transition using a Dugdale model, *Journal of colloid and interface science*, 150 (**1992**) 243-269.

[27] J.W. Suk, S.R. Na, R.J. Stromberg, D. Stauffer, J. Lee, R.S. Ruoff, K.M. Liechti, Probing the adhesion interactions of graphene on silicon oxide by nanoindentation, *Carbon*, 103 (**2016**) 63-72.

[28] T.D. Jacobs, K.E. Ryan, P.L. Keating, D.S. Grierson, J.A. Lefever, K.T. Turner, J.A. Harrison, R.W. Carpick, The effect of atomic-scale roughness on the adhesion of nanoscale asperities: a combined simulation and experimental investigation, *Tribology Letters*, 50 (**2013**) 81-93.

[29] Y.I. Rabinovich, J.J. Adler, A. Ata, R.K. Singh, B.M. Moudgil, Adhesion between nanoscale rough surfaces: I. Role of asperity geometry, *Journal of Colloid and Interface Science*, 232 (**2000**) 10-16.

[30] S. Na, D. Sarceno, K. Liechti, Ultra long-range interactions between silicon surfaces, *International Journal of Solids and Structures*, 80 (**2016**) 168-180.

[31] P. Gong, Q. Li, X.-Z. Liu, R.W. Carpick, P. Egberts, Adhesion mechanics between nanoscale silicon oxide tips and few-layer graphene, *Tribology Letters*, 65 (**2017**) 61.

[32] S.P. Koenig, N.G. Boddeti, M.L. Dunn, J.S. Bunch, Ultrastrong adhesion of graphene membranes, *Nature Nanotechnology*, 6 (**2011**) 543.

[33] X.Z. Liu, Q. Li, P. Egberts, R.W. Carpick, Nanoscale adhesive properties of graphene: the effect of sliding history, *Advanced Materials Interfaces*, 1 (**2014**) 1300053.

[34] J. Torres, Y. Zhu, P. Liu, S.C. Lim, M. Yun, Adhesion energies of 2D graphene and MoS_2 to silicon and metal substrates, *Physica Status Solidi (A)*, 215 (**2018**) 1700512.

[35] Q. Ouyang, K. Ishida, K. Okada, Investigation of micro-adhesion by atomic force microscopy, *Applied Surface Science*, 169 (**2001**) 644-648.

[36] R. Jones, H.M. Pollock, J.A. Cleaver, C.S. Hodges, Adhesion forces between glass and silicon surfaces in air studied by AFM: Effects of relative humidity, particle size, roughness, and surface treatment, *Langmuir*, 18 (**2002**) 8045-8055.

[37] M. Paajanen, J. Katainen, O.H. Pakarinen, A.S. Foster, J. Lahtinen, Experimental humidity dependency of small particle adhesion on silica and titania, *Journal of Colloid and Interface Science*, 304 (**2006**) 518-523.

[38] O. Stukalov, C.A. Murray, A. Jacina, J.R. Dutcher, Relative humidity control for atomic force microscopes, *Review of Scientific Instruments*, 77 (**2006**) 033704.

[39] X. Li, W. Cai, J. An, S. Kim, J. Nah, D. Yang, R. Piner, A. Velamakanni, I. Jung, E. Tutuc, Large-area synthesis of high-quality and uniform graphene films on copper foils, *Science*, 324 (**2009**) 1312-1314.

[40] A. Krajewska, I. Pasternak, G. Sobon, J. Sotor, A. Przewloka, T. Ciuk, J. Sobieski, J. Grzonka, K.M. Abramski, W. Strupinski, Fabrication and applications of multi-layer graphene stack on transparent polymer, *Applied Physics Letters*, 110 (**2017**) 041901.

[41] N. Yoshihara, M. Noda, Chemical etching of copper foils for single-layer graphene growth by chemical vapor deposition, *Chemical Physics Letters*, 685 (**2017**) 40-46.

[42] S. Huang, V.N. Mochalin, Hydrolysis of 2D transition-metal carbides (MXenes) in colloidal solutions, *Inorganic Chemistry*, 58 (**2019**) 1958-1966.

[43] A. Lipatov, M. Alhabeb, M.R. Lukatskaya, A. Boson, Y. Gogotsi, A. Sinitskii, Effect of synthesis on quality, electronic properties and environmental stability of individual monolayer Ti_3C_2 MXene flakes, *Advanced Electronic Materials*, 2 (**2016**) 1600255.

[44] M. Naguib, O. Mashtalir, M.R. Lukatskaya, B. Dyatkin, C. Zhang, V. Presser, Y. Gogotsi, M.W. Barsoum, One-step synthesis of nanocrystalline transition metal oxides on thin sheets of disordered graphitic carbon by oxidation of MXenes, *Chemical Communications*, 50 (**2014**) 7420-7423.

[45] Y. Cao, Q. Deng, Z. Liu, D. Shen, T. Wang, Q. Huang, S. Du, N. Jiang, C.-T. Lin, J. Yu, Enhanced thermal properties of poly (vinylidene fluoride) composites with ultrathin nanosheets of MXene, *RSC Advances*, 7 (**2017**) 20494-20501.

[46] C. Zhang, S. Pinilla, N. McEvoy, C.P. Cullen, B. Anasori, E. Long, S.H. Park, A. Seral-Ascaso, A. Shmeliov, D. Krishnan, Oxidation stability of colloidal 2D titanium carbides (MXenes), *Chemistry of Materials*, 29 (**2017**) 4848-4856.

[47] F. Liu, A. Zhou, J. Chen, H. Zhang, J. Cao, L. Wang, Q. Hu, Preparation and methane adsorption of two-dimensional carbide Ti_2C, *Adsorption*, 22 (**2016**) 915-922.

[48] J.E. Spanier, S. Gupta, M. Amer, M.W. Barsoum, Vibrational behavior of the $M_{n+1}AX_n$ phases from first-order Raman scattering (M= Ti, V, Cr, A= Si, X= C, N), *Physical Review B*, 71 (**2005**) 012103.

[49] I. Childres, L.A. Jauregui, W. Park, H. Cao, Y.P. Chen, Raman spectroscopy of graphene and related materials, *New Developments in Photon and Materials Research*, 1 (**2013**) 1-20.

[50] A.C. Ferrari, J. Meyer, V. Scardaci, C. Casiraghi, M. Lazzeri, F. Mauri, S. Piscanec, D. Jiang, K. Novoselov, S. Roth, Raman spectrum of graphene and graphene layers, *Physical Review Letters*, 97 (**2006**) 187401.

[51] W. Feng, H. Luo, Y. Wang, S. Zeng, L. Deng, X. Zhou, H. Zhang, S. Peng, Ti_3C_2 MXene: a promising microwave absorbing material, *RSC Advances*, 8 (**2018**) 2398-2403.

[52] X. Li, X. Yin, M. Han, C. Song, X. Sun, H. Xu, L. Cheng, L. Zhang, A controllable heterogeneous structure and electromagnetic wave absorption properties of Ti_2CT_x MXene, *Journal of Materials Chemistry C*, 5 (**2017**) 7621-7628.

[53] B. Cappella, G. Dietler, Force-distance curves by atomic force microscopy, *Surface Science Reports*, 34 (**1999**) 1-104.

[54] R.W. Carpick, D.F. Ogletree, M. Salmeron, A general equation for fitting contact area and friction vs load measurements, *Journal of Colloid and Interface Science*, 211 (**1999**) 395-400.

[55] W. Gao, P. Xiao, G. Henkelman, K.M. Liechti, R. Huang, Interfacial adhesion between graphene and silicon dioxide by density functional theory with van der Waals corrections, *Journal of Physics D: Applied Physics*, 47 (**2014**) 255301.

IV. ACHIEVING SUPERLUBRICITY WITH 2D TRANSITION METAL CARBIDES (MXENES) AND MXENE/GRAPHENE COATINGS

Shuohan Huang[a], Kalyan C. Mutyala[c, d], Anirudha V. Sumant[c, *], Vadym N. Mochalin[a, b, *]
[a]Department of Chemistry, Missouri University of Science & Technology, Rolla, Missouri 65409, United States
[b]Department of Materials Science & Engineering, Missouri University of Science & Technology, Rolla, Missouri 65409, United States
[c]Center of Nanoscale Materials, Argonne National Laboratory, Lemont, Illinois, 60439, USA
[d]Currently at Ford Motor Company, Dearborn, Michigan, 48124, USA
*Correspondence to: sumant@anl.gov and mochalinv@mst.edu

ABSTRACT

Two-dimensional (2D) materials have demonstrated unique friction and anti-wear properties unmatched by their bulk (3D) counterparts. A relatively new, large and quickly growing family of two-dimensional early transition metal carbides and nitrides (MXenes) present a great potential in different applications. There is a growing interest in understanding the mechanical and tribological properties of MXenes, however, no report of MXene superlubricity in a solid lubrication process at the macroscale has been presented. Here we investigate the tribological properties of Ti_3C_2 MXene deposited on SiO_2 coated Si substrates subjected to wear by sliding against a diamond-like carbon coated steel ball counterbody using a ball-on-disc tribometer. We have observed that a reduction of the friction coefficient to the superlubric regime (0.0067 ± 0.0017) can be achieved with Ti_3C_2 MXene in dry nitrogen environment. Moreover, the addition of graphene to Ti_3C_2 further reduced the friction by 37.3% and wear by the factor of 2 as compared to Ti_3C_2

alone, while the superlubricity behavior of the MXene remained unchanged. These results open up new possibilities for exploring the family of MXenes in various tribological applications.

1. INTRODUCTION

Efficiency and lifetime of machinery, which are affected by friction, lubrication, and wear of materials, become increasingly crucial in modern society [1]. Concerns about the increased consumption of non-renewable energy resources, such as coal and petroleum, demand minimization of friction in transportation and industrial sectors [2]. Thus, the discovery and development of excellent lubricant materials to combat friction and wear are of great importance. Solid 2D lubricants such as graphene [2, 3], graphene oxide [4], and molybdenum disulfide (MoS_2) [5] are now gaining much attention for this purpose because of their superior mechanical properties and environmental benignancy compared with oil-based lubricants. Many experimental and theoretical studies have investigated the tribological behavior of 2D materials [6-12]. In particular, graphene has shown outstanding tribological properties as promising lubricant, as well as excellent additive to compositions for wear and friction reduction purposes. The possibility to achieve superlubricity in various atmospheric conditions at the macroscale, utilizing graphene and other 2D materials and their combinations, is another big step [13-16]. MXenes are a new class of two-dimensional early transition metal carbides/nitrides discovered in 2011 [17, 18]. MXenes are produced by etching of the A layers from bulk MAX phases, where M represents transition metal, A is a group IIIA or IVA elemen, and X can be C, N or both

[19]. As a relatively new, large and quickly growing class of 2D materials, MXenes have been studied in various applications, such as supercapacitors [20]. Lasers [21], EMI shielding and THz communication [22], batteries [23-26], sensors [27-30], etc. Thermal stability [31] and mechanical properties [32, 33] of individual MXene flakes have been studied computationally on a large scale, as well as experimentally [34], and their adhesion behavior has also been investigated recently [35, 36]. MXenes are great candidates for tribological applications because of their outstanding mechanical strength and bending rigidity [32, 34, 37] and a possibility for precise control over the monolayer thickness [38-40]. Yang et al. reported that the addition of 1.0 wt% Ti_3C_2 MXene improved the anti-friction properties of base oil [41]. In a similar study published by Zhang et al., 1.0 wt% of 10-20 nm Ti_3C_2 nanosheets effectively improved the friction and anti-wear properties of base oil [42]. Liu et al. reported a lower friction coefficient and ball wear volume achieved with 0.8 wt% of highly exfoliated Ti_3C_2 added to base oil [43].

Ti_3C_2 MXene is also a promising material for solid lubrication. Zhang et al. reported on the synthesis of Ti_3C_2/ultra-high molecular weight polyethylene composites that reduced the plow friction and adhesive wear [44]. Mai et al. designed Ti_3C_2 nanosheets/copper composites with a 19 times lower wear rate and a 46% reduction in the coefficient of friction (COF) compared to the bare copper counterbody under dry sliding [45]. Recently, Yin et al. created Ti_3C_2/nanodiamond composites that showed the ultra-wear resistance when rubbed against a polytetrafluoroethylene ball at room temperature in air. According to the authors, the combination of the rolling action of nanodiamond with the slipping and intercalation of MXene provided the reduction in wear [46]. Hu et al. reported $Ti_3C_2T_x$/Al composites with COF 0.2 in dry sliding test, which is twice lower than

that of bare Al [47]. Zhang et al. predicted using modeling that defects, such as Ti and O vacancies in MXene structure, increase the COF through increasing its surface roughness. And compared with the -O- terminated Ti_3C_2, the -OH terminations of Ti_3C_2 further reduced its interlayer COF [48]. Rosenkranz et al. verified that both surface terminations and intercalated water in $Ti_3C_2T_x$ MXene reduced the interfacial bonding strength, resulting in a lower frictional force under dry conditions on stainless steel surfaces [49]. Researchers have also demonstrated that Ti_3C_2 MXene can act as solid lubricant on different substrates at the nanoscale [36, 50, 51]. All these studies utilizing MXene alone or in combination with other 2D materials have shown that MXenes have great potential as solid lubricants, however, none of these studies reported superlubricity either using MXene itself or in combination with other materials. Moreover, it should be noted that MXenes may be quite reactive towards environment, in particular, water [52-55] and water vapor, as well as other gaseous species [27] may result in MXene degradation or at least, change its surface terminations. Therefore, it becomes important to conduct measurements in an inert atmosphere.

In this work, we investigate the tribological properties of Ti_3C_2 MXene as well as MXene/graphene films on Si substrates coated with thin film of SiO_2 (~300 nm thick SiO_2, from Silicon Valley Microelectronics, hereafter referred to as “Si substrates”) subjected to wear by sliding against a diamond-like carbon (DLC) coated stainless steel ball using a ball-on-disc tribometer operated in a controlled environment. We demonstrate that it is possible to achieve superlubricity with MXene alone as well as in combination with graphene, with an additional benefit of reduced wear in the latter case.

2. EXPERIMENTAL DETAILS

2.1. PREPARATION OF Ti_3C_2 MXENE AND Ti_3C_2/GRAPHENE COATINGS ON SILICON SUBSTRATES

Ti_3AlC_2 MAX phase was synthesized by heating a mixture of Ti (-325 mesh, 99.5%, Alfa Aesar), Al (-325 mesh, 99.5%, Alfa Aesar), and graphite (-325 mesh, 99%, Alfa Aesar) powders (3:1.1:1.88 molar ratio) at a rate of 10 ^oC/min from RT to 1550 ^oC and holding at this temperature for 2 h. Heating and cooling were entirely conducted under Ar flow. Ti_3C_2 MXene was synthesized according to the published methods [53]. Briefly, the etchant was prepared by adding 0.3 g LiF to 3 mL 9 M HCl in a plastic centrifuge tube and stirring for 5 min. 0.3 g of Ti_3AlC_2 MAX phase powder (-400 mesh, particle size $\leq$ 38 µm) was gradually added to the etchant and left reacting for 36 h at 35 ^oC. The etched powder was washed with deionized water until the pH of the supernatant reached ~6. The Ti_3C_2 colloidal solution was then obtained by 5 min hand-shaking followed by 40 min centrifugation at 3500 rpm.

Samples of Ti_3C_2 on Si substrates (average flake size ~0.8 µm, Figure 1) were produced by 20 min bath sonication of the as-prepared MXene colloidal solution and spray-coated from ~1.5 mL of the diluted as-prepared aqueous colloidal solution (0.017 mg/mL MXene). Ti_3C_2/graphene coatings were prepared by mixing diluted Ti_3C_2 colloidal solution (0.017 mg/mL) and graphene ethanol solution (0.010 mg/mL, Graphene Supermarket, carbon content 99.99%, average flake size ~550 nm) in a 1:1 volume ratio followed by 20 min bath sonication. ~1.5 mL of this dispersion was spray-coated on the Si substrates. All samples were dried in ambient environment for more than 24 h before testing. All Si

substrates used in this work were treated overnight in piranha solution (concentrated sulfuric acid: hydrogen peroxide = 3: 1) prior to film deposition.

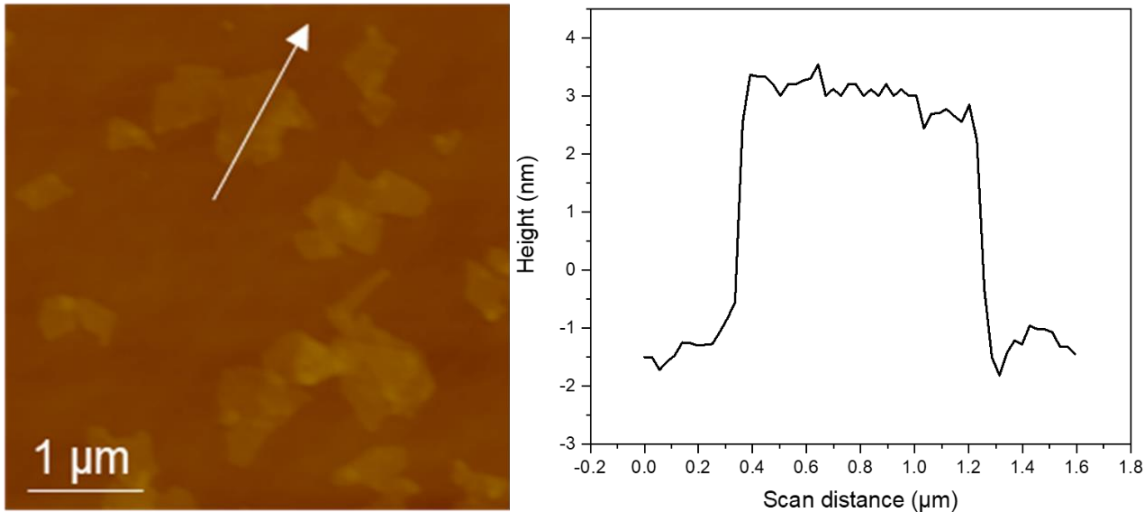

Figure 1. AFM images of Ti_3C_2 coatings on Si substrates.

2.2. FRICTION AND WEAR TESTS

Friction and wear tests were conducted in dry nitrogen atmosphere (Dew Point Temperature -40 ^{o}C, ≤ RH 0.1%) at room temperature using a multifunctional ball-on-disc type tribometer (MFT-5000, Rtec Instruments). The Si substrates with deposited films were clamped on a sample platform and slid against a 9.526 mm diameter stainless steel ball coated with DLC as described elsewhere [56, 57]. The applied normal load was controlled at 2 N (maximum contact pressure 0.60 GPa) with 0.1 m/s linear velocity for a total running time of 1 hour. Zero calibration of the machine was carried out automatically before each test.

2.3. CHARACTERIZATION

Raman spectroscopy was performed using Renishaw InVia confocal Raman micro-spectrometer with 532 nm laser, 100x objective and a 1200 l/mm grating. The spectra were acquired with 500 s exposure time, 0.5% of laser power and 1 accumulation.

Atomic force microscopy (AFM) was performed using Digital Instruments Nanoscope IIIA under ambient atmosphere. The AFM image of Ti_3C_2 was recorded in tapping mode with a silicon tip (App Nano, Tip radius < 10nm).

3. RESULTS AND DISCUSSION

3.1. TRIBOLOGICAL BEHAVIOR OF MXENE COATING

Friction tests were first conducted on the Si substrates *vs* DLC coated balls for comparison. The experimental COFs for a Si substrate and Ti_3C_2 MXene against the DLC coated ball are shown in Figure 2 where the dash-dotted line represents superlubric threshold (COF = 0.01). The average measured COF for Si substrate against DLC in the range 700-1800 s (before the failure point) is 0.0222 ± 0.0035, whereas the average COF for Ti_3C_2 against DLC in the range 700-3100 s, i.e., before the failure point, is in the superlubricity range, 0.0067 ± 0.0017, as shown in Figure 2(b). The COF value for Ti_3C_2 is 3.3 times lower than for the Si substrate. Failure points at ~1800 s and 3100 s for the Si substrate and Ti_3C_2 coating, respectively (Figure 2(a)), are due to wearing out of DLC coating on the ball as explained below based on the wear marks observed on the counterbody after wear tests.

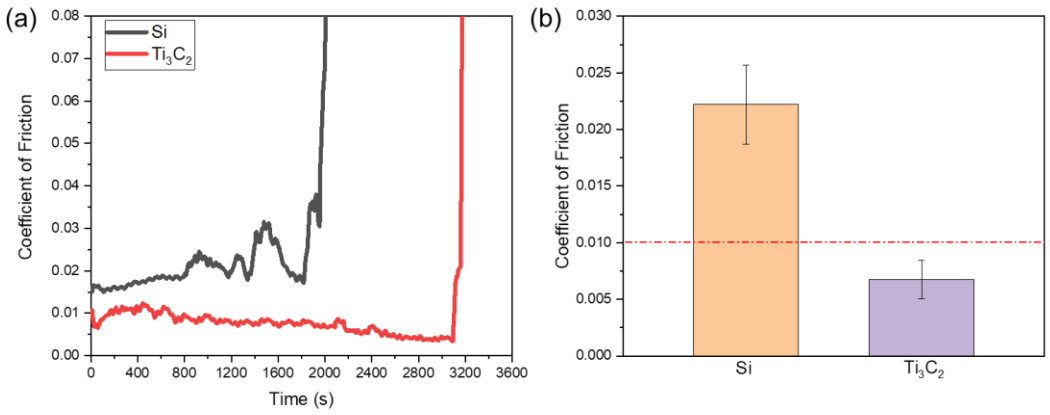

Figure 2. (a) Tribological behavior of Si substrate and Ti_3C_2 on Si substrate against a DLC coated steel ball and; (b) comparison of COF values demonstrating the onset of superlubricity. Error bars represent standard deviations of the average COF values.

X-ray photoelectron spectroscopy (XPS) data for similar MXene samples published before [22, 35] showed the presence of Ti, C, O, F, and Cl elements, indicating that our MXenes are terminated with different functional groups (T = -OH, -F, -O- and -Cl), in good agreement with other literature data [58]. As hypothesized in prior studies, the surface terminations may affect friction by changing the interlayer binding/adhesion energy of MXenes resulting in a lower COF [49, 59]. However, in this case, we believe the inert nature of the DLC counterbody as well as graphene like shearing of of MXene flakes was mostly responsible for reducing the friction to superlubric regime. Since we did not passivate MXene, it may react over time of the experiment, which may eventually degrade the 2D nature of the MXene. When this happens, shearing becomes disturbed, which results in high friction that wears down DLC and leads to a sudden increase of friction to very high values towards the end of the tribo tests as shown in Figure 2(a). Optical microscopy images of the wear tracks for the Si substrate and Ti_3C_2 samples are shown in Figure 3(a,b).

Raman spectroscopy was further conducted on the wear tracks of the samples. Figure 3(c,d) show Raman spectra recorded from the wear tracks on the Si substrate and Ti_3C_2 coatings, respectively. Only Si peaks at 300, 520, and ~960 cm^{-1} were observed in four representative spots on Si substrate (Figure 3(c)) [60]. The Ti_3C_2 sample showed superlubric COF after 700 s and high friction after 3100 s when DLC coating has worn out exposing the underlying steel on the counterbody surface (Figure 2(a)). Raman spectra show only crystalline and amorphous Si peaks for spots 2-4 within the wear track (Figure 3(d)) and no signs of MXene. Figure 3(e,f) show the optical microscopy images of the balls worn against the Si substrate and Ti_3C_2, respectively. The DLC coatings were worn out in both tests on the Si substrate and Ti_3C_2 samples, clearly exposing the underlying steel surface of the balls. Although in case of Ti_3C_2 superlubricity was achieved, the wear was still high. This could be due to a relatively sparse coverage exposing Si in gaps between the flakes, as shown in AFM image (Figure 1), and leading to the intermittent contact between Si and DLC, thus increasing the overall wear. However, this did not affect COF on average since the flakes shear easily and are mobile within the wear track, thus despite the sparse nature of the coating, Ti_3C_2 maintained low friction over a long time. This behavior is similar to that of graphene flakes observed previously on steel surfaces [2].

3.2. TRIBOLOGICAL BEHAVIOR OF MXENE/GRAPHENE COATING

From the experiments described above, Ti_3C_2 reaches the superlubic regime but the coating is worn out finally. To check if it is possible to maintain superlubricity and reduce wear of the counterbody even further, we have also tried to fabricate a composite MXene-graphene coating prepared from mixing solution-processed graphene with Ti_3C_2 using

sonication. A similar strategy, when MXene was combined with another 2D material, was shown to improve mechanical properties of the resulting composite [61]. Another benefit of adding graphene to MXene coating is to protect MXene from the effects of the environment, where the hydrophobic nature of graphene may reduce exposure of MXene to humidity that is detrimental to its structure [52, 53]. A recent high-resolution microscopy study [62] also showed that the introduction of graphene nanosheets induces the formation of the lubricating tribofilm, so that it can protect the contact surface. Figure 4(a, b) display the friction test results of graphene, Ti_3C_2, and Ti_3C_2/graphene coatings, respectively, on Si substrate tested against DLC. The average friction coefficient for graphene versus DLC was 0.0138 ± 0.0014 (700-3600 s), while for the Ti_3C_2/graphene (~37 wt% of graphene) coating, it was reduced to 0.0042 ± 0.0011 (700-3600 s), which not only reached the superlubricity range but indeed reduced the wear of the DLC ball significantly. The lower friction coefficient of Ti_3C_2/graphene *vs* DLC could be attributed to the additional shearing and covering of MXene by graphene during the sliding process thereby reducing wear on the DLC side. It is also possible that graphene may have helped in passivating the reactive surface of MXene during friction. However, while the addition of 37 wt% graphene to MXene reduced the COF from 0.0067 ± 0.0017 to 0.0042 ± 0.0011, a 100 wt% graphene coating yielded a higher COF of 0.0138 ± 0.0014 indicating that a balance between graphene and MXene concentrations must be maintained to achieve the best performance. Thus, we experimentally demonstrated that a combination of Ti_3C_2 MXene with graphene provides the lowest friction coefficient and lower wear than Ti_3C_2 alone.

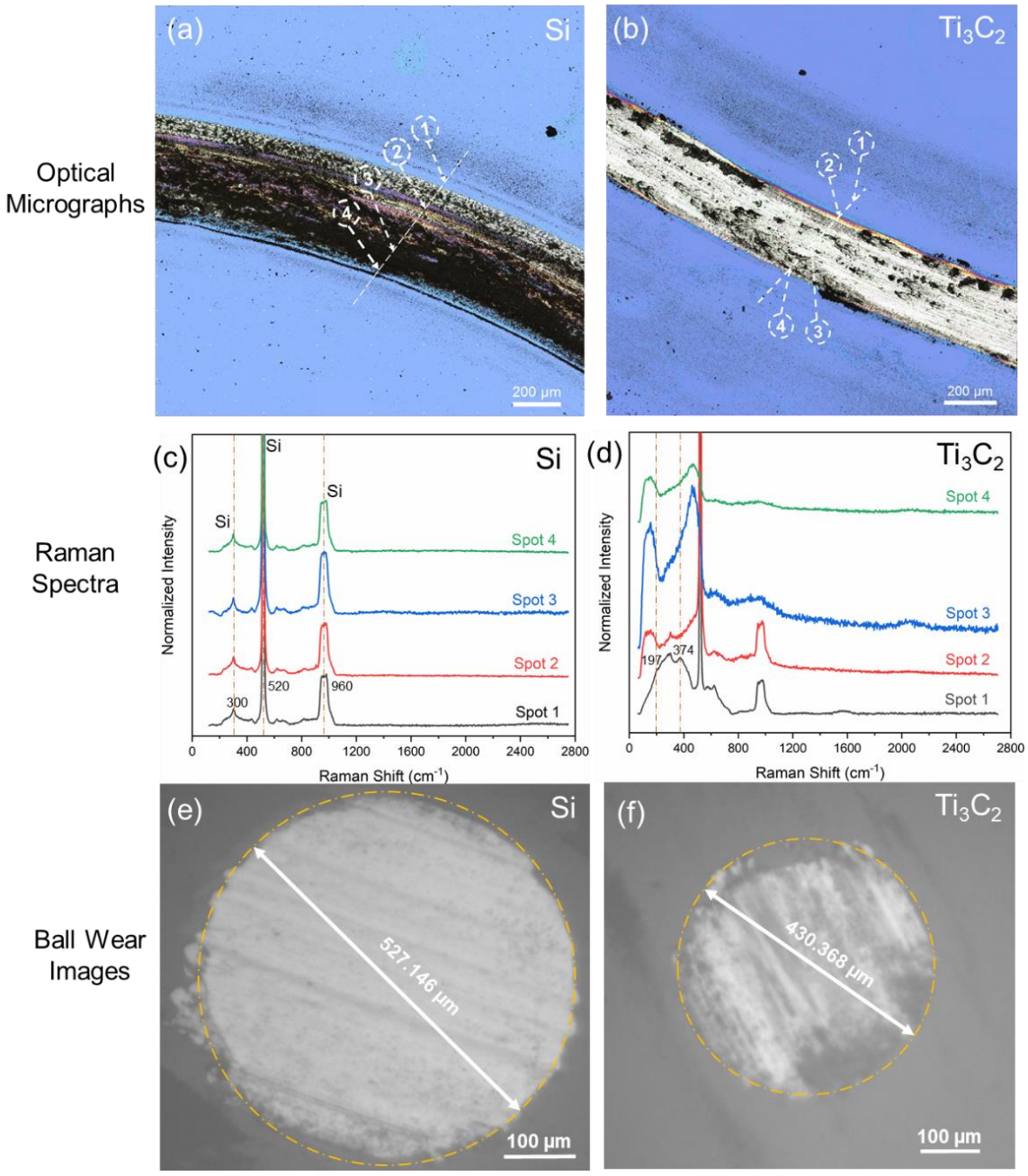

Figure 3. Top row: optical microscopy of the wear tracks on (a) Si substrate and (b) Ti_3C_2 samples; middle row: Raman spectra from representative spots on (c) Si substrate and (d) Ti_3C_2 samples; bottom row: optical microscopy of the balls worn against (e) Si substrate and (f) Ti_3C_2 samples.

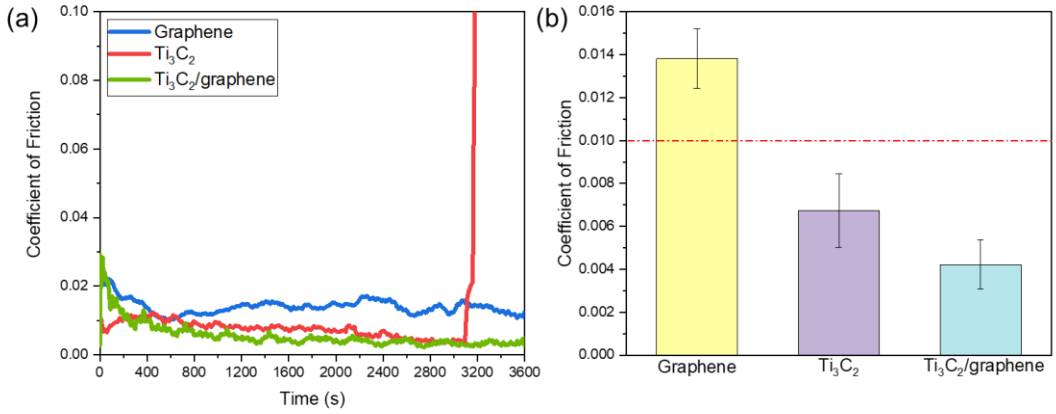

Figure 4. (a) Tribological behavior of graphene, Ti_3C_2, and Ti_3C_2/graphene coatings against DLC coated steel balls and (b) comparison of the corresponding COF values. Error bars represent standard deviations of average COF values.

Optical microscopy and Raman spectra of the wear track on graphene coated Si substrate are shown in Figure 5(a, c), respectively. Raman signature of graphene was observed in spots 1, 2, and 4 in Figure 5(c) with an increasing intensity of D band, indicating progressive amorphization when moving from the edges to the center of the wear track. The Raman spectrum from spot 3 shows amorphous carbon, which might be part of the transfer layer from DLC coating of the counterbody. Compared with Ti_3C_2 (Figure 3(b)), the wear track on Ti_3C_2/graphene coating *vs* DLC after the test appears to be less abrasive (Figure 5(b)).

Raman spectra from the wear track on Ti_3C_2/graphene sample showed amorphous carbon originating either from graphene remaining in the track or from DLC coating on the ball. In case of graphene, the wear is smaller according to Raman results (Figure 5) and friction test (Figure 4). It is clear that neat graphene has more complete coverage and therefore friction interface is mostly between DLC and graphene and not with the

underlaying SiO_2, resulting in a lower wear rate of the DLC ball. In case of Ti_3C_2/graphene, the coverage is sparse as can be deduced indirectly by looking at the intensity of the SiO_2 peak in the Raman spectra of the wear track (Figure 5(d)) and comparing it with Raman spectra shown in Figure 5(c). The higher intensity of SiO_2 peak in case of Ti_3C_2/graphene indicates that more SiO_2 is exposed and therefore the friction interface is mixed increasing the likelihood of intermittent contact between DLC and SiO_2. Although the overall friction is dominated by DLC vs Ti_3C_2 (hence the superlubricity is unchanged), the intermittent contact with the SiO_2 must be responsible for the higher wear rate.

Images of the wear scars on the counterbody were also analyzed. For graphene and Ti_3C_2/graphene coated samples, relatively small wear scars were observed after the tests (Figure 5(e, f)). The ball wear volume was estimated using the equation:

$$V = \left(\frac{\pi h}{6}\right)\left(\frac{3d^2}{4} + h^2\right) \quad (1)$$

$$\text{where } h = r - \sqrt{r^2 - d^2/4} \quad (2)$$

d is the diameter of the ball wear cap, and r is the radius of the DLC coated ball (4.763 mm).

The ball wear rate was estimated using Archard's equation [63, 64]:

$$K_B = \frac{V}{SW} \quad (3)$$

where V is the ball wear volume, S is the sliding distance (360 m in our study), and W is the applied load.

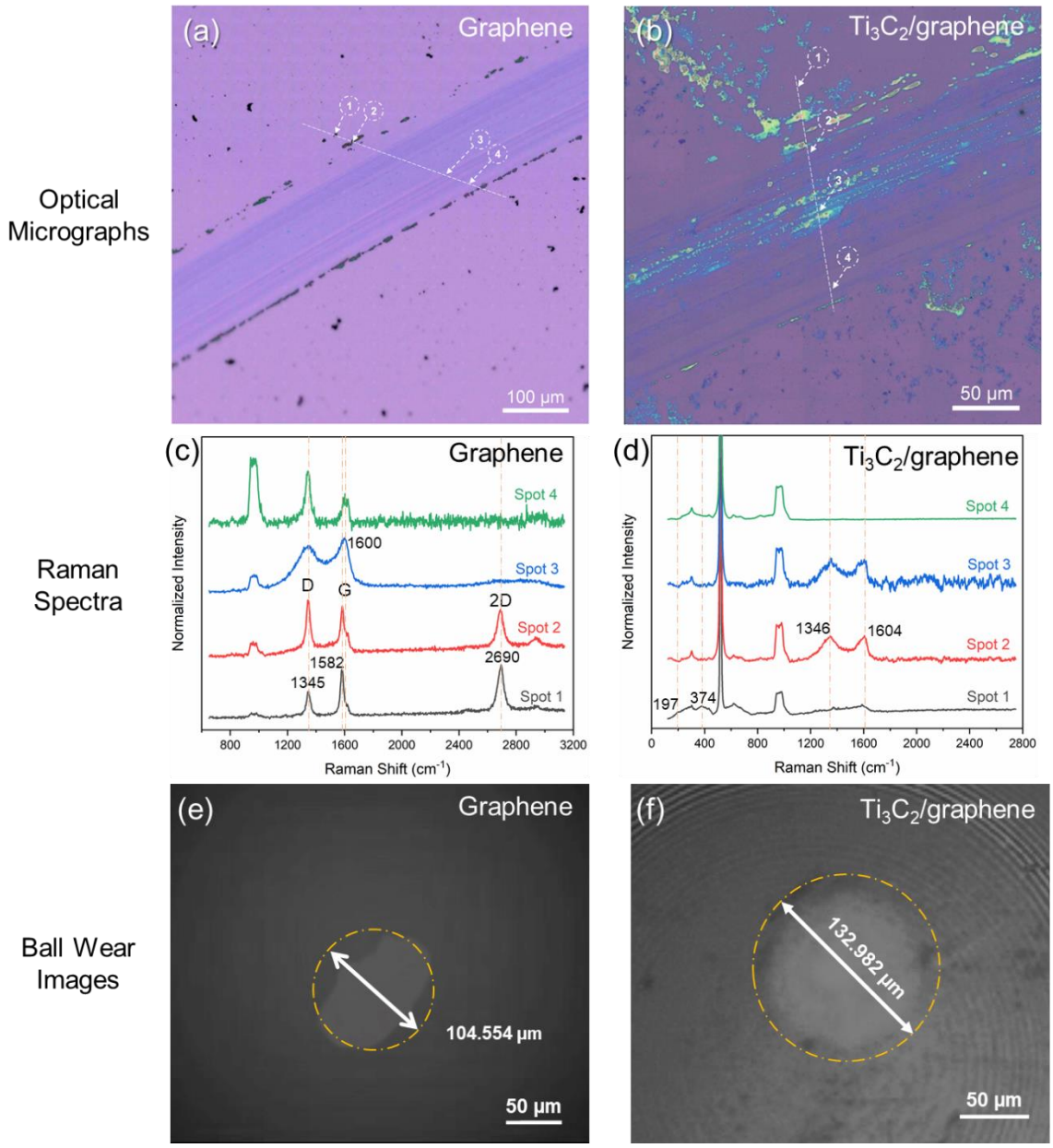

Figure 5. Top row: optical microscopy images of the wear tracks on (a) graphene and (b) Ti_3C_2/graphene coatings; middle row: Raman spectra from representative spots for (c) graphene and (d) Ti_3C_2/graphene samples; bottom row: optical microscopy images of the balls worn against (e) graphene, and (f) Ti_3C_2/graphene samples.

The ball wear rates against the Si substrate, Ti_3C_2, graphene, and Ti_3C_2/graphene coatings are summarized in Figure 6. The Si substrate showed the largest wear rate as

expected. Although achieving superlubricity, Ti_3C_2 MXene also showed a high wear rate (4.9×10^{-7} $mm^3/(N\cdot m)$). It is worth noting that after adding 37 wt% of graphene, the wear rate of Ti_3C_2 was reduced by a factor of 2, to 4.5×10^{-9} $mm^3/(N\cdot m)$, with COF further reduced by 37.3%. Thus, graphene prolonged the running time of Ti_3C_2 in the friction tests by reducing abrasion while the superlubricity of MXene remained unchanged.

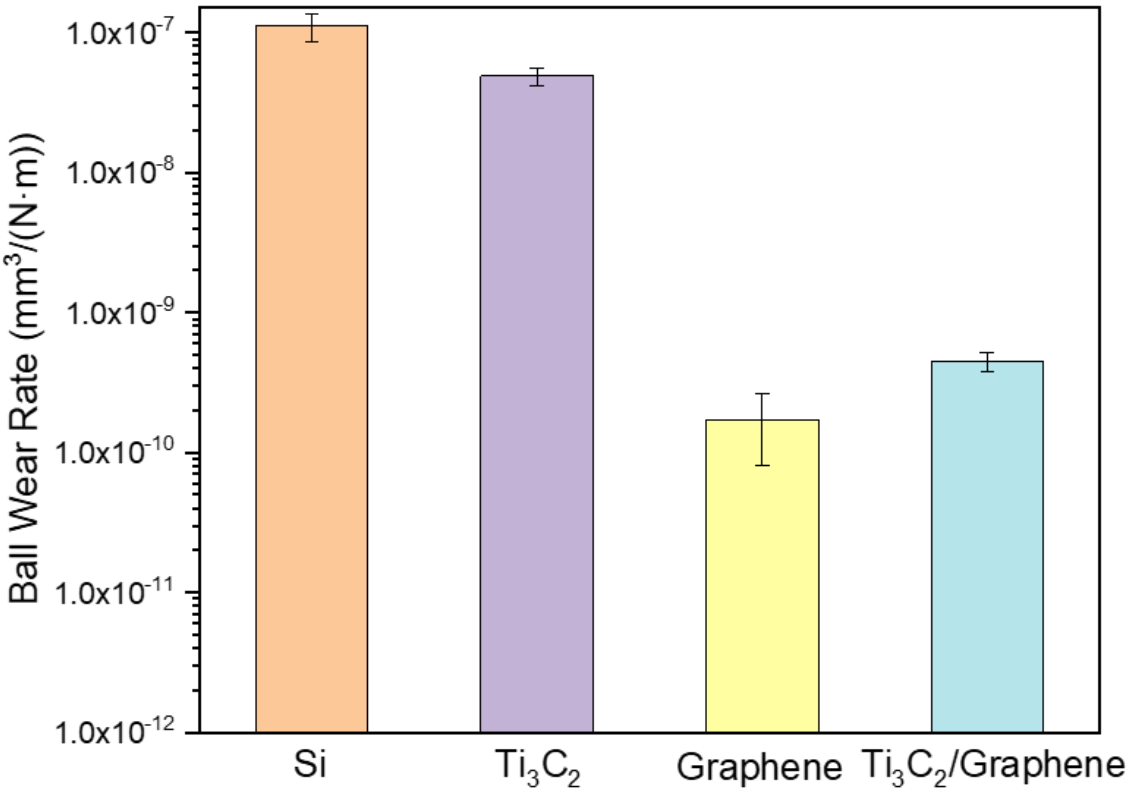

Figure 6. Ball wear rate against Si substrate, Ti_3C_2, graphene, and Ti_3C_2/graphene coated Si substrates.

4. CONCLUSIONS

In summary, the tribological properties of Ti_3C_2 MXene coatings on the Si substrate have been investigated in a controlled environment. The ball-on-disk friction tests were conducted against the DLC coated steel ball counterbody in dry nitrogen atmosphere and the results show that the average measured COF for Ti_3C_2 is 0.0067 ± 0.0017, falling into the superlubricity range. This COF value is 3.3 times lower than for the Si substrate. Moreover, with the introduction of 37 wt% graphene to Ti_3C_2, the COF was further reduced by 37.3% (to 0.0042 ± 0.0011) compared with Ti_3C_2, while the ball wear rate of Ti_3C_2 was reduced by a factor of 2. Thus, superlubricity against DLC can be achieved with MXene, furthermore, with the addition of graphene to MXene, the superlubricity of the coating remained unchanged while abrasion was further reduced. This work opens opportunities for exploring the potential of MXenes and MXene/graphene coatings as novel solid lubricants for various applications.

CREDIT AUTHORSHIP CONTRIBUTION STATEMENT

Shuohan Huang: Conceptualization, Investigation, Formal analysis, Validation, Writing - original draft. Kalyan C. Mutyala: Conceptualization, Investigation, Supervision, Writing - review & editing. Anirudha V. Sumant: Conceptualization, Supervision, Resources, Project administration, Funding acquisition, Writing - review & editing. Vadym N. Mochalin: Conceptualization, Supervision, Resources, Project administration, Funding acquisition, Writing - review & editing

ACKNOWLEDGEMENTS

The authors acknowledge access to the Center for Nanoscale Materials, an Office of Science user facility. This work was supported by the U.S. Department of Energy, Office of Science, Office of Basic Energy Sciences, under Contract No. DE-AC02-06CH11357. Part of this work was supported by the National Science Foundation under Grant No. 1930881 CMMI.

DATA AVAILABILITY STATEMENT

The raw/processed data required to reproduce these findings cannot be shared at this time due to technical or time limitations.

REFERENCES

[1] K. Holmberg, A. Erdemir, Influence of tribology on global energy consumption, costs and emissions, Friction, 5 (2017) 263-284.

[2] D. Berman, A. Erdemir, A.V. Sumant, Graphene: a new emerging lubricant, Mater. Today, 17 (2014) 31-42.

[3] X. Zeng, Y. Peng, H. Lang, A novel approach to decrease friction of graphene, Carbon, 118 (2017) 233-240.

[4] H. Liang, Y. Bu, J. Zhang, Z. Cao, A. Liang, Graphene oxide film as solid lubricant, ACS Appl. Mater. Interfaces, 5 (2013) 6369-6375.

[5] C. Donnet, J. Martin, T. Le Mogne, M. Belin, Super-low friction of MoS_2 coatings in various environments, Tribol. Int., 29 (1996) 123-128.

[6] W. Guo, J. Yin, H. Qiu, Y. Guo, H. Wu, M. Xue, Friction of low-dimensional nanomaterial systems, Friction, 2 (2014) 209-225.

[7] O. Penkov, H.J. Kim, H.J. Kim, D.E. Kim, Tribology of graphene: a review, Int. J. Precis. Eng. Manuf., 15 (2014) 577-585.

[8] J. Lin, L. Wang, G. Chen, Modification of graphene platelets and their tribological properties as a lubricant additive, Tribol. Lett., 41 (2011) 209-215.

[9] S.S. Kandanur, M.A. Rafiee, F. Yavari, M. Schrameyer, Z.-Z. Yu, T.A. Blanchet, N. Koratkar, Suppression of wear in graphene polymer composites, Carbon, 50 (2012) 3178-3183.

[10] P. Zhu, R. Li, Study of nanoscale friction behaviors of graphene on gold substrates using molecular dynamics, Nanoscale Res. Lett., 13 (2018) 34.

[11] P.C. Uzoma, H. Hu, M. Khadem, O.V. Penkov, Tribology of 2D nanomaterials: a review, Coatings, 10 (2020) 897.

[12] A. Rosenkranz, Y. Liu, L. Yang, L. Chen, 2D nano-materials beyond graphene: from synthesis to tribological studies, Appl. Nanosci., 10 (2020) 3353-3388.

[13] D. Berman, S.A. Deshmukh, S.K. Sankaranarayanan, A. Erdemir, A.V. Sumant, Macroscale superlubricity enabled by graphene nanoscroll formation, Science, 348 (2015) 1118-1122.

[14] D. Berman, B. Narayanan, M.J. Cherukara, S.K. Sankaranarayanan, A. Erdemir, A. Zinovev, A.V. Sumant, Operando tribochemical formation of onion-like-carbon leads to macroscale superlubricity, Nat. Commun., 9 (2018) 1-9.

[15] D. Berman, A. Erdemir, A.V. Sumant, Approaches for achieving superlubricity in two-dimensional materials, ACS Nano, 12 (2018) 2122-2137.

[16] D. Berman, K.C. Mutyala, S. Srinivasan, S.K. Sankaranarayanan, A. Erdemir, E.V. Shevchenko, A.V. Sumant, Iron-nanoparticle driven tribochemistry leading to superlubric sliding interfaces, Adv. Mater. Interfaces, 6 (2019) 1901416.

[17] M. Naguib, M. Kurtoglu, V. Presser, J. Lu, J. Niu, M. Heon, L. Hultman, Y. Gogotsi, M.W. Barsoum, Two-dimensional nanocrystals produced by exfoliation of Ti_3AlC_2, Adv. Mater., 23 (2011) 4248-4253.

[18] M. Naguib, V.N. Mochalin, M.W. Barsoum, Y. Gogotsi, 25th anniversary article: MXenes: a new family of two-dimensional materials, Adv. Mater., 26 (2014) 992-1005.

[19] M. Naguib, O. Mashtalir, J. Carle, V. Presser, J. Lu, L. Hultman, Y. Gogotsi, M.W. Barsoum, Two-dimensional transition metal carbides, ACS Nano, 6 (2012) 1322-1331.

[20] M. Ghidiu, M.R. Lukatskaya, M.Q. Zhao, Y. Gogotsi, M.W. Barsoum, Conductive two-dimensional titanium carbide 'clay' with high volumetric capacitance, Nature, 516 (2014) 78-81.

[21] J. Yi, L. Du, J. Li, L. Yang, L. Hu, S. Huang, Y. Dong, L. Miao, S. Wen, V.N. Mochalin, Unleashing the potential of Ti_2CT_x MXene as a pulse modulator for mid-infrared fiber lasers, 2D Mater., 6 (2019) 045038.

[22] G. Li, N. Amer, H. Hafez, S. Huang, D. Turchinovich, V.N. Mochalin, F.A. Hegmann, L.V. Titova, Dynamical control over terahertz electromagnetic interference shielding with 2D $Ti_3C_2T_y$ MXene by ultrafast optical pulses, Nano Lett., 20 (2019) 636-643.

[23] M. Naguib, J. Halim, J. Lu, K.M. Cook, L. Hultman, Y. Gogotsi, M.W. Barsoum, New two-dimensional niobium and vanadium carbides as promising materials for Li-ion batteries, J. Am. Chem. Soc, 135 (2013) 15966-15969.

[24] Y. Xie, M. Naguib, V.N. Mochalin, M.W. Barsoum, Y. Gogotsi, X. Yu, K.-W. Nam, X.-Q. Yang, A.I. Kolesnikov, P.R. Kent, Role of surface structure on Li-ion energy storage capacity of two-dimensional transition-metal carbides, J. Am. Chem. Soc, 136 (2014) 6385-6394.

[25] J. Jiang, W. Yang, H. Wang, Y. Zhao, J. Guo, J. Zhao, M. Beidaghi, L. Gao, Electrochemical performances of MoO_2/C nanocomposite for sodium ion storage: an insight into rate dependent charge/discharge mechanism, Electrochim. Acta, 240 (2017) 379-387.

[26] A. VahidMohammadi, A. Hadjikhani, S. Shahbazmohamadi, M. Beidaghi, Two-dimensional vanadium carbide (MXene) as a high-capacity cathode material for rechargeable aluminum batteries, ACS Nano, 11 (2017) 11135-11144.

[27] S. Chertopalov, V.N. Mochalin, Environment-sensitive photoresponse of spontaneously partially oxidized Ti_3C_2 MXene thin films, ACS Nano, 12 (2018) 6109-6116.

[28] Y. Guo, M. Zhong, Z. Fang, P. Wan, G. Yu, A wearable transient pressure sensor made with MXene nanosheets for sensitive broad-range human-machine interfacing, Nano Lett., 19 (2019) 1143-1150.

[29] M. Mojtabavi, A. VahidMohammadi, W. Liang, M. Beidaghi, M. Wanunu, Single-molecule sensing using nanopores in two-dimensional transition metal carbide (MXene) membranes, ACS Nano, 13 (2019) 3042-3053.

[30] E. Lee, A. VahidMohammadi, Y.S. Yoon, M. Beidaghi, D.-J. Kim, Two-dimensional vanadium carbide MXene for gas sensors with ultrahigh sensitivity toward nonpolar gases, ACS Sens., 4 (2019) 1603-1611.

[31] V. Borysiuk, V.N. Mochalin, Thermal stability of two-dimensional titanium carbides $Ti_{n+1}C_n$ (MXenes) from classical molecular dynamics simulations, MRS commun., 9 (2019) 203-208.

[32] V.N. Borysiuk, V.N. Mochalin, Y. Gogotsi, Molecular dynamic study of the mechanical properties of two-dimensional titanium carbides $Ti_{n+1}C_n$ (MXenes), Nanotechnology, 26 (2015) 265705.

[33] G. Plummer, B. Anasori, Y. Gogotsi, G.J. Tucker, Nanoindentation of monolayer $Ti_{n+1}C_nT_x$ MXenes via atomistic simulations: The role of composition and defects on strength, Comput. Mater. Sci., 157 (2019) 168-174.

[34] A. Lipatov, H. Lu, M. Alhabeb, B. Anasori, A. Gruverman, Y. Gogotsi, A. Sinitskii, Elastic properties of 2D $Ti_3C_2T_x$ MXene monolayers and bilayers, Sci. Adv., 4 (2018) eaat0491.

[35] Y. Li, S. Huang, C. Wei, C. Wu, V.N. Mochalin, Adhesion of two-dimensional titanium carbides (MXenes) and graphene to silicon, Nat. Commun., 10 (2019) 1-8.

[36] Y. Guo, X. Zhou, D. Wang, X. Xu, Q. Xu, Nanomechanical properties of Ti_3C_2 Mxene, Langmuir, 35 (2019) 14481-14485.

[37] V.N. Borysiuk, V.N. Mochalin, Y. Gogotsi, Bending rigidity of two-dimensional titanium carbide (MXene) nanoribbons: A molecular dynamics study, Comput. Mater. Sci, 143 (2018) 418-424.

[38] Y. Dong, S. Chertopalov, K. Maleski, B. Anasori, L. Hu, S. Bhattacharya, A.M. Rao, Y. Gogotsi, V.N. Mochalin, R. Podila, Saturable absorption in 2D Ti_3C_2 MXene thin films for passive photonic diodes, Adv. Mater., 30 (2018) 1705714.

[39] C. Li, S. Kota, C. Hu, M. Barsoum, On the synthesis of low-cost, titanium-based MXenes, J. Ceram. Sci. Technol, 7 (2016) 301-306.

[40] P. Collini, S. Kota, A.D. Dillon, M.W. Barsoum, A.T. Fafarman, Electrophoretic deposition of two-dimensional titanium carbide (MXene) thick films, J. Electrochem. Soc., 164 (2017) D573-D580.

[41] J. Yang, B. Chen, H. Song, H. Tang, C. Li, Synthesis, characterization, and tribological properties of two-dimensional Ti_3C_2, Cryst. Res. Technol., 49 (2014) 926-932.

[42] X. Zhang, M. Xue, X. Yang, Z. Wang, G. Luo, Z. Huang, X. Sui, C. Li, Preparation and tribological properties of $Ti_3C_2(OH)_2$ nanosheets as additives in base oil, RSC Adv., 5 (2015) 2762-2767.

[43] Y. Liu, X. Zhang, S. Dong, Z. Ye, Y. Wei, Synthesis and tribological property of $Ti_3C_2T_x$ nanosheets, J. Mater. Sci., 52 (2017) 2200-2209.

[44] H. Zhang, L. Wang, Q. Chen, P. Li, A. Zhou, X. Cao, Q. Hu, Preparation, mechanical and anti-friction performance of MXene/polymer composites, Mater. Des., 92 (2016) 682-689.

[45] Y.J. Mai, Y.G. Li, S.L. Li, L.Y. Zhang, C.S. Liu, X.H. Jie, Self-lubricating Ti_3C_2 nanosheets/copper composite coatings, J. Alloys Compd., 770 (2019) 1-5.

[46] X. Yin, J. Jin, X. Chen, A. Rosenkranz, J. Luo, Ultra-wear-resistant MXene-based composite coating via in situ formed nanostructured tribofilm, ACS Appl. Mater. Interfaces, 11 (2019) 32569-32576.

[47] J. Hu, S. Li, J. Zhang, Q. Chang, W. Yu, Y. Zhou, Mechanical properties and frictional resistance of Al composites reinforced with $Ti_3C_2T_x$ MXene, Chin. Chem. Lett., 31 (2019) 996-999.

[48] D. Zhang, M. Ashton, R.G. Hennig, S.B. Sinnott, D. Zhang, A. Ostadhossein, D.A.C.T. van, Computational study of low interlayer friction in $Ti_{n+1}C_n$ (n = 1, 2, and 3) MXene, ACS Appl. Mater. Interfaces, 9 (2017) 34467-34479.

[49] A. Rosenkranz, P.G. Grutzmacher, R. Espinoza, V.M. Fuenzalida, E. Blanco, N. Escalona, F.J. Gracia, R. Villarroel, L. Guo, R. Kang, F. Mucklich, S. Suarez, Z. Zhang, Multi-layer $Ti_3C_2T_x$-nanoparticles (MXenes) as solid lubricants - role of surface terminations and intercalated water, Appl. Surf. Sci., 494 (2019) 13-21.

[50] A. Rodriguez, M. Jaman, O. Acikgoz, B. Wang, J. Yu, P. Grutzmacher, A. Rosenkranz, M. Baykara, The potential of Ti_3C_2 nano-sheets (MXenes) for nanoscale solid lubrication revealed by friction force microscopy, Appl. Surf. Sci., 535 (2020) 147664.

[51] X. Zhou, Y. Guo, D. Wang, Q. Xu, Nano friction and adhesion properties on Ti3C2 and Nb2C MXene studied by AFM, Tribol. Int., 153 (2021) 106646.

[52] S. Huang, V.N. Mochalin, Understanding chemistry of two-dimensional transition metal carbides and carbonitrides (MXenes) with gas analysis, ACS Nano, 14 (2020) 10251-10257.

[53] S. Huang, V.N. Mochalin, Hydrolysis of 2D transition-metal carbides (MXenes) in colloidal solutions, Inorg. Chem., 58 (2019) 1958-1966.

[54] X. Zhao, A. Vashisth, J.W. Blivin, Z. Tan, D.E. Holta, V. Kotasthane, S.A. Shah, T. Habib, S. Liu, J.L. Lutkenhaus, pH, nanosheet concentration, and antioxidant affect the oxidation of Ti3C2Tx and Ti2CTx MXene dispersions, Adv. Mater. Interfaces, (2020) 2000845.

[55] V. Natu, J.L. Hart, M. Sokol, H. Chiang, M.L. Taheri, M.W. Barsoum, Edge capping of 2D-MXene sheets with polyanionic salts to mitigate oxidation in aqueous colloidal suspensions, Angew. Chem. Int., 58 (2019) 12655-12660.

[56] K.C. Mutyala, H. Singh, R. Evans, G. Doll, Deposition, characterization, and performance of tribological coatings on spherical rolling elements, Surf. Coat. Technol., 284 (2015) 302-309.

[57] K.C. Mutyala, H. Singh, R. Evans, G. Doll, Effect of diamond-like carbon coatings on ball bearing performance in normal, oil-starved, and debris-damaged conditions, Tribol. Trans., 59 (2016) 1039-1047.

[58] K. Li, X. Wang, X. Wang, M. Liang, V. Nicolosi, Y. Xu, Y. Gogotsi, All-pseudocapacitive asymmetric MXene-carbon-conducting polymer supercapacitors, Nano Energy, 75 (2020) 104971.

[59] T. Hu, M. Hu, Z. Li, H. Zhang, C. Zhang, J. Wang, X. Wang, Interlayer coupling in two-dimensional titanium carbide MXenes, Phys. Chem. Chem. Phys., 18 (2016) 20256-20260.

[60] C. Glynn, O. Lotty, W. McSweeney, J.D. Holmes, C. O'Dwyer, Raman scattering spectroscopy of metal-assisted chemically etched rough Si nanowires, ECS Trans., 35 (2011) 73-86.

[61] T. Zhou, C. Wu, Y. Wang, A.P. Tomsia, M. Li, E. Saiz, S. Fang, R.H. Baughman, L. Jiang, Q. Cheng, Super-tough MXene-functionalized graphene sheets, Nat. Commun., 11 (2020) 1-11.

[62] X. Yin, F. Wu, X. Chen, J. Xu, P. Wu, J. Li, C. Zhang, J. Luo, Graphene-induced reconstruction of the sliding interface assisting the improved lubricity of various tribo-couples, Mater. Des., 191 (2020) 108661.

[63] J. Archard, Contact and rubbing of flat surfaces, J. Appl. Phys., 24 (1953) 981-988.

[64] K.C. Mutyala, Y.A. Wu, A. Erdemir, A.V. Sumant, Graphene-MoS_2 ensembles to reduce friction and wear in DLC-Steel contacts, Carbon, 146 (2019) 524-527.

SECTION

2. CONCLUSIONS

In this dissertaion, we have studied stability of MXenes in water and water-less colloidal solutions saturated with O_2 or Ar, using UV−vis and Raman spectroscopy. We demonstrated that water, rather than O_2, is the main factor leading to MXene degradation in aqueous colloidal solutions. Analysis of gaseous products of MXene degradation in aqueous environment by using GC and Raman further demonstrates that CH_4, rather than carbon oxides, is formed during the reactions of carbide MXenes in water, whereas both CH_4 and NH_3 are formed during degradation of the Ti_3CN MXene in water.

By investigating the degradation kinetics of different MXenes we have concluded that within the same chemical composition (Ti_2C and Ti_3C_2), Ti_3C_2 with a thicker monolayer is more stable than thinner Ti_2C. Within the same monolayer thickness (Ti_3C_2 and Ti_3CN – both having five atomic layer thick monolayers), Ti_3C_2 with a more regular structure is more stable than Ti_3CN, in which X layer is heterogenous (stochastic mix of C and N). However, two MXenes with the same monolayer thickness but different transition metals in their structure (Ti_2C and Nb_2C – both having three atomic layer thick monolayers) may have vastly different chemical reactivities, thus demonstrating that chemical properties of 2D materials also depend on their chemical composition and type of bonding within the monolayer when the monolayer thickness and structure are otherwise same. These results will be important for fundamental studies into chemistry of MXenes and other

2D materials and will also provide guidelines for development of many practical applications of MXenes where their stability is of importance.

We have investigated the adhesion energies between SiO_2 and MXenes (Ti_2C and Ti_3C_2) using AFM. The results show that the adhesion energies of MXenes with Si are in the range of adhesion of monolayer graphene with Si. However, unlike graphene, no number-of-monolayers dependence has been observed for MXenes. A larger measured value of adhesion energy for Ti_3C_2 ($0.90 \pm 0.03\ J/m^2$) than Ti_2C ($0.40 \pm 0.02\ J/m^2$) can be attributed to the thicker monolyer. The role of surface chemistry in adhesion interactions of MXenes with SiO_2 still remains unclear, but potentially it can be used to control the adhesion, provided we could better understand MXene chemistry and tailor the functional groups terminating MXene surfaces.

Tribological properties of MXene (Ti_3C_2) films on Si have been studied in a dry N_2 environment to suppress MXene reactivity towards oxygen and humidity. The ball-on-disk friction test results show that the average measured COF for Ti_3C_2 MXene against DLC is 0.0067 ± 0.0017, falling into the superlubricity regime, but with a high ball wear rate. With the addition of 37 wt% of graphene to MXene, the COF has been further reduced to 0.0042 ± 0.0011, while the ball wear rate has been reduced by a factor of 2. These results show a great potential of MXenes and MXene/graphene coatings performing as solid lubricants, especially in oxygen- and water-deficient environments.

The fundamental chemical and mechanical properties that have been investigated in this dissertation open new opportunities for rational desing of many applications for 2D transition metal carbides and/or nitrides (MXenes).

BIBLIOGRAPHY

[1] M. Naguib, M. Kurtoglu, V. Presser, J. Lu, J.J. Niu, M. Heon, L. Hultman, Y. Gogotsi, M.W. Barsoum, Two-dimensional nanocrystals produced by exfoliation of Ti_3AlC_2, *Advanced Materials*, 23 (**2011**) 4248-4253.

[2] M. Naguib, V.N. Mochalin, M.W. Barsoum, Y. Gogotsi, 25th anniversary article: MXenes: A new family of two‐dimensional materials, *Advanced Materials*, 26 (**2014**) 992-1005.

[3] M. Alhabeb, K. Maleski, B. Anasori, P. Lelyukh, L. Clark, S. Sin, Y. Gogotsi, Guidelines for synthesis and processing of two-dimensional titanium carbide ($Ti_3C_2T_x$ MXene), *Chemistry of Materials*, 29 (**2017**) 7633-7644.

[4] M. Ghidiu, M.R. Lukatskaya, M.Q. Zhao, Y. Gogotsi, M.W. Barsoum, Conductive two-dimensional titanium carbide 'clay' with high volumetric capacitance, *Nature*, 516 (**2014**) 78-81.

[5] A. Lipatov, H. Lu, M. Alhabeb, B. Anasori, A. Gruverman, Y. Gogotsi, A. Sinitskii, Elastic properties of 2D $Ti_3C_2T_x$ MXene monolayers and bilayers, *Science Advances*, 4 (**2018**) eaat0491.

[6] V.N. Borysiuk, V.N. Mochalin, Y. Gogotsi, Molecular dynamic study of the mechanical properties of two-dimensional titanium carbides $Ti_{n+1}C_n$ (MXenes), *Nanotechnology*, 26 (**2015**) 265705.

[7] N. Zhang, Y. Hong, S. Yazdanparast, M.A. Zaeem, Superior structural, elastic and electronic properties of 2D titanium nitride MXenes over carbide MXenes: a comprehensive first principles study, *2D Materials*, 5 (**2018**) 045004.

[8] V.N. Borysiuk, V.N. Mochalin, Y. Gogotsi, Bending rigidity of two-dimensional titanium carbide (MXene) nanoribbons: A molecular dynamics study, *Computational Materials Science*, 143 (**2018**) 418-424.

[9] K. Chaudhuri, M. Alhabeb, Z. Wang, V.M. Shalaev, Y. Gogotsi, A. Boltasseva, Highly broadband absorber using plasmonic titanium carbide (MXene), *ACS Photonics*, 5 (**2018**) 1115-1122.

[10] Y. Dong, S. Chertopalov, K. Maleski, B. Anasori, L. Hu, S. Bhattacharya, A.M. Rao, Y. Gogotsi, V.N. Mochalin, R. Podila, Saturable absorption in 2D Ti_3C_2 MXene thin films for passive photonic diodes, *Advanced Materials*, 30 (**2018**) 1705714.

[11] Y. Dong, S.S.K. Mallineni, K. Maleski, H. Behlow, V.N. Mochalin, A.M. Rao, Y. Gogotsi, R. Podila, Metallic MXenes: A new family of materials for flexible triboelectric nanogenerators, *Nano Energy*, 44 (**2018**) 103-110.

[12] M.R. Lukatskaya, O. Mashtalir, C.E. Ren, Y. Dall'Agnese, P. Rozier, P.L. Taberna, M. Naguib, P. Simon, M.W. Barsoum, Y. Gogotsi, Cation intercalation and high volumetric capacitance of two-dimensional titanium carbide, *Science*, 341 (**2013**) 1502-1505.

[13] C. Zhang, M.P. Kremer, A. Seral‐Ascaso, S.H. Park, N. McEvoy, B. Anasori, Y. Gogotsi, V. Nicolosi, Stamping of flexible, coplanar micro‐supercapacitors using MXene inks, *Advanced Functional Materials*, 28 (**2018**) 1705506.

[14] Y. Xie, M. Naguib, V.N. Mochalin, M.W. Barsoum, Y. Gogotsi, X. Yu, K.W. Nam, X.Q. Yang, A.I. Kolesnikov, P.R. Kent, Role of surface structure on Li-ion energy storage capacity of two-dimensional transition-metal carbides, *Journal of the American Chemical Society*, 136 (**2014**) 6385-6394.

[15] M. Naguib, J. Halim, J. Lu, K.M. Cook, L. Hultman, Y. Gogotsi, M.W. Barsoum, New two-dimensional niobium and vanadium carbides as promising materials for Li-ion batteries, *Journal of the American Chemical Society*, 135 (**2013**) 15966-15969.

[16] H. Tang, W. Li, L. Pan, C.P. Cullen, Y. Liu, A. Pakdel, D. Long, J. Yang, N. McEvoy, G.S. Duesberg, In situ formed protective barrier enabled by sulfur@ titanium carbide (MXene) ink for achieving high‐capacity, long lifetime Li‐S batteries, *Advanced Science*, 5 (**2018**) 1800502.

[17] J. Yi, L. Du, J. Li, L. Yang, L. Hu, S. Huang, Y. Dong, L. Miao, S. Wen, V.N. Mochalin, Unleashing the Potential of Ti_2CT_x MXene as a Pulse Modulator for Mid-Infrared Fiber Lasers, *2D Mater.*, 6 (**2019**) 045038.

[18] S.J. Kim, H.J. Koh, C.E. Ren, O. Kwon, K. Maleski, S.Y. Cho, B. Anasori, C.K. Kim, Y.K. Choi, J. Kim, Y. Gogotsi, H.T. Jung, Metallic $Ti_3C_2T_x$ MXene Gas Sensors with Ultrahigh Signal-To-Noise Ratio, *ACS Nano*, 12 (**2018**) 986-993.

[19] S. Xu, Y. Dall'Agnese, G. Wei, C. Zhang, Y. Gogotsi, W. Han, Screen-printable microscale hybrid device based on MXene and layered double hydroxide electrodes for powering force sensors, *Nano Energy*, 50 (**2018**) 479-488.

[20] S. Huang, K. Mutyala, A. Sumant, V. Mochalin, Achieving superlubricity with 2D transition metal carbides (MXenes) and MXene/graphene coatings, *Materials Today Advances*, 9 (**2021**) 100133.

[21] X. Yin, J. Jin, X. Chen, A. Rosenkranz, J. Luo, Ultra-wear-resistant MXene-based composite coating via in situ formed nanostructured tribofilm, *ACS Appl. Mater. Interfaces*, 11 (**2019**) 32569-32576.

[22] G. Li, N. Amer, H. Hafez, S. Huang, D. Turchinovich, V.N. Mochalin, F.A. Hegmann, L.V. Titova, Dynamical control over terahertz electromagnetic interference shielding with 2D $Ti_3C_2T_y$ MXene by ultrafast optical pulses, *Nano Letters*, 20 (**2019**) 636-643.

[23] G. Deysher, C.E. Shuck, K. Hantanasirisakul, N.C. Frey, A.C. Foucher, K. Maleski, A. Sarycheva, V.B. Shenoy, E.A. Stach, B. Anasori, Synthesis of Mo4VAlC4 MAX phase and two-dimensional Mo4VC4 MXene with five atomic layers of transition metals, *ACS nano*, 14 (**2019**) 204-217.

[24] M. Radovic, M.W. Barsoum, MAX phases: bridging the gap between metals and ceramics, *American Ceramics Society Bulletin*, 92 (**2013**) 20-27.

[25] M. Magnuson, M. Mattesini, Chemical bonding and electronic-structure in MAX phases as viewed by X-ray spectroscopy and density functional theory, *Thin Solid Films*, 621 (**2017**) 108-130.

[26] Z. Guo, L. Zhu, J. Zhou, Z. Sun, Microscopic origin of MXenes derived from layered MAX phases, *RSC Advances*, 5 (**2015**) 25403-25408.

[27] M. Khazaei, A. Ranjbar, K. Esfarjani, D. Bogdanovski, R. Dronskowski, S. Yunoki, Insights into exfoliation possibility of MAX phases to MXenes, *Physical Chemistry Chemical Physics*, 20 (**2018**) 8579-8592.

[28] M. Naguib, Y. Gogotsi, Synthesis of two-dimensional materials by selective extraction, *Accounts of chemical research*, 48 (**2015**) 128-135.

[29] K. Maleski, M. Alhabeb, Top-Down MXene Synthesis (Selective Etching), in: 2D Metal Carbides and Nitrides (MXenes), Springer, **2019**, pp. 69-87.

[30] T. Li, L. Yao, Q. Liu, J. Gu, R. Luo, J. Li, X. Yan, W. Wang, P. Liu, B. Chen, W. Zhang, W. Abbas, R. Naz, D. Zhang, Fluorine-Free Synthesis of High-Purity Ti3C2Tx (T=OH, O) via Alkali Treatment, *Angewandte Chemie International Edition*, 57 (**2018**) 6115-6119.

[31] M.A. Hope, A.C. Forse, K.J. Griffith, M.R. Lukatskaya, M. Ghidiu, Y. Gogotsi, C.P. Grey, NMR reveals the surface functionalization of Ti3C2 MXene, *Phys. Chem. Chem. Phys.*, 18 (**2016**) 5099-5102.

[32] V. Natu, R. Pai, M. Sokol, M. Carey, V. Kalra, M.W. Barsoum, 2D Ti3C2Tz MXene synthesized by water-free etching of Ti3AlC2 in polar organic solvents, *Chem*, 6 (**2020**) 616-630.

[33] S. Zhao, C. Chen, X. Zhao, X. Chu, F. Du, G. Chen, Y. Gogotsi, Y. Gao, Y. Dall'Agnese, Flexible Nb4C3Tx Film with Large Interlayer Spacing for High‐Performance Supercapacitors, *Advanced Functional Materials*, 30 (**2020**) 2000815.

[34] J. Xuan, Z. Wang, Y. Chen, D. Liang, L. Cheng, X. Yang, Z. Liu, R. Ma, T. Sasaki, F. Geng, Organic-Base-Driven Intercalation and Delamination for the Production of Functionalized Titanium Carbide Nanosheets with Superior Photothermal Therapeutic Performance, *Angewandte Chemie International Edition*, 55 (**2016**) 14569-14574.

[35] M. Naguib, O. Mashtalir, J. Carle, V. Presser, J. Lu, L. Hultman, Y. Gogotsi, M.W. Barsoum, Two-Dimensional Transition Metal Carbides, *ACS Nano*, 6 (**2012**) 1322-1331.

[36] Q. Tao, M. Dahlqvist, J. Lu, S. Kota, R. Meshkian, J. Halim, J. Palisaitis, L. Hultman, M.W. Barsoum, P.O. Persson, Two-dimensional Mo 1.33 C MXene with divacancy ordering prepared from parent 3D laminate with in-plane chemical ordering, *Nature communications*, 8 (**2017**) 1-7.

[37] R. Meshkian, M. Dahlqvist, J. Lu, B. Wickman, J. Halim, J. Thörnberg, Q. Tao, S. Li, S. Intikhab, J. Snyder, M.W. Barsoum, M. Yildizhan, J. Palisaitis, L. Hultman, P.O.Å. Persson, J. Rosen, W-Based Atomic Laminates and Their 2D Derivative W1.33C MXene with Vacancy Ordering, *Advanced Materials*, 30 (**2018**) 1706409.

[38] A. Lipatov, M. Alhabeb, M.R. Lukatskaya, A. Boson, Y. Gogotsi, A. Sinitskii, Effect of synthesis on quality, electronic properties and environmental stability of individual monolayer Ti_3C_2 MXene flakes, *Advanced Electronic Materials*, 2 (**2016**) 1600255.

[39] X. Sang, Y. Xie, M.-W. Lin, M. Alhabeb, K.L. Van Aken, Y. Gogotsi, P.R. Kent, K. Xiao, R.R. Unocic, Atomic defects in monolayer titanium carbide (Ti3C2T x) MXene, *ACS nano*, 10 (**2016**) 9193-9200.

[40] J. Halim, M.R. Lukatskaya, K.M. Cook, J. Lu, C.R. Smith, L.-Å. Näslund, S.J. May, L. Hultman, Y. Gogotsi, P. Eklund, Transparent conductive two-dimensional titanium carbide epitaxial thin films, *Chemistry of Materials*, 26 (**2014**) 2374-2381.

[41] S. Husmann, Ö. Budak, H. Shim, K. Liang, M. Aslan, A. Kruth, A. Quade, M. Naguib, V. Presser, Ionic liquid-based synthesis of MXene, *Chemical Communications*, 56 (**2020**) 11082-11085.

[42] M.R. Lukatskaya, J. Halim, B. Dyatkin, M. Naguib, Y.S. Buranova, M.W. Barsoum, Y. Gogotsi, Room ‐ temperature carbide ‐ derived carbon synthesis by electrochemical etching of MAX phases, *Angewandte Chemie*, 126 (**2014**) 4977-4980.

[43] W. Sun, S. Shah, Y. Chen, Z. Tan, H. Gao, T. Habib, M. Radovic, M. Green, Electrochemical etching of Ti 2 AlC to Ti 2 CT x (MXene) in low-concentration hydrochloric acid solution, *J Mater Chem A*, 5 (**2017**) 21663-21668.

[44] S. Yang, P. Zhang, F. Wang, A.G. Ricciardulli, M.R. Lohe, P.W. Blom, X. Feng, Fluoride ‐ free synthesis of two ‐ dimensional titanium carbide (MXene) using a binary aqueous system, *Angewandte Chemie International Edition*, 57 (**2018**) 15491-15495.

[45] M.R. Lukatskaya, S.-M. Bak, X. Yu, X.-Q. Yang, M.W. Barsoum, Y. Gogotsi, Probing the Mechanism of High Capacitance in 2D Titanium Carbide Using In Situ X-Ray Absorption Spectroscopy, *Advanced Energy Materials*, 5 (**2015**) 1500589.

[46] S. Huang, V.N. Mochalin, Hydrolysis of 2D transition-metal carbides (MXenes) in colloidal solutions, *Inorganic Chemistry*, 58 (**2019**) 1958-1966.

[47] K. Maleski, V.N. Mochalin, Y. Gogotsi, Dispersions of two-dimensional titanium carbide MXene in organic solvents, *Chemistry of Materials*, 29 (**2017**) 1632-1640.

[48] A. Jawaid, A. Hassan, G. Neher, D. Nepal, R. Pachter, W.J. Kennedy, S. Ramakrishnan, R.A. Vaia, Halogen Etch of Ti3AlC2 MAX Phase for MXene Fabrication, *ACS nano*, (**2021**).

[49] Q. Ye, P. Xiao, W. Liu, K. Chen, T. Chen, J. Xue, S. Du, Q. Huang, Exploring the potential of exfoliated ternary ultrathin Ti4AlN3 nanosheets for fabricating hybrid patterned polymer brushes, *RSC Advances*, 5 (**2015**) 70339-70344.

[50] P. Urbankowski, B. Anasori, T. Makaryan, D. Er, S. Kota, P.L. Walsh, M. Zhao, V.B. Shenoy, M.W. Barsoum, Y. Gogotsi, Synthesis of two-dimensional titanium nitride Ti4N3 (MXene), *Nanoscale*, 8 (**2016**) 11385-11391.

[51] I. Shein, A. Ivanovskii, Graphene-like titanium carbides and nitrides Tin+ 1Cn, Tin+ 1Nn (n= 1, 2, and 3) from de-intercalated MAX phases: First-principles probing of their structural, electronic properties and relative stability, *Computational Materials Science*, 65 (**2012**) 104-114.

[52] Y. Li, H. Shao, Z. Lin, J. Lu, L. Liu, B. Duployer, P.O. Persson, P. Eklund, L. Hultman, M. Li, A general Lewis acidic etching route for preparing MXenes with enhanced electrochemical performance in non-aqueous electrolyte, *Nature materials*, 19 (**2020**) 894-899.

[53] V. Kamysbayev, A.S. Filatov, H. Hu, X. Rui, F. Lagunas, D. Wang, R.F. Klie, D.V. Talapin, Covalent surface modifications and superconductivity of two-dimensional metal carbide MXenes, *Science*, (**2020**) eaba8311.

[54] M. Alhabeb, K. Maleski, T.S. Mathis, A. Sarycheva, C.B. Hatter, S. Uzun, A. Levitt, Y. Gogotsi, Selective Etching of Silicon from Ti3SiC2 (MAX) To Obtain 2D Titanium Carbide (MXene), *Angewandte Chemie International Edition*, 57 (**2018**) 5444-5448.

[55] R. Meshkian, L.-Å. Näslund, J. Halim, J. Lu, M.W. Barsoum, J. Rosen, Synthesis of two-dimensional molybdenum carbide, Mo2C, from the gallium based atomic laminate Mo2Ga2C, *Scripta Materialia*, 108 (**2015**) 147-150.

[56] J. Halim, S. Kota, M.R. Lukatskaya, M. Naguib, M.Q. Zhao, E.J. Moon, J. Pitock, J. Nanda, S.J. May, Y. Gogotsi, Synthesis and characterization of 2D molybdenum carbide (MXene), *Advanced Functional Materials*, 26 (**2016**) 3118-3127.

[57] O. Mashtalir, M. Naguib, V.N. Mochalin, Y. Dall'Agnese, M. Heon, M.W. Barsoum, Y. Gogotsi, Intercalation and delamination of layered carbides and carbonitrides, *Nature communications*, 4 (**2013**) 1-7.

[58] Y. Sun, S. Li, Y. Zhuang, G. Liu, W. Xing, W. Jing, Adjustable interlayer spacing of ultrathin MXene-derived membranes for ion rejection, *Journal of Membrane Science*, 591 (**2019**) 117350.

[59] G.R. Berdiyorov, K.A. Mahmoud, Effect of surface termination on ion intercalation selectivity of bilayer Ti3C2T2 (T= F, O and OH) MXene, *Applied Surface Science*, 416 (**2017**) 725-730.

[60] M. Shekhirev, C.E. Shuck, A. Sarycheva, Y. Gogotsi, Characterization of MXenes at Every Step, from Their Precursors to Single Flakes and Assembled Films, *Progress in Materials Science*, (**2020**) 100757.

[61] S. Huang, V.N. Mochalin, Understanding chemistry of two-dimensional transition metal carbides and carbonitrides (MXenes) with gas analysis, *ACS nano*, 14 (**2020**) 10251-10257.

[62] C. Zhang, S. Pinilla, N. McEvoy, C.P. Cullen, B. Anasori, E. Long, S.H. Park, A. Seral-Ascaso, A. Shmeliov, D. Krishnan, Oxidation stability of colloidal 2D titanium carbides (MXenes), *Chemistry of Materials*, 29 (**2017**) 4848-4856.

[63] D.B. Lioi, G. Neher, J.E. Heckler, T. Back, F. Mehmood, D. Nepal, R. Pachter, R. Vaia, W.J. Kennedy, Electron-Withdrawing Effect of Native Terminal Groups on the Lattice Structure of Ti3C2T x MXenes Studied by Resonance Raman Scattering: Implications for Embedding MXenes in Electronic Composites, *ACS Applied Nano Materials*, 2 (**2019**) 6087-6091.

[64] A. Sarycheva, Y. Gogotsi, Raman Spectroscopy Analysis of the Structure and Surface Chemistry of Ti3C2T x MXene, *Chemistry of Materials*, 32 (**2020**) 3480-3488.

[65] Y. Li, S. Huang, C. Wei, D. Zhou, B. Li, C. Wu, V.N. Mochalin, Adhesion Between MXenes and Other 2D Materials, *ACS Applied Materials & Interfaces*, (**2021**).

[66] K.L. Firestein, J.E. von Treifeldt, D.G. Kvashnin, J.F. Fernando, C. Zhang, A.G. Kvashnin, E.V. Podryabinkin, A.V. Shapeev, D.P. Siriwardena, P.B. Sorokin, Young's modulus and tensile strength of Ti3C2 MXene nanosheets as revealed by in situ TEM probing, AFM nanomechanical mapping, and theoretical calculations, *Nano Letters*, 20 (**2020**) 5900-5908.

[67] Y. Li, S. Huang, C. Wei, C. Wu, V.N. Mochalin, Adhesion of two-dimensional titanium carbides (MXenes) and graphene to silicon, *Nature Communications*, 10 (**2019**) 1-8.

[68] X. Zhou, Y. Guo, D. Wang, Q. Xu, Nano friction and adhesion properties on Ti3C2 and Nb2C MXene studied by AFM, *Tribology International*, 153 (**2021**) 106646.

[69] K. Maleski, C.E. Shuck, A.T. Fafarman, Y. Gogotsi, The Broad Chromatic Range of Two‐Dimensional Transition Metal Carbides, *Advanced Optical Materials*, (**2020**) 2001563.

[70] L. Verger, C. Xu, V. Natu, H.-M. Cheng, W. Ren, M.W. Barsoum, Overview of the synthesis of MXenes and other ultrathin 2D transition metal carbides and nitrides, *Current Opinion in Solid State and Materials Science*, 23 (**2019**) 149-163.

[71] F. Shahzad, M. Alhabeb, C.B. Hatter, B. Anasori, S.M. Hong, C.M. Koo, Y. Gogotsi, Electromagnetic interference shielding with 2D transition metal carbides (MXenes), *Science*, 353 (**2016**) 1137-1140.

[72] J. Halim, K.M. Cook, M. Naguib, P. Eklund, Y. Gogotsi, J. Rosen, M.W. Barsoum, X-ray photoelectron spectroscopy of select multi-layered transition metal carbides (MXenes), *Applied Surface Science*, 362 (**2016**) 406-417.

[73] J. Halim, K.M. Cook, P. Eklund, J. Rosen, M.W. Barsoum, XPS of cold pressed multilayered and freestanding delaminated 2D thin films of Mo2TiC2Tz and Mo2Ti2C3Tz (MXenes), *Applied Surface Science*, 494 (**2019**) 1138-1147.

[74] T. Schultz, N.C. Frey, K. Hantanasirisakul, S. Park, S.J. May, V.B. Shenoy, Y. Gogotsi, N. Koch, Surface termination dependent work function and electronic properties of Ti3C2T x MXene, *Chemistry of Materials*, 31 (**2019**) 6590-6597.

[75] K.J. Harris, M. Bugnet, M. Naguib, M.W. Barsoum, G.R. Goward, Direct Measurement of Surface Termination Groups and Their Connectivity in the 2D MXene V2CTx Using NMR Spectroscopy, *J. Phys. Chem. C*, 119 (**2015**) 13713-13720.

[76] K.J. Griffith, M.A. Hope, P.J. Reeves, C.P. Grey, K.J. Griffith, M. Anayee, Y. Gogotsi, Bulk and Surface Chemistry of the Niobium MAX and MXene Phases from Multinuclear Solid-State NMR Spectroscopy, *J Am Chem Soc*, 142 (**2020**) 18924-18935.

[77] T. Kobayashi, Y. Sun, K. Prenger, D.-e. Jiang, M. Naguib, M. Pruski, Nature of Terminating Hydroxyl Groups and Intercalating Water in Ti3C2Tx MXenes: A Study by 1H Solid-State NMR and DFT Calculations, *J. Phys. Chem. C*, 124 (**2020**) 13649-13655.

[78] W. Sun, H.-W. Wang, L. Vlcek, J. Peng, A.B. Brady, N.C. Osti, E. Mamontov, M. Tyagi, J. Nanda, S.G. Greenbaum, P.R.C. Kent, M. Naguib, Multiscale and Multimodal Characterization of 2D Titanium Carbonitride MXene, *Adv. Mater. Interfaces*, 7 (**2020**) 1902207.

[79] M. Seredych, C.E. Shuck, D. Pinto, M. Alhabeb, E. Precetti, G. Deysher, B. Anasori, N. Kurra, Y. Gogotsi, High-temperature behavior and surface chemistry of carbide MXenes studied by thermal analysis, *Chemistry of Materials*, 31 (**2019**) 3324-3332.

[80] J.L. Hart, K. Hantanasirisakul, A.C. Lang, B. Anasori, D. Pinto, Y. Pivak, J.T. van Omme, S.J. May, Y. Gogotsi, M.L. Taheri, Control of MXenes' electronic properties through termination and intercalation, *Nature Communications*, 10 (**2019**) 1-10.

[81] M. Anayee, N. Kurra, M. Alhabeb, M. Seredych, M.N. Hedhili, A.-H. Emwas, H.N. Alshareef, B. Anasori, Y. Gogotsi, Role of acid mixtures etching on the surface chemistry and sodium ion storage in $Ti_3C_2T_x$ MXene, *Chemical Communications*, 56 (**2020**) 6090-6093.

[82] P.E. Rina Ibragimova, Patrick Rinke, and Hannu-Pekka Koms, Surface Functionalization of 2D MXenes: Trends in Distribution, Composition, and Electronic Properties, *The Journal of Physical Chemistry Letters*, 12 (**2021**) 2377-2384.

[83] C. Chen, M. Boota, P. Urbankowski, B. Anasori, L. Miao, J. Jiang, Y. Gogotsi, Effect of glycine functionalization of 2D titanium carbide (MXene) on charge storage, *J Mater Chem A*, 6 (**2018**) 4617-4622.

[84] M.B. Hanna Pazniak, Thomas Bilyk, Andrea Liedl, Yan Busby, Céline Noël, Patrick Chartier, Simon Hurand, Marc Marteau, Laurent Houssiau, Rosanna Larciprete, Paolo Lacovig, Daniel Lizzit, Ezequiel Tosi, Silvano Lizzit, Jérôme Pacaud, Stéphane Célérier, Vincent Mauchamp, and Marie-Laure David, Ion Implantation as an Approach for Structural Modifications and Functionalization of Ti3C2Tx MXenes, *ACS Nano*, (**2021**).

[85] O. Mashtalir, K.M. Cook, V.N. Mochalin, M. Crowe, M.W. Barsoum, Y. Gogotsi, Dye adsorption and decomposition on two-dimensional titanium carbide in aqueous media, *J Mater Chem A*, 2 (**2014**) 14334-14338.

[86] V. Natu, J.L. Hart, M. Sokol, H. Chiang, M.L. Taheri, M.W. Barsoum, Edge capping of 2D‐MXene sheets with polyanionic salts to mitigate oxidation in aqueous colloidal suspensions, *Angewandte Chemie International Edition*, 58 (**2019**) 12655-12660.

[87] X. Zhao, A. Vashisth, E. Prehn, W. Sun, S.A. Shah, T. Habib, Y. Chen, Z. Tan, J.L. Lutkenhaus, M. Radovic, Antioxidants Unlock Shelf-Stable $Ti_3C_2T_x$ (MXene) Nanosheet Dispersions, *Matter*, 1 (**2019**) 513-526.

[88] G. Li, K. Jiang, S. Zaman, J. Xuan, Z. Wang, F. Geng, Ti_3C_2 sheets with an adjustable surface and feature sizes to regulate the chemical stability, *Inorganic Chemistry*, 58 (**2019**) 9397-9403.

[89] F. Xia, J. Lao, R. Yu, X. Sang, J. Luo, Y. Li, J. Wu, Ambient oxidation of Ti3C2 MXene initialized by atomic defects, *Nanoscale*, 11 (**2019**) 23330-23337.

[90] Y. Chae, S.J. Kim, S.-Y. Cho, J. Choi, K. Maleski, B.-J. Lee, H.-T. Jung, Y. Gogotsi, Y. Lee, C.W. Ahn, An investigation into the factors governing the oxidation of two-dimensional Ti3C2 MXene, *Nanoscale*, 11 (**2019**) 8387-8393.

[91] J. Zhang, N. Kong, D. Hegh, K.A.S. Usman, G. Guan, S. Qin, I. Jurewicz, W. Yang, J.M. Razal, Freezing Titanium Carbide Aqueous Dispersions for Ultra-long-term Storage, *ACS Applied Materials & Interfaces*, 12 (**2020**) 34032-34040.

[92] J. Kim, Y. Yoon, S.K. Kim, S. Park, W. Song, S. Myung, H.K. Jung, S.S. Lee, D.H. Yoon, K.S. An, Chemically Stabilized and Functionalized 2D ‐ MXene with Deep Eutectic Solvents as Versatile Dispersion Medium, *Advanced Functional Materials*, (**2021**) 2008722.

[93] T. Mathis, M. Maleski, A. Goad, A. Sarycheva, M. Anayee, A.C. Foucher, K. Hantanasirisakul, E. Stach, Y. Gogotsi, Modified MAX Phase Synthesis for Environmentally Stable and Highly Conductive Ti3C2 MXene, *ChemRxiv*, (**2020**).

VITA

Shuohan Huang was born in 1994, in Shenyang, Liaoning province, China. She received her Bachelor of Engineering in Polymer Materials and Engineering from Donghua University, Shanghai, China in June 2016. After graduation, she joined BASF, Shanghai, China, as an assistant chemist, working on the synthesis and characterization of emulsions for constructions. Shuohan Huang joined Prof. Vadym Mochalin's lab as a Ph.D. student in September 2017, when she started work on the synthesis, characterization, and fundamental chemistry of 2D transition metal carbides and/or nitrides (MXenes). She received her Doctor of Philosophy in Chemistry from Missouri University of Science and Technology, Rolla, Missouri, United States in May 2021.

.